Remaining Machining Tool Life Prediction Using Machine Learning

Von der Fakultät für Ingenieurwissenschaften,
Abteilung Elektrotechnik und Informationstechnik
der Universität Duisburg-Essen

zur Erlangung des akademischen Grades

Doktor der Ingenieurwissenschaften

genehmigte Dissertation

von
Lukas Krupp
aus
Homburg

Datum der Einreichung: 13.04.2023

Gutachter: Prof. Dr. rer. nat. Anton Grabmaier
Gutachter: Prof. Dr.-Ing. Norbert Wehn

Tag der mündlichen Prüfung: 02.11.2023

Acknowledgements

This thesis was written during my time as a research assistant at the Fraunhofer Institute for Microelectronic Circuits and Systems IMS in Duisburg between 2020 and 2023. I want to thank everyone who supported and encouraged me during these years and thus contributed to the success of the work. Special thanks go to my direct supervisors Prof. Dr. rer. nat. Anton Grabmaier, Prof. Dr.-Ing. Andreas Hennig and Dr.-Ing. Christian Wiede. The numerous conversations and discussions with them were the beacon of my research work. I would also like to thank Prof. Dr.-Ing. Norbert Wehn for reviewing the thesis and for his helpful input and advice.

I am incredibly grateful to my former colleague Hans-Christian Müller, who acquired and managed the BMBF research project KI-MUSIK 4.0, which provided the framework for my dissertation. I would also like to acknowledge my colleagues at Fraunhofer IMS, with whom I was able to work during this time and who supported me with technical discussions, organizational advice, and distraction through joint activities outside of work: Burkhard Heidemann, Cornelia Metz, Lars Wulfert, Johannes Kühnel, Carolin Würich, Felix Wichum, Dr.-Ing. Gongbo Chen, Dennis Latoschewski, Martin Verbunt, Thorben Grenter, Felix Essingholt, Sebastian Böller, Ingo Hoyer, Kunj Vora, Dr.-Ing. Maren Kasischke, Dr.-Ing. Pierre Gembaczka, Alexander Stanitzki, and Dr.-Ing. Gerd vom Bögel. I also greatly appreciate all the students I supervised during my thesis: Zero Liß, Shadrach Simon Sundar, Kushal Kumar Kasina, Leon Sabel, Orkhan Ahmadov, and Preetham Ganadalu Jayaram.

I would like to thank Rene Grünke from Schaeffler Technologies AG as consortium leader of the BMBF research project KI-MUSIK 4.0 and all my consortium colleagues with whom I was able to collaborate. Furthermore, I would like to thank Prof. Dr.-Ing. Joachim Friedhoff, Romas Auder, and Frederik Simon from

the University of Applied Sciences Ruhr West, as well as Markus Künkler and Niclas Georg from Aura Frästechnik GmbH for their continuous support in the implementation of my experiments as part of the dissertation.

I want to especially thank my partner, Laura Sohmann, for her unwavering support, her firm belief in my abilities, and the sacrifices she has made over the last few years. Even in the darkest moments, she has managed to awaken positive energy and perseverance in me. Lastly, I would like to thank my family and friends. I thank my parents, Matthias and Brigitte Krupp, and my grandparents, Heinz and Barbara Krupp, for their constant support. They have enabled me to discover the joy of learning and researching and to follow my path to this day. I would also like to thank Dirk, Kerstin, and Jana Sohmann, who have always believed in me and supported me. Finally, I want to thank my friends Nico Mai, Marvin Guth, Helene Wemmert, Jana Balzer, Lucas Deutschmann, Lukas Steiner, Jonas Ney, and Yannick Robin.

Abstract

The machinery and equipment manufacturing industry is decisive in achieving a sustainable economy with a savings potential of 37 % of global CO_2 emissions. Machining production is a significant factor, accounting for over 15 % of global product development costs. As a result of technological innovation in its application areas, the demands on machining continue to increase, particularly in terms of product quality, flexibility, and component complexity. Examples are the aerospace or tool- and die-making industries, where computer-aided manufacturing of free-form components based on multi-axis machining is standard. At the same time, manufacturing companies are facing the challenges of increasing competition and cost pressure.

In order to manufacture at consistently high quality and minimal costs, process and tool monitoring and the subsequent derivation of remaining tool life is of interest. However, due to the increasing customization of production, the prediction of remaining tool life is currently not applicable in the abovementioned areas. Previous process and tool monitoring approaches are too rigid for flexible manufacturing scenarios as they are mainly designed for series production. Accordingly, a methodology for small-batch and single-part production requirements opens up optimization potentials that could not be used so far.

Process and tool monitoring methods generally consist of the four components of sensor technology, signal processing and feature extraction, inference of tool and process condition, and prediction of remaining tool life.

This work first analyzes the influence of small-batch and single-part production conditions on process and tool monitoring. Mechanical vibration is identified as a particularly suitable monitoring variable. It allows a permanent and process-independent sensor integration without being affected by tool or workpiece adaptations. Based on a physical vibration source model of the machine

tool, it is possible to demonstrate the machine independence of the acceleration signals used for vibration sensing. The correlation of the machine-independent signal information with the tool and process state is proven. Thus, the sensor system architecture developed in this work can be used to determine the tool and process state in arbitrary machine tools and flexible machining systems.

A limiting factor in previous process and tool monitoring methods is the low adaptivity and explainability of tool and process state determination. Since the methods are designed for series production, the underlying black box models are manually developed once and cannot be adapted or transferred to other applications afterwards. In order to solve this problem, this thesis proposes an explainable and automatically adaptable method for tool and process condition determination. The method uses the automated machine learning approach to enable modeling based on large multivariate sensor datasets without complex feature engineering. An integrated feature evaluation mechanism visually represents the significant features. It is finally possible to determine the tool and process state in a robust, transferable, and performance-optimized way. A 21 % improvement in tool wear prediction error can be achieved.

In order to improve the remaining tool life prediction under the random variation of the process conditions in the context of small-batch and single-part production, a new tool and process condition forecasting method was proposed. A reduction of the prediction uncertainty due to the random process variations is achieved by combining temporal machine learning-based models and information about arbitrary future machining operations from process simulations. The method reduces the remaining tool life prediction error by 22 % on average. The remaining tool life prediction is performed with an accuracy of approximately 5 minutes. In relation to the average lifetime of the underlying tools of 85 minutes, the relative error is 6 %.

The methods and models developed in this thesis comprehensively extend the applicability of tool and process monitoring to small-batch and single-part production. It is thus possible to perform remaining tool life prediction in flexible manufacturing systems under variable process conditions. The knowledge of the future tool and process conditions enables an optimized production sequence control and cognitive process control to ensure quality and increase productivity.

Kurzzusammenfassung

Der Maschinen- und Anlagenbau ist mit einem Einsparungspotenzial von 37 % der weltweiten CO_2-Emissionen entscheidend für die Umsetzung einer nachhaltigen Gesamtwirtschaft. Die zerspanende Fertigung ist hierbei ein bedeutender Faktor, da sie über 15 % der globalen Produktentwicklungskosten ausmacht. Infolge der technologischen Innovation in ihren Anwendungsbereichen steigen die Anforderungen an die spanende Fertigung kontinuierlich, insbesondere in Bezug auf Produktqualität, Flexibilität und Komplexität der Bauteile. Beispiele hierfür sind die Luft- und Raumfahrtindustrie oder der Werkzeug- und Formenbau, wo die computergestützte Fertigung von Freiformteilen auf der Grundlage der Mehrachsenbearbeitung zum Standard gehört. Gleichzeitig sehen sich die Fertigungsunternehmen mit den Herausforderungen des zunehmenden Wettbewerbs und Kostendrucks konfrontiert.

Um mit gleichbleibend hoher Qualität und minimalen Kosten zu fertigen, ist die Prozess- und Werkzeugüberwachung sowie die anschließende Ableitung der Werkzeugreststandzeit von Interesse. Aufgrund der zunehmenden Individualisierung der Produktion ist die Vorhersage der Reststandzeit in den oben genannten Bereichen jedoch derzeit nicht anwendbar. Bisherige Prozess- und Werkzeugüberwachungsansätze sind für flexible Fertigungsszenarien nicht adaptiv genug, da sie hauptsächlich für die Serienfertigung ausgelegt sind. Eine Methodik für die Anforderungen der Kleinserien- und Einzelteilfertigung eröffnet daher Optimierungspotenziale, die bisher nicht genutzt werden konnten.

Prozess- und Werkzeugüberwachungsmethoden bestehen allgemein aus den vier Komponenten der Sensorik, der Signalverarbeitung und Merkmalsextraktion, der Inferenz von Werkzeug- und Prozesszustand und der Vorhersage der Werkzeugreststandzeit.

In dieser Arbeit wird zunächst der Einfluss von Kleinserien- und Einzelteil-

fertigungsbedingungen auf die Prozess- und Werkzeugüberwachung analysiert. Als eine besonders geeignete Überwachungsgröße wird die mechanische Schwingung identifiziert. Sie ermöglicht eine permanente und prozessunabhängige Sensorintegration ohne Beeinflussung durch Werkzeug- oder Werkstückanpassungen. Basierend auf einem physikalischen Schwingungsquellenmodell der Werkzeugmaschine kann die Maschinenunabhängigkeit der zur Schwingungserfassung verwendeten Beschleunigungssignale nachgewiesen werden. Außerdem wird die Korrelation der maschinenunabhängigen Signalinformation mit dem Werkzeug- und Prozesszustand gezeigt. Somit kann die in dieser Arbeit entwickelte Sensorsystemarchitektur zur Bestimmung des Werkzeug- und Prozesszustandes in beliebigen Werkzeugmaschinen und flexiblen Bearbeitungssystemen eingesetzt werden.

Ein limitierender Faktor bisheriger Prozess- und Werkzeugüberwachungsmethoden ist die geringe Adaptivität und Erklärbarkeit der Werkzeug- und Prozesszustandsbestimmung. Da die Methoden für die Serienfertigung konzipiert sind, werden die zugrundeliegenden Black-Box-Modelle einmalig manuell entwickelt und können anschließend nicht mehr angepasst oder auf andere Anwendungen übertragen werden. Um dieses Problem zu lösen, wird in dieser Arbeit eine erklärbare und automatisch anpassbare Methode zur Werkzeug- und Prozesszustandsbestimmung vorgeschlagen. Die Methode nutzt den Ansatz des automatisierten maschinellen Lernens, um die Modellierung auf Basis großer multivariater Sensordatenmengen ohne komplexes Feature Engineering zu ermöglichen. Ein integrierter Merkmalsbewertungsmechanismus stellt die signifikanten Merkmale visuell dar. Damit ist es möglich, den Werkzeug- und Prozesszustand auf robuste, übertragbare und performanceoptimierte Weise zu bestimmen. Der Fehler bei der Vorhersage des Werkzeugverschleißes kann hierdurch um 21 % gesenkt werden.

Um die Vorhersage der verbleibenden Werkzeugstandzeit unter der zufälligen Variation der Prozessbedingungen bei der Kleinserien- und Einzelteilfertigung zu verbessern, wurde eine neue Methode zur Prognose der Werkzeug- und Prozessbedingungen vorgeschlagen. Eine Reduzierung der Vorhersageunsicherheit aufgrund der zufälligen Prozessvariationen wird durch die Kombination von temporalen, auf maschinellem Lernen basierenden Modellen und Informationen über zukünftige Bearbeitungsvorgänge aus Prozesssimulationen erreicht. Die Methode reduziert den Fehler bei der Vorhersage der verbleibenden Werkzeugstandzeit im Durchschnitt um 22 %. Die Vorhersage der verbleibenden Werkzeugstandzeit erfolgt

mit einer Genauigkeit von etwa 5 Minuten. Bezogen auf die durchschnittliche Lebensdauer der zugrunde liegenden Werkzeuge von 85 Minuten beträgt der relative Fehler somit 6 %.

Die in dieser Arbeit entwickelten Methoden und Modelle erweitern die Anwendbarkeit der Werkzeug- und Prozessüberwachung umfassend auf die Kleinserien- und Einzelteilfertigung. Damit ist es möglich, eine Reststandzeitvorhersage von Zerspanungswerkzeugen in flexiblen Fertigungssystemen unter variablen Prozessbedingungen durchzuführen. Die Kenntnis des Werkzeug- und Prozesszustandes, auch in der Zukunft, ermöglicht eine optimierte Ablaufsteuerung der Produktion und eine kognitive Prozessregelung zur Sicherung der Qualität und Steigerung der Produktivität.

Contents

Abbreviations and Symbols

List of Acronyms

AAS	Asset Administration Shell
ADC	Analog-to-Digital Converter
AAF	Anti-aliasing Filter
ASIC	Application-specific Integrated Circuit
API	Application Programming Interface
ASHA	Asynchronous Successive Halving Algorithm
CAD	Computer-aided Design
CAM	Computer-aided Manufacturing
CNC	Computerized Numerical Control
CNN	Convolutional Neural Network
COTS	Commercial off-the-shelf
CPPS	Cyber-Physical Production System
CPU	Central Processing Unit
DAC	Digital-to-Analog Converter
DFT	Discrete Fourier Transform
ENBW	Equivalent Noise Bandwidth
FDA	Fully-differential Amplifier
FEM	Finite Element Method
FFT	Fast Fourier Transform
FPGA	Field-programmable Gate Array
GPU	Graphics Processing Unit
IEPE	Integrated Electronics Piezo-Electric
IIO	Industrial I/O

IIoT	Industrial Internet of Things
IIRA	Industrial Internet Reference Architecture
IPC	Industrial PC
ISA	Instruction Set Architecture
IT	Information Technology
LPF	Low-pass Filter
LOTO	Leave-One-Tool-Out
LSB	Least Significant Bit
LSTM	Long-short Term Memory
MAE	Mean Absolute Error
MAPE	Mean Absolute Percentage Error
MSE	Mean Squared Error
MEMS	Micro-Electro-Mechanical System
MCU	Microcontroller Unit
NAS	Neural Architecture Search
NC	Numerical Control
NURBS	Non-uniform Rational Basis Spline
OS	Operating System
OT	Operational Technology
PLC	Programmable Logic Controller
PoE	Power-over-Ethernet
PSD	Power Spectral Density
RAMEC	Reference Architecture Model Edge Computing
RAMI 4.0	Reference Architecture Model for Industry 4.0
RMSE	Root-Mean-Square Error
RAM	Random-access Memory
RNN	Eecurrent Neural Network
SOA	Service-Oriented Architecture
SBC	Single-board Computer
STFT	Short-time Fourier Transform
STEP	Standard for the Exchange of Product Model Data
SoC	System-on-Chip
SPI	Serial Peripheral Interface

SNR	Signal-to-Noise Ratio
SQNR	Signal-to-Quantization Noise Ratio
TPU	Tensor Processing Unit
WCET	Worst-case Execution Time

List of Symbols

A	[mm^2]	Cross-sectional Area of Cut
$\vec{F}$	[N]	Machining Force Vector
F_c	[N]	Cutting Force
F_f	[N]	Feed Force
F_p	[N]	Passive Force
F_t	[N]	Tangential Force
F_r	[N]	Radial Force
F_a	[N]	Axial Force
F_x	[N]	x-Axis Force
F_y	[N]	y-Axis Force
F_z	[N]	z-Axis Force
G	[Pa]	Shear Modulus
KB	[mm]	Crater Width
KM	[mm]	Crater Center Distance
KT	[mm]	Crater Depth
P_c	[W]	Cutting Power
P_{diss}	[W]	Dissipated Power
P_e	[W]	Effective Machining Power
P_f	[W]	Feed Power
P_th	[W]	Thermal Power
P_vib	[W]	Vibration Power
P_{xx}	$\left[\frac{\mathrm{V}^2}{\sqrt{\mathrm{Hz}}}\right]$	Power Spectral Density
R_{eff}	[mm]	Effective Cutter Radius
R_a^i	[mm]	Average Roughness per Segment i
R_p^i	[mm]	Maximum Roughness Profile Peak per Segment i
R_v^i	[mm]	Minimum Roughness Profile Valley per Segment i

R_z^i	[mm]	Distance between R_p^i and R_v^i
R_z	[mm]	Ten Point Height of Irregularities
SV_α	[mm]	Rake Face Displacement
SV_γ	[mm]	Flank Face Displacement
T_c	[min]	Instantaneous Cutting Time
$T_c^{VB_t}$	[min]	Cutting Time at Wear Mark Width Threshold
Q	$\left[\frac{\text{mm}^3}{\text{min}}\right]$	Material Removal Rate
V	[mm^3]	Removed Material during a Milling Operation
VB	[mm]	Flank Wear Mark Width
VB_{max}	[mm]	Maximum Flank Wear Mark Width
VB_t	[mm]	Flank Wear Mark Width Threshold
$\underline{Z}$	$\left[\frac{\text{Pa}\cdot\text{s}}{\text{m}}\right]$	Sound Wave Impedance
a_e	[mm]	Radial Depth of Cut
a_p	[mm]	Axial Depth of Cut
b	[mm]	Chip Width
c_L	$\left[\frac{\text{m}}{\text{s}}\right]$	Longitudinal Wave Velocity
c_T	$\left[\frac{\text{m}}{\text{s}}\right]$	Transverse Wave Velocity
f_C	[Hz]	Machine Component-related Frequency
f_N	[Hz]	Natural Frequency
f_s	[Hz]	Sampling Frequency
f_z	[mm]	Feed per Tooth
h	[mm]	Undeformed Chip Thickness
h_{ch}	[mm]	Deformed Chip Thickness
h_{min}	[mm]	Minimum Chip Thickness
n	[rpm]	Rotation Speed
r	[mm]	Cutting Edge Radius
$\vec{s}$	[m]	Sound Deflection
t_c	[min]	Cutting Time
Δt_c	[min]	Cutting Duration of Contiguous Machining Operation
t_r	[min]	Remaining Cutting Time
$\vec{v}$	$\left[\frac{\text{m}}{\text{s}}\right]$	Sound Velocity
v_c	$\left[\frac{\text{mm}}{\text{min}}\right]$	Cutting Speed
v_f	$\left[\frac{\text{mm}}{\text{min}}\right]$	Feed Speed

z_c	[-]	Number of Cutting Edges
Φ	[°]	Shear Angle
Ω_z	[Hz]	Tooth Engagement Frequency
α	[°]	Clearance Angle
α_L	[°]	Lead Angle
β	[°]	Wedge Angle
β_T	[°]	Tilt Angle
γ	[°]	Rake Angle
θ	[°]	Tool Engagement Angle
κ	[°]	Cutting Edge Angle
μ	[-]	Poisson's Ratio
ρ	$\left[\frac{\mathrm{kg}}{\mathrm{m}^3}\right]$	Density
φ	[°]	Instantaneous Engagement Angle

1. Introduction

1.1 Motivation

The machinery and equipment manufacturing industry is critical to achieving a sustainable economy. Through innovative technologies, there is a saving potential of up to 37 % of global CO_2 emissions [1]. Machining is essential to industrial manufacturing due to its significant share in the value-creation process. At the beginning of the 21^{st} century, machining directly or indirectly accounted for more than 15 % of all product creation costs [2]. This value is still rising today due to constantly expanding fields of application, such as electromobility or renewable energies [3]. The avoidance of material waste and rework in machining production represents an elementary goal for increasing sustainability and, at the same time, for securing the competitiveness of manufacturing companies. It goes hand in hand with the optimal management and use of raw materials and machining tools and the energy-efficient operation of machine tools.

The progress of technical systems requires the availability of high-quality components, e.g., in the automotive, aerospace, tool- and die-making, or prosthetic manufacturing industries. In this context, the dimensional accuracy and surface quality requirements and the complexity of the manufactured workpiece shapes constantly increase [4]. For example, even minor deviations from the dimensional and roughness specifications of injection and die-casting molds for plastics production can lead to defective end products. In addition, the increasing customization of products is causing a higher proportion of small-batch and single-part production [5, 6]. In order to cope with the increasing requirements, three main pillars have developed in industrial practice: computer-aided design (CAD) and computer-aided manufacturing (CAM) software systems for the automation and optimization of machining process planning, flexible machine tools, such as five-

axis machining centers, and process monitoring of quality-relevant and -related parameters [7].

Machining process monitoring is crucial to ensuring high product quality as problems can be detected directly during machining and corrected quickly. Its establishment is favored by the development of Industry 4.0, with the objective of digitizing production. Based on condition monitoring and predictive maintenance, Industry 4.0 is a core driver of resource efficiency, lifecycle management, and networking [8]. In addition to process monitoring using standard manufacturing metrology, methods usable during ongoing machining processes have been developed. In-process monitoring is based on process-integrated sensors for data acquisition and microelectronic components for the processing and transmission of the data [9]. Sensors are retrofitted into the machine tool, e.g., force or structure-borne sound transducers, or the digital drive-related signals used by the machine tool controller are acquired.

Since the sensor data generated during the process contain only indirect information about the quality-relevant parameters of interest, their processing is indispensable for information extraction. However, with the advancement of Industry 4.0, the number of connected sensors in the production environment is increasing, accumulating high volumes of multivariate data. Data-driven modeling based on machine learning methods represents a suitable solution to the resulting complication of information extraction [10, 11]. Concerning modeling of quality-relevant parameters, two approaches are distinguished, which build on each other: the prediction of parameters as a substitute for the direct measurement of the workpiece or tool using manufacturing metrology and the prognosis of future parameter values in case of temporal process changes, e.g., due to tool wear. Together, the approaches form the basis for determining the remaining tool life, which allows estimating when quality criteria are violated and process adaptations become necessary [12].

Up to now, the determination of tool life in industrial practice is performed by default before tool use based on empirical knowledge and is assumed to be a constant value depending only on the tool type [13, 14, 15]. However, this assumption is valid only for the case of series production, where the process conditions do not change during tool life and are known beforehand. Data-driven methods for predicting the remaining tool life, which currently receive attention

in research, have also been limited exclusively to considering series production scenarios. Applying the approaches for the increasing proportion of small batch and single-part production is impossible due to their low degree of flexibility from a sensor and algorithm perspective. In addition to using flexible machine tools, producing complex workpiece shapes as single parts or in small batches leads to frequent changes in the process and machine tool configuration. Sensor-based process monitoring approaches described in the state-of-the-art do not consider this high degree of adaptivity or change of process components. So far, sensor system concepts based on process-independent monitoring variables, which allow permanent process monitoring of small-batch and single-part production, have not yet been investigated. Furthermore, small-batch and single-part production are characterized by the variation of workpiece shapes and cutting parameters during the tool life, which leads to variable load on the tool. The variable load significantly influences the tool life, but on the other hand also affects the sensor signals, making pattern recognition for information extraction more difficult. The prediction of quality-related parameters, such as tool wear, and the remaining tool life prediction under the influence of the variable process conditions has not yet been investigated in previous works.

Against the background of the above described, this work aims to extend the state-of-the-art by presenting a machine learning-based method and machine learning models that enable the sensor-driven prediction of the remaining tool life based on quality-relevant parameters for the manufacturing of complex-shaped single-part workpieces.

1.2 Contributions

The main contributions of this work are listed in the following:

1. First, a **process-independent sensor system architecture** is proposed, enabling cutting process monitoring in flexible manufacturing systems such as multi-axis machine tools under single-part manufacturing conditions. The sensor system architecture is primarily based on the monitoring variable of vibration, but also allows the acquisition of controller signals. Due to the propagation property of vibration, permanent sensor integration is enabled, making it independent of process components that frequently change

during single-part production, such as tool or workpiece clamping. The integrated signal processing method allows the local extraction of information about the current process and tool state and local data reduction to reduce transmission bandwidth for data provisioning. Its optimization for energy-constrained systems is possible, further simplifying sensor integration.

2. Based on the sensor system architecture and the acquirable data, an **automated and explainable method for regression of tool wear** as a tool life criterion is proposed. The method enables the investigation and identification of relevant sensor-based and process-describing features for modeling at reduced effort without the intervention of a human expert. In previous works, process monitoring models were rigid due to the assumed series production conditions. In contrast, automating the modeling process allows a high degree of model adaptivity under the variable process conditions of single-part production. At the same time, the explainability enables the optimization of the predictive models, e.g., in terms of robustness and transferability.
3. The regression of tool wear is the foundation of the **remaining tool life prediction method** proposed in this work. The method is based on the tool wear forecast. It thus maintains the relationship to the tool life criterion at all times, which can, e.g., be fed back into process simulations. The method extends the state-of-the-art by enabling the inclusion of future, potentially varying influencing factors on tool life. This reduces the prediction uncertainty for the variable process conditions of the single-part production. Furthermore, more comprehensive data sources, such as the CAD/CAM software systems or the process simulation, can be included in modeling the remaining tool life.

1.3 Thesis Outline

The rest of the thesis is structured as follows. Chapter 2 describes the relevant foundations for this work, summarizes and discusses the state-of-the-art of the remaining tool life prediction, and details the research gap to be filled in this thesis. Chapter 3 introduces this work's objectives, core research questions, and general approach. Chapter 4 then describes the sensor system architecture for flexible

manufacturing systems, its implementation and evaluation. Chapter 5 presents the method for residual life prediction based on the wear forecast and regression and the evaluation results. Chapter 6 summarizes the thesis and identifies areas of future work.

2. Fundamentals and State of the Art

Since this work covers an interdisciplinary subject area, a summary of the most important fundamentals is required for the further course. The following presents and discusses the relevant concepts, models, and functional principles. In addition, the current state of research on the remaining life prognosis of machining tools using machine learning is presented, and the research gaps targeted by this work are identified.

2.1 Modern Production Systems

Since its beginning, industrial manufacturing has been subject to constant change. Automating manufacturing systems as part of the third industrial revolution has led to a rapid increase in productivity. Driven by the networking of technical systems, a fundamental change in the architecture of established automation systems is taking place as part of the fourth industrial revolution, summarized under the term Industry 4.0 [16, 17]. The following sections introduce the underlying concepts of Industry 4.0 and their significance for machining production.

2.1.1 Automation System Architecture

Networked mechatronic systems with a dedicated virtual representation form the basis of Industry 4.0 with the overarching goal of digitized and self-organizing value chains [18]. Networking and digitization enable the permanent availability of real-time information about the systems and the modeling, prediction, and optimization of their behavior and interaction. The two central concepts of Indus-

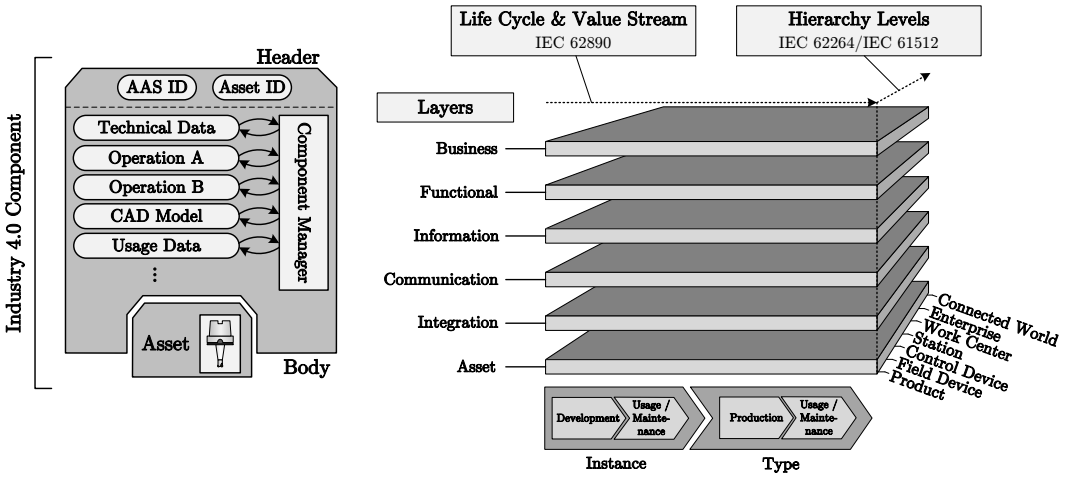

(a) AAS **(b)** RAMI 4.0 [23, 24]

Figure 2.1: Asset administration shell (AAS) and the reference architecture model for Industry 4.0 (RAMI 4.0). The concepts form the foundation for the networking and digitization of production in the context of Industry 4.0.

try 4.0 are the asset administration shell (AAS) [19, 20, 21, 22] and the reference architecture model for Industry 4.0 (RAMI 4.0) [23] shown in Figures 2.1a and 2.1b, respectively.

An entity involved in the production is called an asset. Hence, physical objects such as machines, drives or materials, and non-physical objects such as software or manufacturing processes are assets. An asset is virtually represented by its AAS, the digital interface to its features, capabilities, and operations. The AAS serves as the basis for services that describe the externally provided functionality of an asset. The combination of asset and AAS is referred to as an Industry 4.0 component. Figure 2.1a shows the AAS of a milling tool as an example, making the milling tool an Industry 4.0 component. The AAS consists of a header and a body. The header enables the unique identification of the Industry 4.0 component by asset and AAS ID, and the body manages the submodels associated with the asset. The submodels group functional aspects of an Industry 4.0 component and contain data or references to databases (technical data, real-time usage data), the operations and capabilities of the asset and references to virtual models of the asset and its functionalities (simulation or CAD models). Machine learning models assigned to an Industry 4.0 component, as targeted in this work, are also referenced in the AAS [25]. The component manager coordinates the local submodels

and the communication between AASs. If Industry 4.0 components are part of a higher-level system, the relationships between the Industry 4.0 components are part of a submodel in the overall AAS [26].

With its three dimensions *Layers*, *Life Cycle & Value Stream* and *Hierarchy Levels*, as shown in Figure 2.1b, RAMI 4.0 provides a framework for implementing AAS of entities on all factory levels along their lifecycle [23, 24, 27]. In the following, the dimensions are specified in detail:

- **Layers:** The *Layers* axis views the Industry 4.0 component from an information technology perspective. The physical or virtual entity is described on the *Asset* layer including all its components. The *Integration* layer represents the interface between the entity and its AAS. Typical interface components of physical assets include software modules to read sensors or control actuators. The *Communication* layer defines the information exchange with other AAS and services, including the particular communication protocols. The information required by services to provide the functionality of an asset is specified on the *Information* layer. The services are defined on the *Functional* layer and embedded into their particular business model on the *Business* layer.
- **Life Cycle & Value Stream:** The *Life Cycle & Value Stream* axis enables to model the whole life cycle of production-related entities. The corresponding standard IEC 62890 [28] includes the *Type* and *Instance* stages. The *Type* stage describes the development process of the entity from the idea to the first model or prototype. After development and availability of the prototype, the entity is produced, entering the *Instance* stage. Both *Type* and *Instance* stages include a usage and maintenance phase after the availability of the prototype and the start of the component production, respectively. During the lifecycle of an entity, it is always accompanied by an AAS.
- **Hierarchy Levels:** The *Hierarchy Levels* of RAMI 4.0 represent the levels of functionality in a factory or plant. They extend the traditional automation pyramid defined in the standards IEC 62264 [29] and IEC 61512 [30] by the levels *Product* to allow for their digital representation and *Connected World* enabling services that span across multiple factories. The *Hierarchy Levels* account for the requirements of services concerning information aggregation and functional separation. For example, collecting data from

multiple machines may be necessary within a work cell, a production line or a factory.

AAS and RAMI 4.0 form the basis for a service-oriented architecture (SOA) of automation, whereby the functionalities of entities are provided to other entities in the form of software-defined services [31, 32]. From a technical perspective, specific requirements must be fulfilled for implementing a SOA: Besides the mechanical production systems and processes, sensors, actuators, computing and communication capabilities must be available to implement connected services. Systems meeting these requirements are referred to as cyber-physical production system (CPPS) [33]. Industry 4.0 technologies based on RAMI 4.0 as well as the AAS and the reference models themselves are subject of continuous standardization [34, 35].

2.1.2 Edge Computing

Apart from RAMI 4.0, similar frameworks providing a basis for connected systems in the industry have been developed. Complementary to Industry 4.0, the industrial internet reference architecture (IIRA) is most important [36]. It provides the foundation for the Industrial Internet of Things (IIoT) with the goal of convergence between operational technology (OT) and information technology (IT). OT includes the physical industrial systems as well as the hard- and software used to control them, e.g., programmable logic controllers (PLCs). IT comprises the hard- and software used to handle, i.e., input, process, transmit and output, digital data, e.g., gateways or cloud servers. A difference between the frameworks is the broad view of IIRA across all industrial sectors while RAMI 4.0 is specific to industrial production. The IIRA focuses on the data handling and information flow within IIoT systems.

The edge computing paradigm is a central concept of the IIRA important to CPPS and Industry 4.0 [37, 38]. Edge computing describes the migration of computing capabilities and data processing from centralized locations like cloud servers toward the network's edge and, thus, the data sources. The IIRA views the edge as a logical layer reflecting the continuum between the dispersed and concentrated computational deployment patterns [39]. OT and IT in industrial production are distributed across the factory by default, as reflected in the hierar-

chy levels of RAMI 4.0. Furthermore, since the digital representation of an asset in its AAS can only be implemented based on computing and communication capabilities, edge computing forms a decisive basis for this.

Due to the significant overlap between RAMI 4.0 and the IIRA, especially concerning the edge computing paradigm, aligning both architectures is an important goal [40]. With respect to AAS, approaches have been developed to consider their management in naturally distributed CPPS [41]. Asset- and repository-deployed AAS are distinguished, depending on whether the asset has dedicated computing and communication capabilities [42]. Passive Industry 4.0 components, i.e., without computing and communication capabilities, cannot provide their AAS by themselves. Hence, their AASs are managed in repositories, e.g., hosted on an edge gateway. The reference architecture model edge computing (RAMEC) [43] provides a formal basis for applying edge computing in Industry 4.0. It allows specifying the application- and implementation-related aspects of edge computing systems on the hardware and software levels. At the same time, it retains the relation to the hierarchy levels of the factory as considered in RAMI 4.0.

2.1.3 Autonomous Machining Systems

Machining forms a central part of manufacturing and is directly affected by the change in automation system architecture due to Industry 4.0. While the production of workpieces in machining is automated through Computerized numerical control (CNC) technology, other steps in the process chain, such as process planning or quality control, are primarily performed manually [44]. Applying the concepts according to the previous Sections 2.1.1 and 2.1.2 offers the potential of quality- and resource-optimized production by networking along the process chain and increasing autonomy. In the literature, many attempts have been made to define autonomy in the context of technical systems [45]. The present work shares the definition according to [46] as the ability of the system to successfully perform a specific task without having been explicitly programmed or requiring significant human intervention. Figure 2.2 shows the system components of a general autonomous system [47].

In the production context, the components of autonomous systems can be represented using AAS and RAMI 4.0. The edge computing paradigm forms the

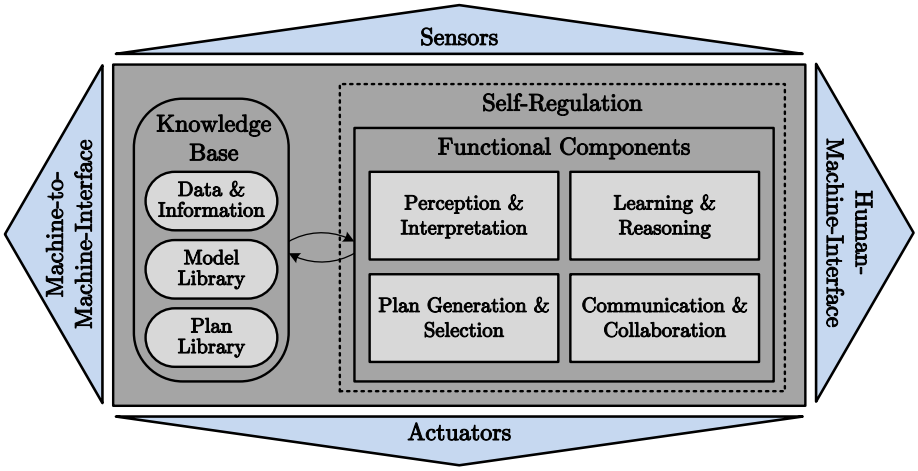

Figure 2.2: Functional and technical components of a general autonomous system [47, 46].

technical basis for their implementation, such that the desired characteristics of autonomous production systems are supported by design [47, 48]. According to Figure 2.2, sensors are used to collect data related to the specific application or environment. The data is then processed to extract relevant information (*Perception & Interpretation*). In addition, contextual data from other systems or human operators can be included via the machine-to-machine and human-machine interfaces. The multiple data sources form the basis for learning the relationships relevant to the system's tasks (*Learning & Reasoning*). An essential technological foundation for this is provided by machine learning methods, enabling the generation of models from data without direct programming. Thus, the system can adapt to changes in the application or to new tasks. After the task-related information and knowledge about the current state of the system and its environment are available, the following steps are planned to accomplish the tasks (*Plan Generation & Selection*). All relevant data, information, models, and plans are stored in a knowledge base that is continuously adapted. *Actuators* finally execute the plans or messages are passed to other machines or human operators when collaboration or transfer of control is required (*Communication & Collaboration*).

Figure 2.3 shows the structure of an autonomous machining system with its information processing components. The CNC machine tool is the system's core and executes the machining processes. The execution is based on the control loops defined by the CNC programming. The control loops are non-cognitive

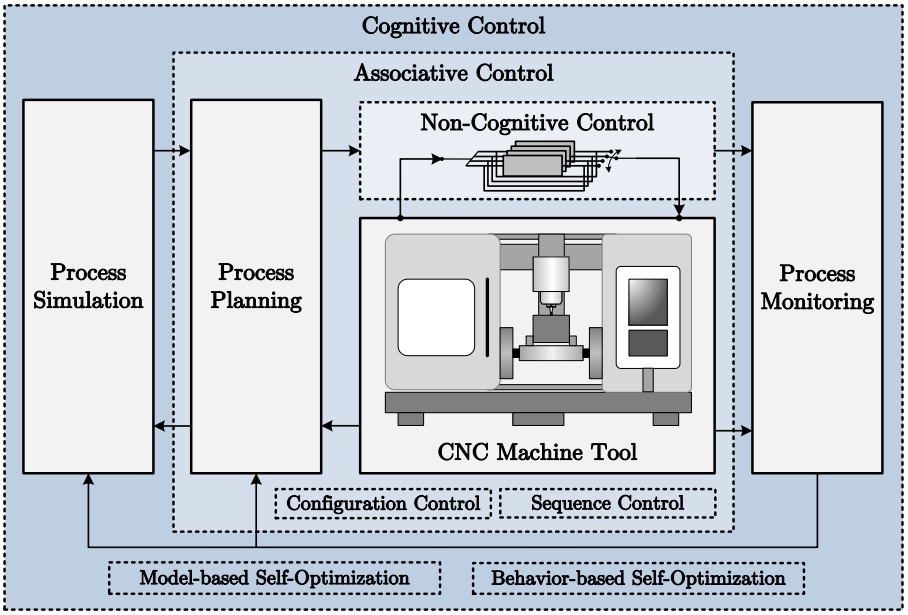

Figure 2.3: Architecture of an autonomous machining system, adapted from [49, 50].

and executed under hard real-time requirements based on the machine-internal sensors and actuators. The programming and configuration of the CNC machine tool and the high-level sequential control of the processes are performed as part of the process planning. Process planning represents the associative control. A process planner can use experience from past machining operations and link them to future ones for optimization. Process simulation and monitoring are the information processing components necessary for the cognitive control [51] of machining processes. These form the basis for complete virtual representations of the machining process and its components (CNC machine tool, cutting tool, workpiece), so-called digital twins [52]. Process simulation and monitoring enable the identification of problems and optimization potentials of currently running and future machining processes. Therefore, behavior and model-based self-optimization of the machining processes can be performed.

Digital twins in manufacturing are specified in the standard ISO 23247 [53]. The provided framework covers all aspects of process simulation and monitoring necessary for cognitive process control and can be implemented using AAS [25]. Digital twins of machining systems and their components are current research topics [54, 55, 56]. Machining tool-centered approaches, e.g., based on the stan-

dard ISO 13399 [57], are particularly important for tool life cycle management and process productivity optimization [58, 59].

2.2 Machining Process

Machining processes and systems are essential for today's value chains, leading to high overall importance for production. Machining is used to manufacture end products and components directly or to produce tools for other production technologies such as stamping, casting or forming. In order to manage high workpiece complexities and the increasing individualization of production, flexible CNC machine tools are used in combination with advanced CAD and CAM software [60]. Therefore, the following sections describe the relationships that apply in today's machining systems, especially to understand the significance of the resulting load on the cutting tools. The considerations are the basis for process monitoring and, ultimately, the application of machine learning techniques in today's machining industry.

2.2.1 Machining Fundamentals

Before considering complex machining processes, as they are state of the art today, one must first understand the fundamentals of machining [13, 61, 62, 63]. The interaction between the cutting tool and the workpiece through relative movements characterizes machining. This work focuses on machining with a geometrically defined cutting edge, to which all the following explanations refer. Geometrically defined cutting edges of the tools lead to the formation of geometrically defined chips during machining. Chip formation is a process of plastic deformation induced by the cutting edge of the tool entering the workpiece material and exceeding its maximum bearable shear stress. The chip slides over the rake face of the cutting edge. The opposite flank or clearance face is oriented towards the newly emerging surface of the workpiece as the chip runs off. The geometrical parameters of the tool and the process parameters guide the chip formation. Figure 2.4 illustrates the chip formation and the relevant parameters during machining for a general turning process.

Plastic deformation during the chip formation occurs in five areas. The primary

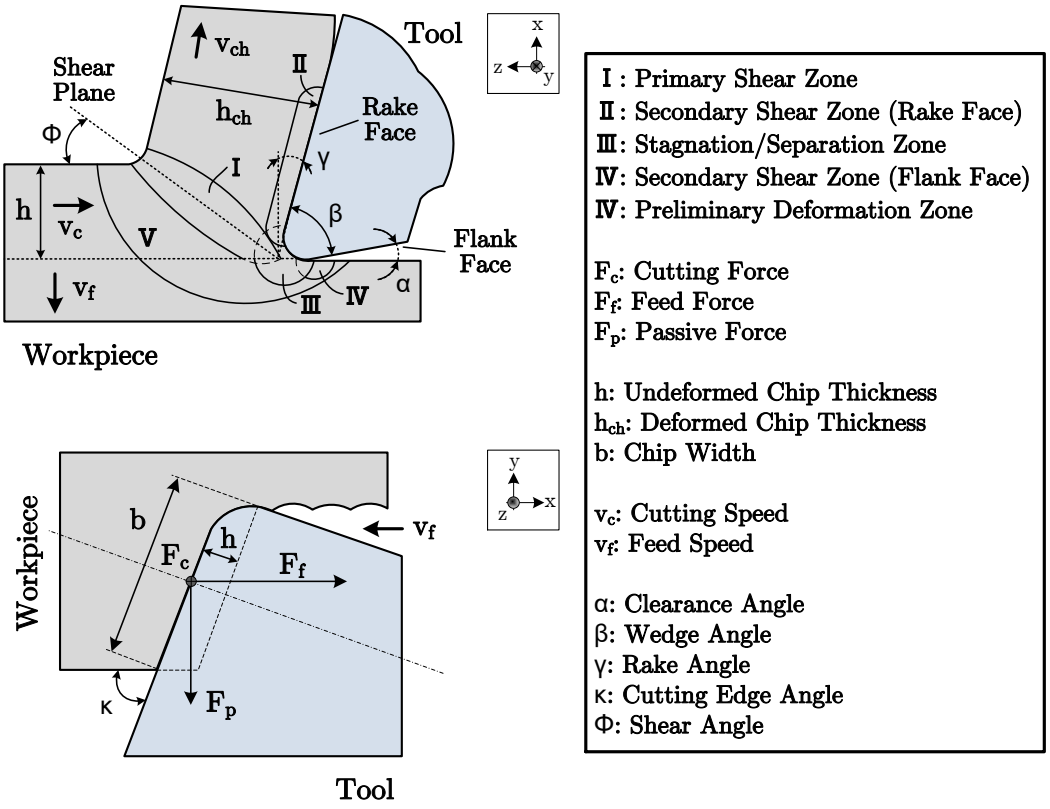

Figure 2.4: Chip formation in a machining process using the example of turning with geometric parameters, deformation zones and resulting forces, adapted from [13, 62].

shear zone (I) is the central area of deformation. In the secondary shear zones at the rake and flank faces (II, IV), plastic deformation occurs due to friction forces resulting from the contact between the cutting edge faces and the workpiece material. The friction in the secondary shear zones is the major source of heat generated during the machining process. In the separation and stagnation zone in front of the cutting edge (III), the actual separation of the material occurs. As there is maximum pressure from all sides, built-up edges can occur due to particles of the workpiece material being bonded onto the rake face of the cutting edge. The preliminary deformation zone (V) is in immediate proximity to the chip and the primary shear zone. The deformation results from significant stress, as the material in the area will be split off next. The force required to exceed the shear stress necessary to detach the chip from the workpiece and the friction forces at the cutting edges result in the overall machining force $\vec{F}$. $\vec{F}$ is a vector

and can be split into its three spatial components: the cutting force F_c, the feed force F_f and the passive force F_p. Section 2.2.3 will further detail the machining force.

2.2.2 Free-Form Surface Machining

Manufacturing complex workpiece shapes, such as for mold- and die-making or in the context of the aerospace industry, requires advanced methods of machining process planning [60]. For this purpose, 3D computer modeling is used, enabling the design of arbitrary objects and shapes through CAD technologies. The 3D models form the basis for the subsequent generation of CNC machine instructions using CAM technologies [64]. Arbitrarily shaped workpieces are generated during 3D computer modeling by employing free-form surfaces based on the non-uniform rational basis spline (NURBS) functions [65]. A surface is described using NURBS functions according to Equations 2.1a and 2.1b.

$$S(u,v) = \sum_{i=0}^{n}\sum_{j=0}^{m} R_{i,j}(u,v)\mathbf{P}_{i,j} \tag{2.1a}$$

$$R_{i,j}(u,v) = \frac{N_{i,p}(u)N_{i,q}(v)w_{i,j}}{\sum_{k=0}^{n}\sum_{l=0}^{m} N_{k,p}(u)N_{l,q}(v)w_{k,l}} \tag{2.1b}$$

The central components of NURBS-based modeling are the control points $\mathbf{P}_{i,j}$ and the rational basis functions $R_{i,j}(u,v)$. The rational basis functions are weighted combinations of B-spline basis functions $N_{i,p}(u)$ and $N_{i,q}(v)$, which are polynomials of orders p and q, respectively. The weighting is based on the matrix $\mathbf{W}$ containing the weights $w_{i,j}$ with $i \in [0,n]$ and $j \in [0,m]$. A rational basis function is assigned a control point $\mathbf{P_{i,j}}$ and by combining the rational basis functions into a series over the control points, a surface can be modeled using the function $S(u,v)$. $S(u,v)$ is parametric, i.e., it returns points for a specific pair of input values u and v. By evaluating the function $S(u,v)$ for $u \in [a,b]$ and $v \in [c,d]$, the points $\mathbf{S}$ constituting the surface are generated. Figure 2.5 shows an example of a convex surface using the control points to illustrate the NURBS-based modeling.

The tensors $\mathbf{S_{i,1}}$ and $\mathbf{S_{1,j}}$ represent the points when evaluating $S(u,v)$ over the intervals of u and v, assuming i and j fixed at a value of 1, respectively. Hence, the points constitute the lines highlighted in blue and red in Figure 2.5.

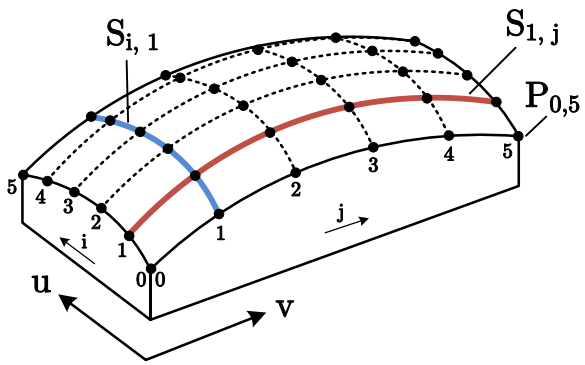

Figure 2.5: Concave surface illustrating the parameters and working principle of NURBS-based surface modeling.

2.2.3 Multi-Axis Milling

Due to its high flexibility regarding the workpiece shapes to be produced, the milling process is the core technology in free-form surface machining [60, 66]. Therefore, this work focuses primarily on free-form surface milling. The term free-form surface machining will be used synonymously in the following. In addition to the 3D computer modeling of workpieces described in the previous section, the multi-axis capability of modern machine tools is an essential foundation for free-form surface milling. Manufacturing complex sculptured surfaces requires the movement of the cutting tool on at least the three spatial axes. However, machines with more degrees of freedom are standard to avoid changing the workpiece setup and thus increase the overall productivity. In particular, five-axis machine tools, which allow the additional rotation and tilting of the machine table, are state-of-the-art in manufacturing [67, 68]. Due to the arbitrary orientation of the milling tool to the workpiece surface (working plane) during five-axis milling, the tool engagement conditions and thus the mechanical load on the milling tool change frequently. The kinematic and geometric principles and the cutting forces during five-axis milling are considered in the following.

The standard DIN 8589-3 [69] defines milling according to its kinematic characteristics as a circular movement of the tool cutting edges with the non-parallel orientation of the feed direction with respect to the tool's rotational axis. The standard distinguishes multiple milling techniques, whereby the main category of interest in this work is form milling. Form milling describes the manufacturing

of arbitrary 3D surfaces that do not directly depend on the geometry of the used milling tool. The form milling methodologies are further subdivided concerning the applied process control. Today, the milling of free-form surfaces is exclusively based on CNC machine tools [44, 67] due to the geometric complexity and the required shape and surface accuracy.

The milling of free-form surfaces is an end milling process, as defined in DIN 8985-3. Surface milling is generally subdivided according to the orientation of the tool's rotational axis with respect to the working plane and the cutting edge part generating new surface layers of the workpiece. During face milling, the rotational axis of the tool is perpendicular to the working plane, while during peripheral milling the orientation is horizontal. Face and peripheral milling have the purpose of generating a single surface with the end or side cutting edges of the tool, respectively. On the other hand, end milling allows to generate new surfaces with both cutting edges. Especially in form milling operations, the rotational axis of the end milling tool is arbitrarily oriented with respect to the working plan.

The two variants up- and down-milling [63] are distinguished depending on the relationship between cutting direction and feed direction. Up- and down-milling result in different loads on the tool's cutting edges. The up-milling process is characterized by opposite cutting and feed directions. Therefore, the cutting edge enters the material at a chip thickness of $h = 0$ mm, followed by a continuous increase. As long as the chip thickness is below the characteristic minimum chip thickness h_{min}, i.e., $h \in [0, h_{min}]$, no shearing but only friction and squeezing occurs, leading to high thermal stress on the cutting edges. In addition, the feed and cutting forces act in opposite directions, resulting in increased vibration excitation. Hence, up-milling is considered unfavorable. During down-milling, characterized by the same cutting and feed direction, the cutting edge enters the material abruptly and the cutting process terminates at a chip thickness of $h = 0$ mm.

Figure 2.6 illustrates up- and down-milling and introduces the main cutting parameters and geometric relationships relevant to milling. Different shapes of tool bodies and cutting edges are used in milling based on the series of standards DIN 11529 [70] and DIN 6581 [71]. Due to its importance for multi-axis milling, toroidal tools with circular tool cutting edges are used in this work [72, 73]. All the following explanations, equations and figures are based on them, but can be

transferred to other tool types without loss of generality.

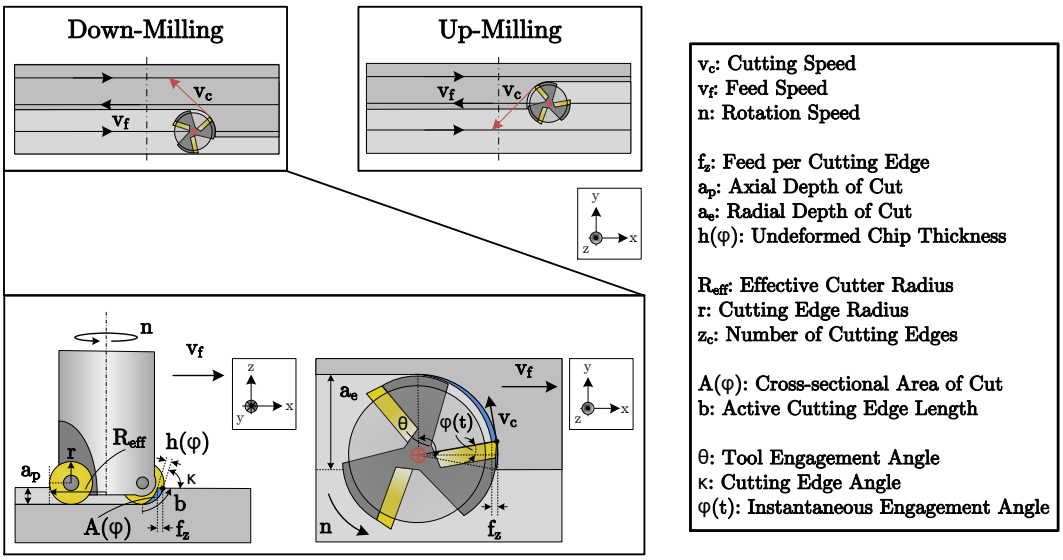

Figure 2.6: Comparison between up- and down-milling with cutting parameters of the milling process and geometric relationships for a toroidal tool with circular cutting edges, adapted from [72, 73].

The cutting parameters v_c and f_z of the milling process and the tool parameters z_c and R_{eff} define the rotational speed n of the spindle and the feed speed v_f, which are calculated according to Equations 2.2a and 2.2b:

$$n = \frac{v_c \cdot 1000}{\pi \cdot R_{eff}} \tag{2.2a}$$

$$v_f = f_z \cdot n \cdot z_c \tag{2.2b}$$

Based on n and z_c, the cutting edge engagement frequency Ω_z is calculated according to Equation 2.3:

$$\Omega_z = \frac{z_c \cdot n}{60} \tag{2.3}$$

The cutting edge angle κ and the effective tool radius R_{eff} depend on the axial cut depth a_p for circular cutting edges, since the contact point of cutting edge and workpiece changes with a_p. The cross-sectional area of the cut A, i.e., the area of the cutting edge in contact with the workpiece during its engagement, is calculated according to Equation 2.4:

$$A(\varphi) = \frac{f_z \cdot a_p \cdot \sin\varphi}{\kappa} \tag{2.4}$$

As the tool rotates, A changes with time, depending on the instantaneous engagement angle $\varphi(t)$ passing through the interval $[\varphi_{min}, \varphi_{max}]$ per currently engaged cutting edge. The length of the interval depends on the radial depth of the cut a_e and is denoted as tool engagement angle θ, defined according to Equation 2.5:

$$\theta = \varphi_{max} - \varphi_{min} \tag{2.5}$$

In addition to the movement along the three spatial axes, the tool can be inclined relative to the working plane in five-axis milling. The lead angle α_L and the tilt angle β_T describe this geometrically. The lead angle specifies the tool inclination in the feed direction, while the tilt angle describes the tool inclination orthogonally to the feed direction. Figure 2.7 illustrates both inclination parameters.

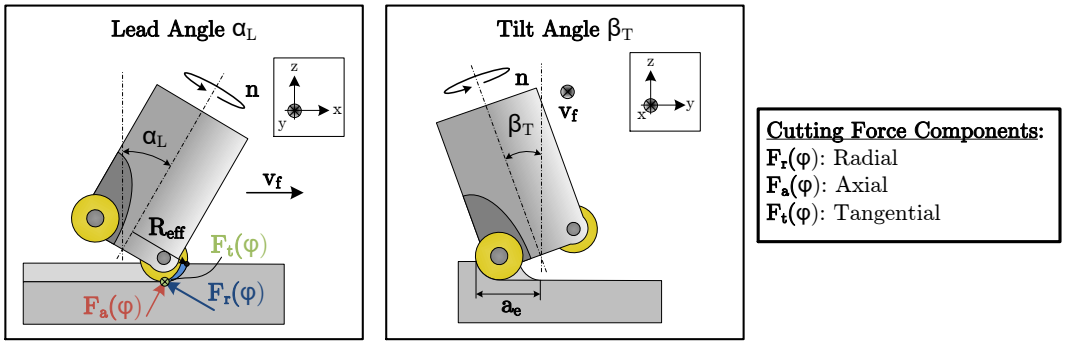

Figure 2.7: Engagement conditions during five-axis milling with lead and tilt angle of the cutting tool's axis with respect to the working plane normal vector, adapted from [72, 73].

As shown on the right for β_T, the tool inclination with respect to the working plane affects the radial depth of the cut a_e and, consequently, the engagement angle θ [72, 73]. Furthermore, the illustration of α_L shows that the displacement of the contact point of the cutting edge as a result of the inclination varies R_{eff} and κ. The same variations occur when the relative position between the workpiece and the working plane changes due to the curvature of the workpiece [74].

In addition to the geometric engagement conditions under lead and tilt angle,

Figure 2.7 shows the components of the cutting force that act during milling, which causes the mechanical load on the tool. The force acting on the engaged tool cutting edge consists of a tangential, radial and axial component. The force components are represented relative to the tool cutting edge. According to the empirical-geometric milling force model of Altintas et al. [75], the cutting force $\vec{F}$ can be written as:

$$\vec{F}(\varphi) = \begin{pmatrix} F_t(\varphi) \\ F_r(\varphi) \\ F_a(\varphi) \end{pmatrix} = \vec{K_c} A(\varphi) + \vec{K_e} b = \underbrace{\begin{pmatrix} K_{tc} \\ K_{rc} \\ K_{ac} \end{pmatrix} \cdot A(\varphi)}_{\substack{\text{Cutting} \\ \text{Component}}} + \underbrace{\begin{pmatrix} K_{te} \\ K_{re} \\ K_{ae} \end{pmatrix} \cdot b}_{\substack{\text{Edge Force} \\ \text{Component}}} \tag{2.6}$$

As described in Section 2.2.1, shearing and friction processes occur at the tool cutting edge during chip formation. Shearing in the shear zones and friction at the rake face, represented by $A(\varphi)$, is considered in the cutting force model by the cutting component using the empirical constants K_{tc}, K_{rc} and K_{ac}. In addition, the model considers ploughing and rubbing at the engaging cutting edge of length b using the edge force component, which is derived from the empirical constants K_{te}, K_{re} and K_{ae}. The empirical constants are determined based on milling tests [76]. However, it is known that the cutting constants K_{tc}, K_{rc} and K_{ac} depend on the geometric parameters of the tool cutting edge described in Section 2.2.1 and this section. The wear of the tool cutting edges, changing their geometry over time, is therefore indirectly represented in the cutting force model. The tangential force component of $\vec{F}$ represents the cutting force F_c during milling:

$$F_c(\varphi) = F_t(\varphi) \tag{2.7}$$

Assuming $\alpha_L = 0°$ and $\beta_T = 0°$, the cutting force can be mapped to the Cartesian coordinate system by multiplying the force vector $\vec{F}$ by a transformation matrix dependent on φ and κ [77]:

$$\begin{pmatrix} F_x(\varphi) \\ F_y(\varphi) \\ F_z(\varphi) \end{pmatrix} = \begin{pmatrix} -\cos\varphi & -\sin\varphi\sin\kappa & -\sin\varphi\cos\kappa \\ \sin\varphi & -\cos\varphi\sin\kappa & -\cos\varphi\cos\kappa \\ 0 & -\cos\kappa & -\sin\kappa \end{pmatrix} \begin{pmatrix} F_t(\varphi) \\ F_r(\varphi) \\ F_a(\varphi) \end{pmatrix} \tag{2.8}$$

If α_L and β_T are set arbitrarily, Equation 2.8 transforms the cutting force into the tool coordinate system, i.e., relative to the tool axis. The transformation into the Cartesian coordinate system is then achieved by a second transformation

matrix depending on α_L and β_T [78]. The mapping of the milling force into the Cartesian coordinate system enables the derivation of the feed force F_f, given the feed direction.

2.2.4 Milling Process Chain

3D computer modeling and multi-axis machining are primary enabling factors of free-form surface machining. CNC machine tools are standard in today's manufacturing, due to their high productivity and the complexity of multi-axis machining. The previous Sections 2.2.2 and 2.2.3 do not yet address the required steps between a 3D workpiece model and the finished workpiece. Therefore, the steps of the so-called CAD/CAM process chain [79, 80] are shown in Figure 2.8.

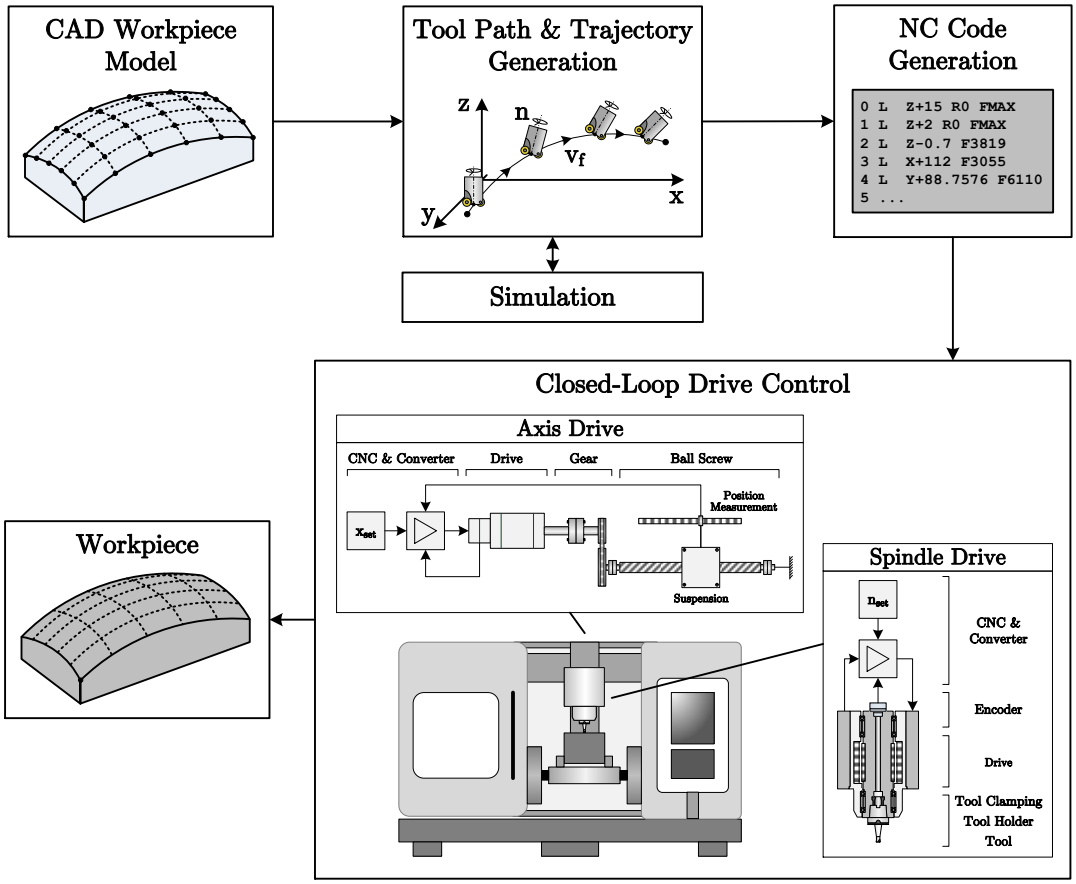

Figure 2.8: Structure of the CAD/CAM process chain and controlled machining process-related components of a CNC tool machine, adapted from [80].

The starting point of the CAD/CAM process chain is the CAD model of the

workpiece, as described in Section 2.2.2. Based on the model, the tool trajectories, i.e., the tool paths and movement patterns (speed, acceleration, jerk) along them, are defined to manufacture the desired surface. The tool trajectory planning also includes determining the tool inclination (lead and tilt angle). The tool trajectory generation in state-of-the-art CAM software tools uses curve- or vector field-based algorithms [81]. During or after trajectory generation, the machining process simulation can be performed to identify problems in the machining process and optimize it. The simulation of the cutting force allows, for example, the optimization of the process concerning its energy efficiency. The effective power P_e to be applied by the drives for machining is based on the cutting and feed force components F_c and F_f according to Equation 2.9 and can therefore be estimated in advance through the force simulation [82].

$$P_e(t) = P_c(t) + P_f(t) = F_c(t) \cdot v_c(t) + F_f(t) \cdot v_f(t) \tag{2.9}$$

Furthermore, optimizing the material removal rate Q according to Equation 2.10, which determines the productivity of the machining process, represents a central simulation objective [83].

$$Q = \frac{\Delta V}{\Delta t_c} \tag{2.10}$$

For this purpose, the volume ΔV to be removed [84, 85] for a certain workpiece and the cutting duration Δt_c required for the production have to be estimated [86, 87]. Both estimation tasks can already be accomplished using state-of-the-art CAM software tools.

The numerical control (NC) code is generated based on the tool trajectories using the so-called post processor module [79]. The NC code is required to control the machine tool and specifies the relative movements between the tool and workpiece. The NC code instructions as well as syntax and structure of NC programs are described in the standards DIN 66025 [88] and ISO 6983 [89]. The machine tool controller interprets the NC program and executes it by instructing the machine drives in a closed-loop manner. In particular, the main axes and spindle drives are crucial for manufacturing the workpieces. Figure 2.8 shows the components of typical axes and spindle drive trains in CNC machine tools [67].

2.3 Machining Process Monitoring

Apart from the milling process simulation, process monitoring is the second major possibility to optimize its execution. Process monitoring ensures process quality and reliability as it enables problem identification based on measurement data and it enables the calibration or optimization of simulation models. Furthermore, problems not representable by simulation can be detected. The following highlights the foundations of process monitoring from a hardware and software perspective.

2.3.1 Data Acquisition

The starting point of process monitoring is the acquisition of measurement data. A distinction is made between online and offline as well as direct and indirect strategies for measuring and quantifying tool- and process quality-related parameters [13]. Online techniques rely on data acquisition during the ongoing machining process, while offline techniques require its interruption or termination. The classification into direct and indirect techniques refers to the measurement of the target parameter. If the direct measurement is not possible, other related variables must be acquired indirectly to infer information on the target parameter.

Quality Target Parameters

The target parameters in machining process monitoring are all related to the workpiece quality. Especially its dimensional accuracy and surface quality are decisive, as they determine and limit the performance of their final applications. The wear of the cutting tools significantly influences both factors, which is why tool wear is also a primary target parameter.

Tool wear includes all changes in the tool's cutting edge geometry resulting from friction processes between the cutting edges and the workpiece material and the general mechanical and thermal stress on the tool material during machining [90]. The main wear mechanisms are abrasion, adhesion, tribo-oxidation, diffusion and surface breakdown [13, 61]. Tool wear depends on the geometry and material of the tool cutting edges, the material of the workpiece, cutting parameters, cutting force and the use of cooling lubricant. The parameters for quantifying tool wear

according to the ISO 3685 standard [91], as shown in Figure 2.9, refer to the material removal at rake and flank faces. They measure the resulting geometric deviation of the edge shape.

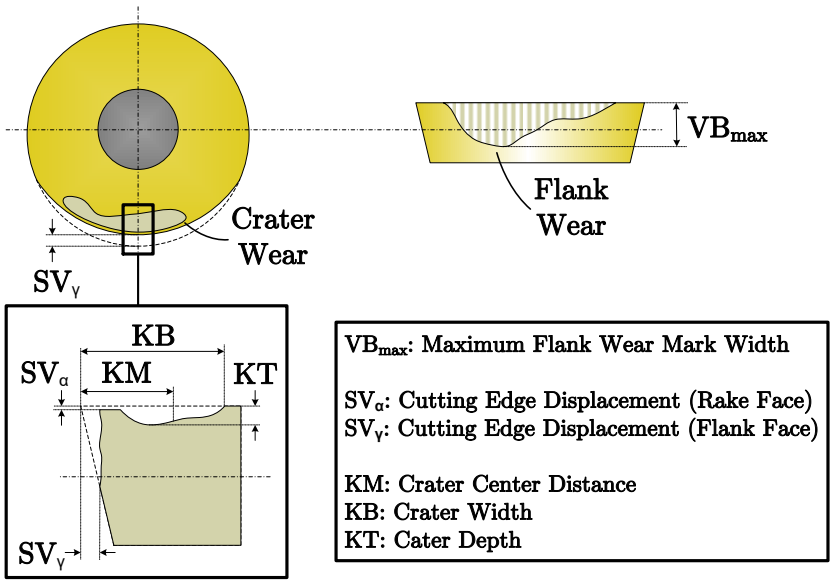

Figure 2.9: Tool wear measurement parameters according to DIN ISO 3685 shown for the cutting edge of a circular insert, adapted from [13, 61].

The formation of flank and crater wear is a gradual, progressive process. It may be accompanied by plastic deformation, notch wear, cracking, chipping, material breakout and built-up edge formation [60]. The gradual wear is to be distinguished from abrupt tool failure caused by the breakage of the tool or cutting edge, which makes the tool unusable. Tool failure is favored by gradual wear, but can also occur independently, e.g., due to mechanical overload. This work considers gradual wear as it mainly causes changes in workpiece quality. The wear mark on the flank face of the cutting edge, as shown in Figure 2.9, mainly influences the workpiece quality. Since it is in direct contact with the newly created workpiece surface, it affects the surface quality. In addition, the formation of the wear mark width is always accompanied by the dimensional change of the cutting edge, i.e., SV_γ, which affects the dimensional accuracy. Accordingly, measuring and monitoring the wear mark width is particularly important and focused in this work. Its maximum value VB_{max} is used for this purpose and is referred to as VB in the following.

Surface quality is determined by quantifying the characteristics of the surface profile of a workpiece [13]. The surface profile (primary or P-profile) contains low- and high-frequency components denoted as waviness (W-profile) and roughness (R-profile), which can be extracted from the P-profile using low- and high-pass filters. Several parameters describing the surface features are determined based on the three profiles according to the standard ISO 21920 [92]. Especially for components of technical applications, the roughness of the surface is of particular importance since it determines their frictional properties [90]. In mold- and die-making, the roughness of the surfaces also determines the quality of the final products [60]. Therefore, the R-profile is mainly considered in this work. The central parameters determined based on an R-profile are shown in Figure 2.10.

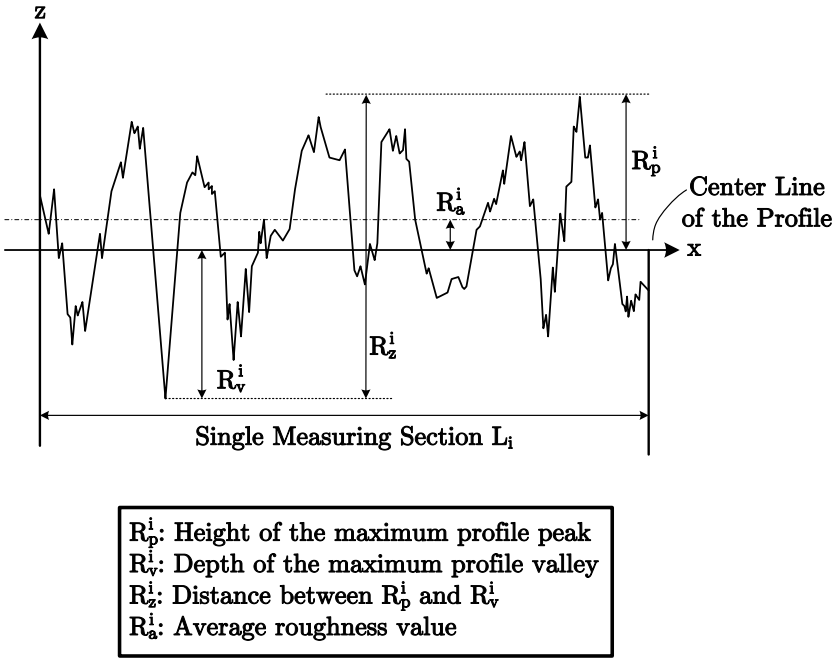

Figure 2.10: Roughness measurement parameters according to ISO 21920 shown for a measuring section of an exemplary roughness profile (R-profile) [13].

To determine the roughness parameters, a measuring section L of a roughness profile is divided into N consecutive subsections of length L_i. As shown in Figure 2.10, the parameters are then determined per subsegment and the average is calculated. The ten-point height of irregularities R_z is particularly important. It represents the mean of the values R_z^i over five consecutive measurement intervals and thus summarizes information on the profile peaks and valleys.

Direct Monitoring

The direct determination of tool wear and workpiece quality parameters is performed using tactile and optical measuring systems [93]. Tactile systems include load cells, probes and profilometers for determining the surface profiles. Optical solutions are microscopy-, laser- or image processing-based. The measuring systems are either machine-integrated or external [44]. Most direct acquisition systems perform measurements offline, i.e., between the manufacturing of workpieces. This is their main disadvantage, as the measurements extend the overall duration of production. In addition, continuous monitoring is impossible and problems cannot be detected immediately. Furthermore, if machining times are long, the machining process must be interrupted for intermittent measurements.

Indirect Monitoring

Online measurement strategies offer a solution to this problem, as they utilize sensors capturing data in-process that is indirectly related to the target parameters [13]. The basis for online measurement strategies are the process outputs of the cutting process resulting from the application of cutting and feed forces for chip removal. As shown in Section 2.2.3, the cutting force during milling is sensitive to changes in the geometry of the cutting edges, as is the case for gradually progressing wear. Therefore, the acting forces or the power expended by the machine tool drives according to Equation 2.9 are feasible monitoring variables. Furthermore, power dissipation occurs during chip formation in the contact zone between the tool and workpiece, generating mainly heat and mechanical vibration, making temperature and vibration also usable monitoring variables. In the following, the monitoring variables suitable for online process monitoring and the sensor principles used for this purpose are examined in detail:

Cutting Force: According to the milling force model of Altintas et al. [75], the cutting force during milling comprises a cutting surface and an edge component. These represent the deformation and friction processes taking place during machining. The cutting force is time-dependent with periodic variation due to the continuous cutting edge entry and exit. In the context of multi-axis milling, the variable engagement conditions also lead to non-periodic force changes during machining. The cutting force is measured using piezoelectric dynamometers and

strain gauges [13]. Strain gauges are applied to the tool structure for this purpose. They exploit the dependence of electrical resistances on their cross-section and length. The resistance varies due to mechanical stretching of the tool structure when the cutting forces act. However, the stiffness of the tool structure results in the low sensitivity of this measurement method.

Through piezoelectric dynamometers, the cutting force can be measured more precisely using the piezoelectric effect. The piezoelectric effect describes the generation of dipoles when the geometry of piezoelectric materials, such as silicon dioxide (SiO_2), changes, resulting in a measurable electrical voltage. The charge shifts caused by elastic deformation can be differentiated according to the direction of the force acting on the piezoelectric crystal. The longitudinal, transversal and shear sensitivity of the materials are differentiated. Static and rotating dynamometers are used for monitoring the cutting process [94]. Three piezoelectric elements, each of longitudinal or transversal sensitivity orientation, are the basis for acquiring the cutting force components in both approaches. Additionally, the torque can be determined in two ways: a fourth shear-sensitive piezoelectric element is used, which allows direct measurement or the torque is calculated via several fixed three-component sensors. In the former case, only the z-axis torque can be determined, while the latter allows the derivation of all three torque components.

Rotating and static dynamometers differ in their mounting location and spatial orientation of the measured forces. Static dynamometers are mounted on the machine tool table and workpieces are clamped directly on it for machining. They allow the cutting force to be measured in the Cartesian coordinate system. Thus, to calculate the forces acting on the tool cutting edges during milling according to Equation 2.6, both the inclination between the tool axis and the working surface normal vector as well as the actual position of the engaging cutting edges and their geometry must be known as described in Section 2.2.3. Rotating dynamometers serve as tool holders and are integrated into the tool clamping system of the spindle. They allow direct measurement of the cutting forces on the tool cutting edges.

Drive Active Power: The active power consumption of the axis and spindle drives depends on the cutting and feed forces [13]. According to Equation 2.9, the cutting force F_c and the feed force F_f have a proportional effect on the cutting

power P_c and the feed power P_f via the cutting speed v_c and the feed speed v_f. To perform the cutting process, the drives of the machine tool must apply the resulting effective power P_e as active power, taking into account their efficiency factor η. The drives are designed such that the torque generation considers the friction of mechanical drive train components (ball screw, bearings), depicted in Figure 2.8 and the effects of the weight force due to their suspension.

As already described above, process changes, e.g., due to tool wear, hence also affect the active power through the force. However, if cutting and feed forces are to be accurately reconstructed from the active power, the factors leading to deviations in the measured values must be compensated [95]. The active power is determined by measuring the voltage, current and phase difference. The external voltage measurement is performed at the connection ports of the drives and the current is acquired using Hall sensors. In addition, modern CNC machine tool controllers also acquire the power consumption of their drives. If the controller offers a communication interface, these digital signals can be used directly for process monitoring.

Temperature: The effective power required for chip formation is dissipated due to the friction and separation processes in the contact zone of the tool cutting edge and the workpiece. A large proportion of the power is converted into heat, of which approximately 75 % is dissipated into the chip, 18 % into the tool and 7 % into the workpiece during steel cutting [13]. As explained in Section 2.2.3, the proportion of the cutting force, representing the friction and separation processes during chip formation, changes due to tool wear. Thus, wear also affects heat dissipation and enables the use of temperature as a process monitoring variable. Thermoelectric or radiation sensors are primarily used for temperature measurement. Thermoelectric sensors (thermocouples, single-wire thermocouples and sheathed thermocouples) must be placed very close to the contact zone to measure the heat streams reliably. This requires integration into or attachment to the tool or workpiece. Radiation sensors (pyrometers, infrared thermometers) are applied externally and do not require direct proximity to the process. However, because an unobstructed view of the contact zone is required, complex components and multi-axis machining can prevent the applicability of radiation sensors.

Vibration: The effective power P_e of the cutting process is not only trans-

formed into heat, but also into mechanical vibrations. The dissipated vibration power leads to the excitation of mass-dependent vibrations of the machine components (machine vibrations) and the deflection of particles of the machine structure from their equilibrium position, resulting in the propagation of mechanical waves within the machine structure (structure-borne sound) [96].

Machine vibrations are described by modeling the machine tool as a mass-spring-damper system, where the machine tool components represent the masses. The vibrations are divided into externally excited and self-excited [97]. The most significant external excitation occurs during milling due to the periodic engagement of the tool cutting edges. In addition, imbalances, defective machine elements or bearing faults cause external excitation of the machine tool system during drive rotation. Due to its mechanical compliance characteristics, the machine structure has natural frequencies at which it oscillates under impulsive excitation. Self-excited vibrations are referred to as chatter and result from the feedback of vibrations due to the machining process, leading to oscillations at the natural frequencies. In today's CNC machines, regenerative chatter is the primary form of self-excited vibrations [98]. It results from excitation due to abrupt variations of the cutting force, leading to waviness and roughness of the surface. If the milling tool reaches the respective area again, the cutting force also varies again due to the modulation of the cutting depth, causing regenerative vibration excitation.

In order to gain an understanding of the generation of structure-borne sound during machining, it is necessary to highlight the fundamentals of structure-borne sound in general [99, 100, 101]. When vibrational energy is introduced into a solid, it propagates in waves through mutual conversion between potential and kinetic energy, distributed in time and space. This results in changes in the shape and volume of the solid in which the potential energy is stored. The resulting wave types can be divided into the basic types of transverse and longitudinal waves, assuming propagation in an isotropic medium. In the case of transverse waves, the direction of particle oscillation and the direction of propagation are orthogonal to each other. In the case of longitudinal waves, the oscillation and propagation directions are the same. Ideally, transverse and longitudinal waves occur when their wavelengths λ_L and λ_T are significantly smaller than the length of the solid. In spatially limited bodies of real components with specific shapes, further types

of waves occur (bending, stretching and surface waves). All types of waves can be described using three fundamental changes in the shape of a surface element: strain, shear deformation and rotation. From this, the general field equations of structure-borne sound are derived:

$$G\left(\Delta\vec{s} + \frac{1}{1-2\mu}\text{grad}\,\text{div}\vec{s}\right) = \rho\frac{\partial^2\vec{s}}{\partial t^2} \tag{2.11a}$$

$$G\left(\Delta\vec{v} + \frac{1}{1-2\mu}\text{grad}\,\text{div}\vec{v}\right) = \rho\frac{\partial^2\vec{v}}{\partial t^2} \tag{2.11b}$$

The field equations contain the material-dependent constants of the shear modulus G, Poisson's ratio μ, density ρ and the sound deflection $\vec{s}$ and sound velocity $\vec{v}$, linked to each other via the partial derivative with respect to time. $\vec{v}$ describes the speed of the particle oscillation in three-dimensional space. It can be shown that the field equations can be decomposed into a source-free and a vortex-free part, describing ideal longitudinal and transverse waves, respectively. The propagation velocities of longitudinal and transverse waves are defined according to:

$$c_L = \sqrt{\frac{G}{\rho}\frac{2(1-\mu)}{1-2\mu}} \tag{2.12a}$$

$$c_T = \sqrt{\frac{G}{\rho}} \tag{2.12b}$$

The above explanations illustrate that combinations of longitudinal and transverse waves can express all other occurring waves. Furthermore, the Equations 2.11a, 2.11b, 2.12a and 2.12b show that the type and propagation of waves are independent of the excitation and are determined only by the material.

In practice, a material's structure-borne sound transmission properties are characterized by the sound wave impedance $\underline{Z}(f)$ [102]. It can be determined metrologically by exciting a body with a force $\vec{F}$ and capturing the resulting sound velocity $\vec{v}$. $\underline{Z}(f)$ is defined according to Equation 2.13, where F and v describe the magnitudes of the vectors $\vec{F}$ and $\vec{v}$:

$$\underline{Z}(f) = \frac{\underline{F}(f)}{\underline{v}(f)} \tag{2.13}$$

$\underline{Z}(f)$ represents a frequency-dependent and, hence, complex transfer function of a material. Since machine tools consist of multiple components of different ma-

terials, the propagation of structure-borne sound in the machine tool structure is influenced accordingly. Refraction and reflection of the waves occur at boundaries of materials with different sound wave impedances and scattering occurs if the size of an obstacle is approximately in the range of the wavelength. Furthermore, the structure-borne sound waves attenuate as a result of energy dissipation.

The measurement of machine vibrations and structure-borne sound is based on the physical vibration quantities of displacement, velocity and acceleration, which are linked to each other via the derivative with respect to time [103]. The displacement is determined through tactile probes and eddy current transducers, while the velocity is measured via inductive transducers or interferometers. Inductive, piezoelectric, piezoresistive and capacitive transducers exist for measuring acceleration. Due to the propagation property of vibrations in mechanical systems and structures, their measurement in cutting process monitoring does not require immediate proximity to the contact zone, as with force or temperature measurement.

Control Signals: As explained in the above description of the active drive power as a process monitoring variable, the digital signals of the machine tool controller are also suitable as process monitoring variables [95, 104]. Axis drives are usually operated via position, speed and current control circuits, while spindle drives require rotation speed control [44]. Hence, the corresponding signals must be available to the machine tool controller via sensors integrated into the machine tool. In addition, the power consumption of the drives is acquired internally. The disadvantage of using the control signals for process monitoring is the machine tool and controller dependency of the interfacing.

2.3.2 Processing Hardware

For indirect process monitoring, information about the target parameters must first be inferred from the sensor data introduced in the previous Section 2.3.1. Information extraction requires processing of the sensor data, enabled by combining the sensors with information and communication technology hardware into sensor systems. Two sensor system architectures for monitoring the machining process exist and will be reviewed in the following. The architectures differ with respect to their proximity to the machining process and resulting level of data

aggregation, as described by the edge computing paradigm in Section 2.1.2.

Component-integrated sensor systems represent the first architecture category. They include sensor systems integrated into the components required for machining, i.e., the cutting tool, the clamping system or the machine tool [105]. Sensor-integrated tools and tool holders are one of the main representatives of this category [106]. Due to their close integration into the machining process and the moving and rotating components of multi-axis machine tools, sensor-integrated tools and tool holders are mostly wireless systems. The sensor systems are either powered using wireless energy transmission [107], energy harvesting [108] or batteries [109]. Due to the resulting restrictions concerning energy consumption, state-of-the-art systems integrate ultra-low-power microcontroller units (MCUs) with the primary tasks of sensor sampling and data transmission. The MCU itself performs no or only limited data processing. The raw sensor signals are transmitted to server systems [110] or mobile end devices [111, 112] like smartphones and tablets for further processing and visualization. Tool-, tool holder- and clamping system-integrated sensor systems utilize vibration, force and temperature as process monitoring variables. One tool-integrated sensor system for monitoring free-form milling processes exists [113, 114]. The sensor system is integrated into a long ball nose tool and monitors the tool vibrations, which significantly affect the surface roughness. Further component-integrated sensor systems are integrated into the machine tool spindle [115, 116] or utilize the digital controller signals and the machine tool controller as a computing platform [117]. Component-integrated sensor systems are the subject of current research. However, commercial off-the-shelf (COTS) systems also already exist on the market [118, 119, 120].

Gateway-level sensor systems form the second architecture category. Gateway-level sensor systems are characterized by the availability of several sensor signals of different monitoring variables and partially across several machine tools on a central computing platform. Component-integrated and dedicated analog sensors can be connected and the machine tool controller may be accessed. The main difference to the component-integrated sensor systems is that sensor data processing, e.g., signal analysis using fast Fourier transform (FFT)-based methods [121, 122] or feature extraction [123], is performed locally to reduce the data volume and directly provide higher-level information. Therefore, the computational

load increases, leading to more powerful computing systems than those used in component-integrated sensor systems. Gateway-level sensor systems are based on industrial PCs (IPCs) [124, 125] or single-board computers (SBCs) [126, 127, 128], while research works also investigate the use of field-programmable gate arrays (FPGAs) [129, 130] or multi-MCU-based gateway systems [131]. COTS gateway-level sensor systems are IPC- or FPGA-based and target the local execution of signal-based monitoring, e.g., threshold-based tool wear detection and the integration into cloud server systems [132, 133, 134, 135, 136, 137, 138].

As the application of machine learning methods increases in machining process monitoring [139], the processing hardware forming the basis of the sensor systems also adapts. As with sensor data processing, the sensor systems perform machine learning tasks locally. The basic machine learning tasks are training and inference of the models. To handle this additional workload alongside the other tasks of the sensor systems, hardware architectures are specialized for machine learning. The first type of specialized hardware architectures used in machining process monitoring are application-specific integrated circuits (ASICs) and tensor processing units (TPUs) enabling in particular the inference of machine learning models [140]. Their training is performed on server systems. First COTS gateway-level sensor systems adopt this principle [137]. The next step is to locally train and infer machine learning, which has been achieved by custom accelerators implemented on FPGA [141]. In addition to ASIC- and FPGA-based acceleration, support for machine learning tasks in embedded systems is added with specialized instruction set architectures (ISAs) of central processing units (CPUs) and the miniaturization of graphics processing units (GPUs), already used in server systems [142]. Another possibility is the distribution of machine learning tasks across multiple sensor systems, leveraging their communication capability [143, 144].

2.3.3 Signal Processing

The sensor systems for cutting process monitoring described in the two previous sections form the basis for processing the sensor signals on the hardware side. Sensor signal processing algorithms are used to extract higher-level information from the sensor signals, which allows the inference of the target parameters. Since machining processes are dynamic, frequency domain analysis is particularly important for monitoring. Frequency domain analysis is used for all process mon-

itoring variables introduced in Section 2.3.1, except for temperature monitoring due to the inertia of heat flow.

The basis of frequency domain analysis is the Fourier transform, which allows a continuous and infinite time domain signal $x(t)$ to be transformed into its frequency domain representation $\underline{X}(f)$ [145]. It is assumed in the following that the time domain sensor signals are always real-valued.

$$\underline{X}(f) = \int_{-\infty}^{+\infty} f(t) e^{-j2\pi ft}\, dt \tag{2.14}$$

In order to be processed using the hardware presented in Section 2.3.1, a sensor signal must be digitized beforehand, i.e., sampled at equidistant time intervals $T_s = \frac{1}{f_s}$ with a sampling frequency of f_s. The result is a discrete signal $\hat{x}(n) = x(nT_s)$ of finite length N whose Fourier transform can be determined using the discrete Fourier transform (DFT):

$$\underline{\hat{X}}(m) = \sum_{n=0}^{N-1} \hat{x}(n) e^{-j2\pi \frac{nm}{N}} \text{ , for } m = 0, \ldots, N-1 \tag{2.15}$$

To reduce the computational complexity of the DFT according to Equation 2.15, in practice it is calculated using the FFT [146].

When analyzing a signal using the Fourier transform, its stationarity, i.e., time invariance, is implicitly assumed. However, this assumption is generally invalid for the machining process since it is dynamic and consists of multiple phases, especially in multi-axis machining. The resulting signals are non-stationary. To enable an analysis of non-stationary signals, the short-time Fourier transform (STFT) is used:

$$\underline{S}(\tau, f) = \int_{-\infty}^{+\infty} x(t) w(\tau - t) e^{-j2\pi ft} \tag{2.16}$$

The STFT of a continuous signal $x(t)$ is based on the multiplication with a moving window function $w(\tau - t)$ and subsequent frequency transform to obtain the time-frequency spectrum $\underline{S}(\tau, f)$. As with the Fourier transform, the STFT is also applicable to a finite, discrete signal $\hat{x}(n)$:

$$\underline{\hat{S}}(l, m) = \sum_{n=l-(N_w-1)}^{l} \hat{x}(n) w(l-n) e^{-j2\pi \frac{nm}{N}} \tag{2.17}$$

The discrete and finite window w is assumed to be non-zero between 0 and $N_w - 1$. Due to its physical significance, the power spectral density (PSD) of a signal, i.e., the distribution of the signal power over frequency, is a crucial part of signal analysis. In addition to the distinction of the stationarity of a signal, it is necessary to distinguish between deterministic and random signals when considering the PSD. The values of a deterministic signal are known at arbitrary time points, whereas this is not valid for random signals. Ideally, signals generated by rotating machines such as machine tools are deterministic. However, in reality, the signals have random components due to the cutting process and the non-ideality of the machine and its components. The periodogram $P_{xx}(f)$ representing the PSD can be generally estimated for a random, discrete and finite signal $\hat{x}(n)$ using the DFT-based frequency spectrum $\underline{\hat{X}}(m)$ according to:

$$P_{xx}(m) = \frac{1}{N}\left|\underline{\hat{X}}(m)\right|^2 \tag{2.18}$$

The quality of the PSD estimate using Equation 2.18 increases with the length of the considered signal segment. In order to increase the quality of the estimate for non-stationary and short signal sections, advanced algorithms are applied, e.g., the Bartlett, Welch or Blackman-Tukey method [145]. In the following, the PSD estimate $P_{xx}(m)$ is denoted as a periodogram.

In addition to signal analysis, feature extraction methods are used to extract condensed information from sensor signals and their frequency as well as time-frequency domain representations [147, 148]. Their goal is to map the characteristics and shape of the signal representations in a minimum possible number of parameters.

2.3.4 Remaining Tool Life Prediction

After signal processing, inference with respect to the quality target parameters of the machining process described in Section 2.3.1 is the final step of machining process monitoring. Based on this, it is possible to estimate how long it will be possible to manufacture further workpieces while complying with the required threshold values of the quality target parameters. This period is referred to as the remaining tool life t_r. The tool life is determined by the cutting time of the tool t_c, indicating how long the tool has been in contact with the workpiece.

The decisive target parameter for the determination of the tool life is denoted as tool life criterion. Progressive tool wear is a common tool life criterion as it significantly influences the quality-relevant parameters of dimensional accuracy and surface quality of the workpieces. The decrease in process quality can be estimated based on future tool wear. Figure 2.11 shows the remaining tool life T_r based on the flank wear mark width VB at an instantaneous cutting time T_c.

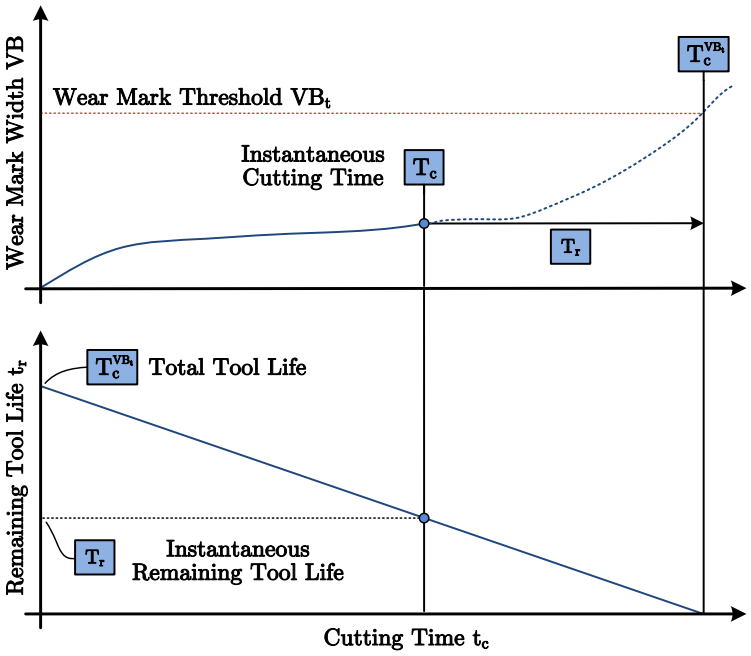

Figure 2.11: Illustration of the remaining tool life and related parameters based on the flank wear mark width VB as a tool life criterion.

The basic method for estimating the total tool life $T_c^{VB_t}$ according to the Taylor formula [13] utilizing VB as a tool life criterion is given by:

$$T_c^{VB_t} = C_v^{VB_t} \cdot v_c^k \text{ , with } k = -\frac{\log C_v^{VB_t}}{\log C_t} \tag{2.19}$$

$T_c^{VB_t}$ is the cutting time until the flank wear mark threshold VB_t is reached. The constant $C_v^{VB_T}$ describes the tool life until VB_t with a cutting speed of $v_c = 1\frac{m}{min}$ and the constant C_T describes the cutting speed for a tool life of one minute. Both constants are empirical values that must be determined separately for every combination of cutting tool and workpiece in machining tests. Equation 2.19 is only based on the cutting speed v_c. Extensions of the Taylor formula include other cutting parameters such as feed per cutting edge f_z and depth of

cut a_p, which also influence the tool life [60].

The Taylor formula represents a physics-based, empirical method for determining the remaining tool life. Further representatives of this variant are wear rate models, which are based on the contact mechanics during the cutting process [149, 150]. Furthermore, simulation-based, stochastic, statistical, machine learning and hybrid approaches exist, as shown in Figure 2.12. Physics- and simulation-based approaches model the tool life criterion, e.g., the wear mark width shown in the upper part of Figure 2.11 and then derive $T_c^{VB_t}$. The other approaches use past or in-process data from direct or indirect monitoring to model the tool life criterion or directly the remaining tool life function, shown in the lower part of Figure 2.11.

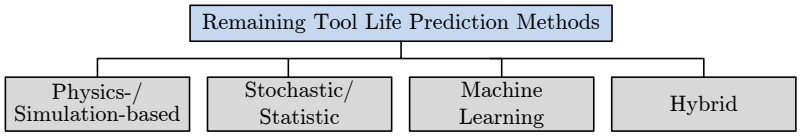

Figure 2.12: Categories of remaining tool life prediction methodologies.

Simulation-based methods mainly utilize the finite element method (FEM) to iteratively model the chip formation process and the resulting wear [151, 152, 153, 154, 155]. The preliminary determination of tool life using pure physics- and simulation-based methods lacks several factors relevant in the machining process, which cannot be described based on univariate parameters or mathematical models. In particular, tool life is additionally influenced by the machine tool and its condition, by production-related variations of the workpiece raw material and the tool and by the workpiece geometry and shape as well as the resulting tool load. Thus, to include real-time information about the process, direct and indirect monitoring is used as the basis for remaining tool life prediction.

Stochastic and statistic methods are based on direct or indirect monitoring data and assumptions on the functions to be modeled, requiring expert knowledge. Examples are parametric regression [156] and forecasting models [157], Bayesian inference [158, 159, 160, 161], Markov models [162, 163] or stochastic processes [164]. Hybrid methods combine physical or simulation models with estimation methods, e.g., particle filters, to optimally determine empirical parameters of the physical models from indirect process monitoring data [165, 166, 167, 168].

Machine learning models are solely monitoring data-based and non-parametric, i.e., neither they neither assumptions on the functions to be modeled nor physics-based models. They will be discussed in detail in the following section.

2.4 Machine Learning

Machine learning methodologies enable extracting information from data such as the indirectly acquired signals of machining process-integrated sensors described in Section 2.3. As a basis for remaining tool life prediction in this work, the corresponding foundations of machine learning are introduced in the following.

2.4.1 Regression and Forecasting

Machine learning methods [169] are based on models whose parameters are adapted during training to a dataset $\mathcal{D}_{train}$, covering the target learning task. The learning tasks are divided into supervised and unsupervised, depending on $\mathcal{D}_{train}$. In supervised learning, a relationship between an input feature space X and a target space Y is established. X consists of feature vectors $\vec{x}_i \in \mathbb{R}^d$, where d denotes their dimension, and targets $y_i \in Y$, resulting in $\mathcal{D}_{train} = \{(\vec{x}_1, y_1), \ldots, (\vec{x}_n, y_n)\}$. A dataset $\mathcal{D}_{test} = \{(\vec{x}_{n+1}, y_{n+1}), \ldots, (\vec{x}_m, y_m)\}$ is used to evaluate the prediction performance of a machine learning model. Depending on Y, classification problems with discrete and regression problems with continuous targets y_i are distinguished. Unsupervised methods do not require information on the target space Y and rely only on the feature vectors. They are used for clustering, dimension reduction and association learning tasks. Figure 2.13 summarizes the differentiation of machine learning problems.

The remaining tool life prediction is generally a regression problem since its target variables are continuous, as described in Section 2.3.4. Therefore, Figure 2.13 shows an overview of regression models focused on in the following. Regression based on machine learning models enables the approximation of arbitrary functional relationships between the input and target spaces. The training and inference, i.e., the application of the models based on sensor data is shown in Figure 2.14.

Machine learning models are characterized by their parameters θ_p, adjusted

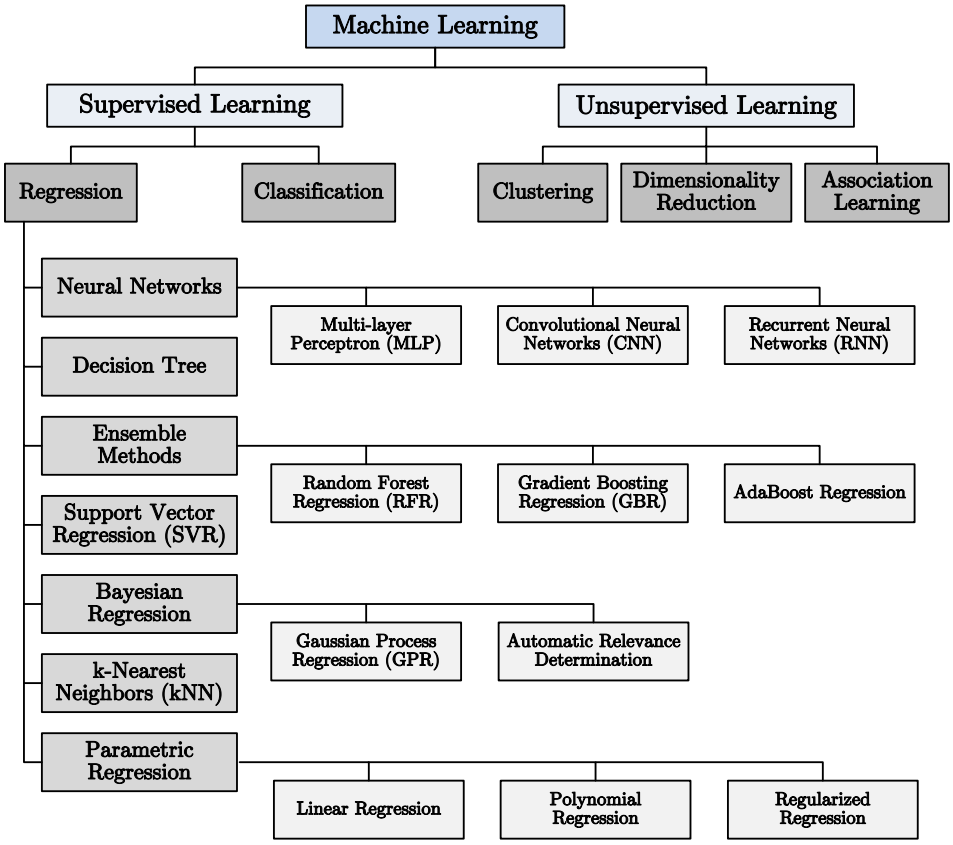

Figure 2.13: Categorization of machine learning tasks and regression models.

during training, and hyperparameters θ_{hp}, fixed during training, parameterizing the architecture and the training of the models. The training is performed by minimizing a loss function $\mathcal{L}$, measuring the error between model prediction and target according to:

$$\theta_p^* = \underset{\theta_p}{\operatorname{argmin}} \sum_{i=1}^{n} \mathcal{L}(y_i, \hat{y}_i) \tag{2.20}$$

θ_p^* denotes the adapted model parameters and $\hat{y}_i$ denotes the model prediction. Loss functions used for regression problems are the R^2 loss, mean absolute error (MAE), mean absolute percentage error (MAPE), mean squared error (MSE) or root-mean-square error (RMSE) [170]. A distinction is made between types of models based on the input data. The models can be preceded by signal processing components, as described in Section 4.1.4, to simplify model building based on already condensed information. However, a selection of a feature subset is

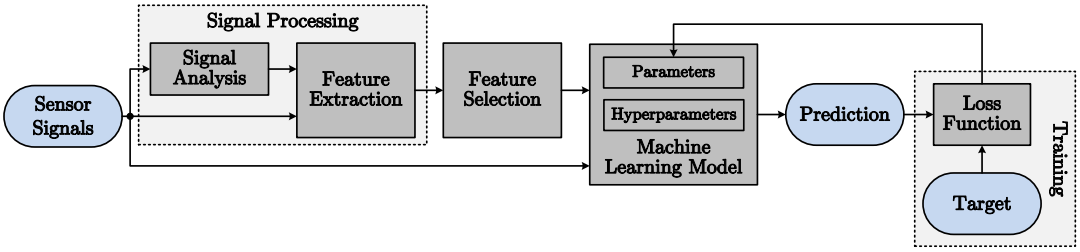

Figure 2.14: Steps of the machine learning pipeline for regression problems based on sensor data.

necessary since the number of extracted features can be arbitrary. The feature selection aims to balance the effect of overfitting, which significantly influences the performance of machine learning models.

Overfitting the model parameters θ_p to the samples of the training dataset limits its generalization capability, i.e., the transferability to samples not included in the training dataset. Not all extracted features contribute equally to the predictive quality of the model. Overfitting is favored if too many features unimportant for approximating the functional target relationship are included in the model input. In addition to the relevance of the features, their increasing number also leads to overfitting, denoted as curse of dimensionality. Each input feature of a machine learning model represents a dimension. The size of the input space grows exponentially with the number of features. As the number of features increases while the number of data points remains the same, searching for meaningful patterns becomes more difficult. Thus, the probability that information can be extracted decreases. Figure 2.15 provides an overview of feature selection methodologies.

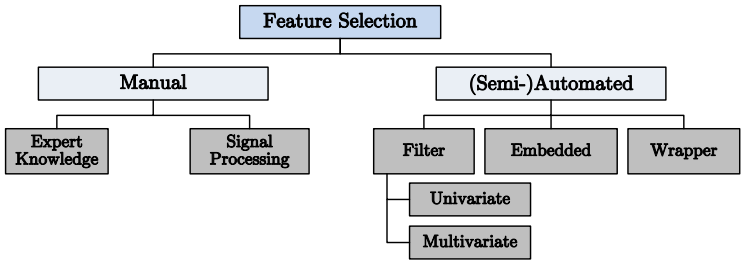

Figure 2.15: Overview of feature selection methodologies [171].

Manual and automated feature selection methods are distinguished. The man-

ual methods are expert-driven and use either a priori known relationships in the process or signal analysis to identify them. Automated methods are solely data-driven and can be further divided into filter, wrapper, and embedded methods. Filter methods use statistical parameters to quantify the relationships between variables. Wrapper and embedded methods directly use machine learning models for feature selection. Wrapper methods search the optimal feature subset based on model performance. Embedded methods perform feature selection as part of the model training. Model types like decision trees or support vector regression shown in Figure 2.13 based on an internal feature ranking are used. Convolutional neural networks (CNNs) represent a special type of machine learning models. Due to the convolution-based structure, both the selection and extraction of features are trained. Thus, raw data can be used as model input.

Forecasting describes a variant of regression for time series data, in which past samples of a target variable are used to predict the future course of the time series [172, 173]. Thus, the target data serves as both model input and output. Standard regression models, shown in Figure 2.13, are frequently used for forecasting. However, there are also models tailored to time series processing, such as recurrent neural networks (RNNs) and long-short term memory (LSTM) networks [174].

2.4.2 Automated Machine Learning

The optimal selection and configuration of the components of machine learning pipelines to achieve the best performance is a complex task due to the large search space. Automated machine learning aims to solve this optimization task in a controlled, data-driven manner [175]. The main areas of automated machine learning are hyperparameter optimization, meta-learning, and neural architecture search.

Hyperparameter optimization targets the complete machine learning pipeline shown in Figure 2.14 and not only the model hyperparameters θ_{hp}. A common problem is the combined pipeline component selection (feature extraction, selection, preprocessing and model) and optimization of model hyperparameters θ_{hp} [176, 177]. Black-box optimization and multi-fidelity approaches are used for hyperparameter optimization. Black-box optimization considers the machine

learning pipeline as an arbitrary function. Hyperparameter search is based on its inputs, outputs, and performance metrics. Therefore, model-free methods such as grid or random search and population-based optimization (genetic, evolutionary or particle-swarm optimization) as well as Bayesian optimization methods are used. Multi-fidelity approaches aim to enable hyperparameter optimization despite the increasing time complexity of model training due to larger models and datasets [178]. They use heuristics to find trade-offs between model performance and the runtime of the hyperparameter search.

Meta-learning describes the learning from past training processes of machine learning models and the optimization of future training processes using the knowledge. It is based on metadata describing the machine learning task, the training process and the model or pipeline configurations.

Unlike other machine learning models, neural networks have hyperparameters that significantly influence their architecture. Therefore, the optimal selection of these hyperparameters is considered separately in the context of the neural architecture search (NAS). NAS is based on the general hyperparameter optimization methods described above. Due to increasing model and dataset sizes in the context of deep learning and thus increasing computational resource complexity of training and inference, hardware-aware NAS is gaining importance. The goal is a multi-objective optimization concerning model performance and computational resource consumption [142].

2.4.3 Application to Machining

Machine learning methods for machining process monitoring are the subject of current research. They offer the possibility to cope with challenges resulting from the constantly increasing requirements of machining production. Increasing quality requirements and resulting demand for process monitoring lead to more connected sensors and process data sources. Machine learning methods enable the extraction of information despite increasing process data volumes, especially from signals of process-integrated sensors, which depict the process quality only indirectly [179, 180]. Furthermore, as shown in Figure 2.13, most machine learning models are non-parametric, which enables their purely data-driven application without physical or expert knowledge. This makes them adaptive, as underlying

models do not need to be manually adjusted when processes change, and offers the potential of automating the process monitoring model development [181]. In the following, the related work is reviewed with a focus on machine learning-based remaining tool life prediction of cutting and particularly milling tools.

As indicated in Section 2.3.4, the remaining tool life prediction methods differ in their objective function. The objective function is to be approximated by the machine learning models and is the foundation for estimating the remaining tool life. The *direct*, *criterion-* and *forecasting-based methods* can be distinguished.

Direct methods approximate the linear remaining tool life function over the cutting time determined based on the tool life criterion and the resulting total tool life, as shown in the lower part of Figure 2.11. Direct methods are easy to apply since a simple regression model is sufficient to perform the prognosis. Moreover, they provide a purely temporal output independent of the tool life criterion, which can be directly used. At the same time, the simple objective function of the method type is its primary drawback. The only target parameter dependent on the tool life criterion is the total tool life. Hence, the machine learning task is the approximation of this parameter from the input data. The indirect reference to the tool life criterion indicates that the generalizability to variable tool life criterion functions, e.g., due to variable process conditions, cannot be guaranteed. Since the total tool life describes only the end point of the tool life criterion, i.e., a single value, intermediate changes cannot be represented. In addition, the explainability of the remaining tool life prediction is not given due to the missing connection with the tool life criterion.

Criterion-based methods approximate the function of the tool life criterion, e.g., the flank wear mark width VB, through a regression model or use criterion-correlated sensor signal-based functions, denoted as health indicators [182]. Subsequently, a simple empirical, non-data-driven model estimates the remaining time until a criterion threshold is reached. For this purpose, linear, physics-based or similarity-based models are used. The advantage of the criterion-based method is the higher degree of explainability compared to the direct method by regressing the tool life criterion. However, due to its empirical nature, the remaining tool life model is bound to fixed process conditions. Adaptation to unknown process conditions or analysis under variable process conditions is impossible.

Forecasting-based methods also use regression of the tool life criterion function

or a related health indicator function. However, based on this, the future course of the function is approximated using a forecasting model. Forecasting-based methods are thus purely data-driven and tool life criterion-based. The disadvantages of the *direct* and *criterion-based methods* in terms of the generalizability and explainability of the remaining tool life prediction can thus be overcome.

Besides the objective function, the methods for remaining tool life prediction described in the state of research differ in terms of the focused production scenarios and the datasets representing them. Production scenarios can be differentiated according to the number of successively manufactured workpieces of the same type into series and single-part production. The production scenario impacts the remaining tool life prediction since it determines the frequency with which the influencing factors of the cutting tools change. In series production, the conditions (especially workpieces and cutting parameters) are mainly constant over the life of a tool. The conditions may differ for different tools, denoted as *inter-tool life variability* in the following. In single-part production, the workpiece geometry and process conditions such as cutting parameters change during the life of a tool, referred to as *intra-tool life variability* in the following. In addition, regardless of the production scenario, the tool load conditions may change while manufacturing a workpiece, e.g., due to complex geometry and multi-axis machining. This is referred to in the following as *intra-workpiece variability* of the conditions. Methods for predicting the remaining tool life are based on publicly available or custom-recorded datasets. Publicly available datasets and their characteristics are summarized in Table 2.1.

Based on the distinction of objective functions and production scenarios of remaining tool life prediction methods described above, Tables 2.2 and 2.3 provide an overview of the current state of research. The tables include the applied machine learning models of the approaches and, in the case of custom datasets, the monitoring variables.

2.5 Research Gap

Based on the review of the related work, the research gap to be filled in this thesis is formulated in the following. This work targets the sensor-driven and machine learning-based prediction of remaining tool life. Therefore, the research gap is

Table 2.1: Literature review of publicly available machining process monitoring datasets that include a tool life criterion and can thus be used for developing machine learning-based remaining tool life prediction methodologies.

Dataset	Production Scenario	Tool Life Criterion	Monitoring Variables
PHM 2010 [183]	Milling series production with **fixed** conditions	Flank wear mark width	Force, Vibration
UC Berkeley [184]	Milling series production with ***inter-tool life*** variation of workpiece material, f_z and a_p	Flank wear mark width	Drive current, Vibration
SMART [185]	Milling series production with ***inter-tool life*** variation of f_z and workpiece clamping force	Binary wear labels	Control signals
Foxconn [186]	Milling series production with ***inter-tool life*** variation of workpiece geometry	Total tool life	Vibration, Drive current, Control signals

Table 2.2: Literature review of machine learning-based remaining tool life prediction methodologies using publicly available datasets.

Ref.	Dataset	Objective Function	Models
[187]	Foxconn	Direct	CNN
[188]	UC Berkeley, PHM 2010	Criterion	CNN-LSTM
[189]	Foxconn	Direct	Ensemble (CNN, LSTM)
[190]	PHM 2010, Foxconn	Criterion, Direct	SVR, GPR, RFR, GBR
[191]	PHM 2010	Forecasting	LSTM
[192]	PHM 2010	Criterion	PCA
[182]	PHM 2010	Criterion	GRU
[193]	PHM 2010	Criterion	CNN-LSTM
[194]	PHM 2010	Criterion	LSTM
[195]	SMART	Criterion	LSTM
[196]	PHM 2010	Forecasting	CNN-LSTM
[186]	Foxconn	Direct	LSTM
[197]	PHM 2010	Direct	MLP
[198]	PHM 2010	Criterion	SVR

derived from the architectural concepts for process monitoring sensor systems described in Section 2.3.2 and the machine learning-based remaining tool life prediction methods described in Section 2.4.3. The state of research in these areas is evaluated against the background of the growing proportion of customized and single-part production in machining with simultaneously increasing workpiece complexity [5].

As explained in Section 2.2.3, increasing workpiece complexity requires flexible manufacturing systems enabling multi-axis machining. Due to changing workpieces and process conditions, single-part production requires a high degree of

Table 2.3: Literature review of machine learning-based remaining tool life prediction methodologies using custom datasets.

Ref.	Production Scenario	Objective Function	Monitoring Variables	Models
[199]	Milling series production with ***inter-tool life*** variation of spindle speed	Criterion	Spindle power	MLP
[200]	Slotting series production with ***inter-tool life*** variation of tool type	Direct	Vibration	LSTM
[201]	Milling series production with ***inter-tool life*** variation of tool path radii and cutting parameters (v_c, f_z, a_p)	Direct	Vibration, Force	MLP, DBN
[202]	Milling series production with ***inter-tool life*** variation of cutting parameters	Direct	Vibration, Drive current, Control signals	CNN-LSTM
[203]	Milling series production with ***inter-tool life*** variation of cutting parameters (v_c, f_z, a_p)	Direct	Vibration, Force, Drive current	CNN
[204]	Milling series production with **fixed** conditions	Direct	Vibration, Force	CNN
[205]	Slotting series production with **fixed** conditions	Direct	Vibration	SVR
[206]	Gear teeth series production with **fixed** conditions	Criterion	Vibration, Drive power	CNN-LSTM
[207, 208]	Milling series production with ***inter-tool life*** variation of cutting parameters (v_c, f_z, a_p)	Direct	Vibration, Force, Drive current	CNN, LSTM
[209]	Milling series production with ***inter-tool life*** variation of cutting parameters (v_c, f_z, a_e)	Criterion	Cutting edge images	CNN-LSTM
[210]	Milling series production with **fixed** conditions	Direct	Force	MLP, SVR
[211]	Milling series production with **fixed** conditions	Forecasting	Vibration	RNNs
[212]	Hole milling series production with ***inter-*** and ***intra-tool life*** variation of cutting parameters (v_c, f_z, a_p)	Criterion	Control signals	LSTM

adaptivity of the manufacturing systems. The previous work on the architectural concepts of component-integrated and gateway-level sensor systems presented in Section 4.1.3 does not yet include these considerations. Although first component-integrated sensor systems for monitoring the production of complex single parts exist [113, 179], there has been no systematic investigation of the impact of the production scenario on sensor-based process monitoring. The requirement analysis of permanent process monitoring in adaptive, flexible machine tools and manufacturing systems is still pending. Due to the resulting high degree of pro-

cess variation, non-invasive and process-independent sensor system concepts are required [5]. From a data processing perspective, the systems must be able to manage the growing number of networked sensors and resulting data volumes and explicitly support the increasing use of machine learning for process monitoring.

The variable production scenarios of single-part production require that not only the manufacturing systems but also the process monitoring models are automatically adapted to the process conditions. Furthermore, for verifying the models, the explainability of their decisions is of particular relevance. Thus, a trade-off between the degree of automation and the explainability of the modeling process is required in machining process monitoring. Despite their adaptivity, this trade-off is a challenge for machine learning methods. As described in Section 2.4.2, automated modeling with machine learning requires not only data-based training, but also the adjustment of model hyperparameters in order to achieve optimal results. Furthermore, machine learning methods are based on black-box models that do not allow direct explainability. So far, only a few automated [190, 213, 214, 181] or explainable modeling approaches [215, 216, 217, 218] exist in the context of machine learning-based machining process monitoring. Combined approaches enabling a trade-off have not been investigated at all. For the remaining tool life prediction, the criterion- and forecasting-based methods presented in Section 2.4.3 enable limited explainability concerning the final model output. However, none of the state-of-the-art approaches listed in Tables 2.2 and 2.3 provide mechanisms for explanation at the sensor signal level. Thus, the relation between sensor signals and tool life criterion is not explainable, making statements regarding the transferability of the approaches, e.g., to other machine tool types, impossible.

The main characteristic of single-part production is the inter-workpiece variability of process conditions introduced in Section 2.4.3. In particular, the change of successive workpiece geometries, resulting tool paths, and cutting parameters influence the cutting time and the load on the tool. In addition, complex workpiece geometries in free-form machining characterized by single-part production lead to intra-workpiece variability of the engagement conditions. The variations in tool load affect the tool life and consequently the remaining tool life prediction. Looking at Tables 2.1 and 2.3, it becomes clear that previous datasets and sensor-based methods of remaining tool life prediction mainly consider fixed process con-

ditions or inter-tool life variation of process conditions in series production. Four series production datasets include intra-workpiece variability [186, 202, 201, 219], and a single one includes changing cutting parameters between subsequently manufactured workpieces [212]. Furthermore, a non-data-driven approach exists that considers a single sequence of varying workpiece geometries [220]. However, the approach requires direct tool wear measurement and linearly interpolates the measurements. Therefore, it is only indirectly related to this work. So far, the sensor-based remaining tool life prediction under variation of geometries of successive workpieces and inter-tool life variation of conditions has not been considered. Hence, there exists no corresponding dataset representing single-part production scenarios.

3. Objectives and Solution Approach

The overall objective of this work is the remaining tool life prediction of machining tools based on sensor-driven process monitoring. The focus is on machining processes characterized by high variability of their influencing factors. They affect the tool load and thus tool life and sensor signals, resulting in multivariate dependencies. The variability of process influencing factors gains importance due to the increasing proportion of small-batch and single-part production and the increasing component complexity. The remaining tool life prediction aims to make the production of components with high quality requirements more reliable and at the same time optimizable. If the remaining time until declining process quality is known, even under changing process conditions, measures can be taken in time to avoid it. In addition, future process parameters can be selected to minimize the overall processing time without the risk of violating quality criteria. Figure 3.1 shows the solution approach followed in this work. The wear-induced surface roughness determines the process quality, making the tool wear the primary tool life criterion. The remaining tool life prediction method developed in this work is demonstrated using the milling of free-form surfaces under single-part production conditions.

From the objective described above, the **main research question** of this work can be derived: Is it possible to predict the tool life under variable process conditions and can the prediction serve as a foundation for optimizing the productivity of the cutting process while ensuring process reliability?

In order to answer the main research question, this work is structured based on **three clusters of sub-research questions**. The areas of the solution approach marked in Figure 3.1 provide the foundation for this:

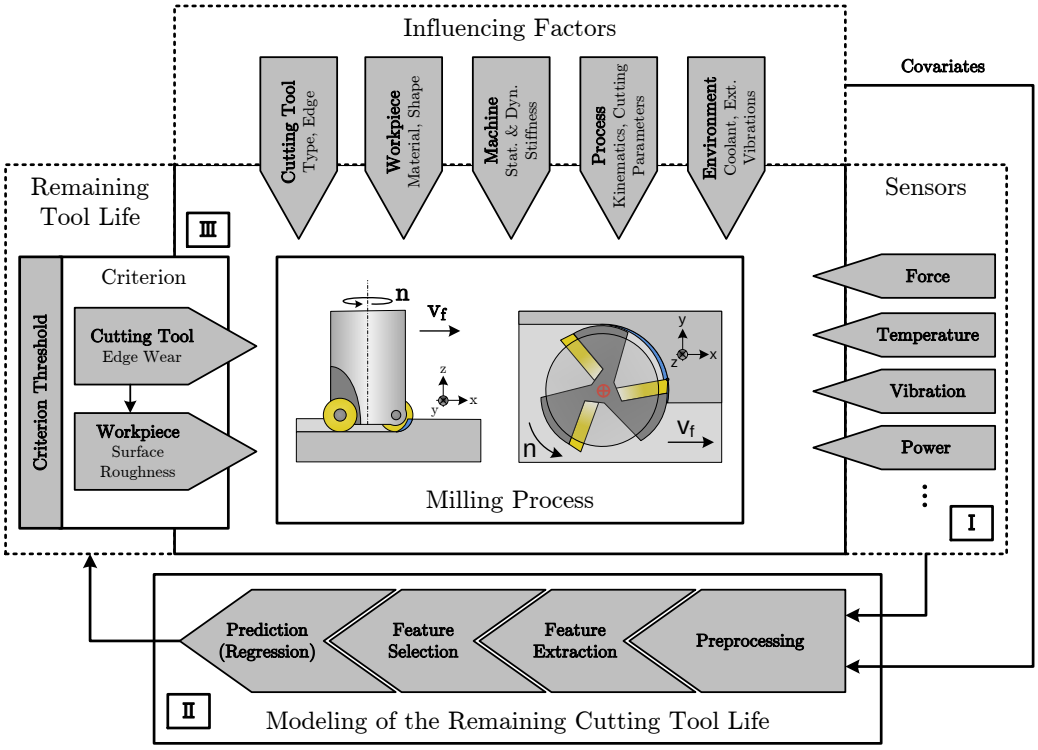

Figure 3.1: Solution approach of this work.

I. Which monitoring variables are suitable for providing machine-independent information for process monitoring concerning surface quality and tool wear. How can the monitoring variables be acquired in a process-independent manner? Process independence refers to components frequently exchanged or adapted in single-part production, such as tools or clamping systems.

II. Which information extractable from the sensor data is necessary for modeling the remaining tool life, and can context information, so-called covariates, e.g., from process planning or simulation, contribute to an improvement? How can the modeling based on the multivariate data be automated while still being explainable?

III. Can the remaining tool life prediction be optimized by incorporating a priori accessible information about future machining operations?

The selection of suitable process monitoring variables and the subsequent development of algorithms for information extraction in the running process is the subject of **Section 4.1**. Suitable process monitoring variables are first determined

and evaluated, which forms the basis for the selection. The focus of the signal processing algorithms lies on extracting high-level process information and wear- as well as roughness-correlated features, which can be used for the subsequent modeling of remaining tool life.

Section 4.2 covers the realization of an overall system based on the previously described methods and algorithms for process monitoring of flexible machine tools. In order to be able to evaluate the methods under variable, realistic conditions, the system is implemented based on a five-axis milling center. Furthermore, the methods for extracting high-level process information are implemented and verified.

Subsequently, the methodology validation for extracting the wear and roughness correlated features is performed in **Section 4.3**. For this purpose, a tool life experiment is conducted based on an exemplary milling process on the five-axis milling center. The evaluation of the experimental results aims to investigate the dependence of the sensor signals and extracted features on the machine to ensure that the method is transferable.

Based on the information and features available according to Chapter 4, the tool life prediction methodology is introduced in **Section 5.1**. For this purpose, an analysis of the tool wear objective function and the multivariate dependencies between process input variables, sensor data and tool wear is performed.

Section 5.2 describes the dataset generation, which is the prerequisite for modeling the remaining tool life. For this purpose, the overall system implemented in Chapter 4 is extended into a testbed, allowing continuous data availability through all steps of the milling process chain. Furthermore, a reference process based on free-form milling is developed, enabling tool life experiments under variable process conditions. A software framework based on the automated machine learning approach, also implemented in Section 5.2, provides the basis for the automated training and evaluation of the machine learning models at the core of the remaining tool life prediction method.

The evaluation of the prediction methodology based on the tool life dataset generated under variable process conditions is presented in **Section 5.3**. The goal of the evaluation is to answer sub-research questions II and III described above and relate to the main research question of this work.

4. Sensor Signals and Information Extraction

Methods for monitoring the cutting process are generally composed of sensor technology and signal processing. They thus aim to extract information about the cutting process and thereby enable the evaluation of its condition as well as the detection of problems and optimization potential. In the following, the requirements resulting from the conditions of single-part production for process monitoring are analyzed, and a corresponding sensor system architecture concept is derived and investigated.

4.1 Process Monitoring Methodology

Single-part production is characterized by the continuous variation of the process conditions, i.e., the workpieces and the cutting parameters. The variation of the process conditions follows a random distribution, which strongly affects the tool life. It is accompanied by flexible manufacturing systems and the frequent adaptation of the process and machine configurations, e.g., the frequent change of tool, tool holder, workpiece clamping, or the entire clamping system. In the following, machining process monitoring is investigated against this background.

4.1.1 Comparison of Process Monitoring Variables

The main foundation for data-based modeling in the context of machining process monitoring is the availability of suitable data sources. The provided data represents the input to the models and is thus crucial for their performance. As described in Section 2.3, process-integrated sensors enable the data acquisition

during machining without the resource-intensive use of manufacturing metrology. Hence, the sensor-based approach is used in this work as the basis for remaining tool life prediction. The first step is to select suitable process monitoring variables as data sources. Initially, the sensor requirements defined by the single-part production of complex free-form surface workpieces have to be analyzed:

- **Process Independence of Sensor Integration**: The application of sensors for machining process monitoring in the context of single-part production is subject to special boundary conditions. The frequent change of products to be manufactured, e.g., of variable size, shape or material, necessitates that process-relevant components, especially the tool, tool holder and workpiece clamping system, have to be adapted. Therefore, sensor integration has to be independent of these directly process-related components to allow the arbitrary process reconfiguration without affecting the data source.
- **Permanence of Sensor Integration**: Predicting the remaining life of cutting tools aims to be a permanent part of tool life cycle management and hence a foundation for overall production optimization. Therefore, modeling the remaining tool life based on sensors as the model's data source requires permanent sensor integration to ensure continuous data availability and consistent data quality. Furthermore, the process reliability must not be compromised by the sensor integration.
- **Generalizability of Information Extraction**: Integrating sensors for monitoring the machining process leads to additional installation and maintenance efforts, especially when retrofitting machines are already in operation. A non-invasive, flexible, and thus scalable integration of its underlying sensors is necessary to ensure the generalizability and transferability of a monitoring approach. Furthermore, machine independence of the information extraction is required. It also prevents adaptations of signal processing due to the frequent adaptation of the machine configuration in single-part production.

Table 4.1 compares the common machining process monitoring variables according to Section 2.3.1 based on the requirements of single-part production derived above.

The comparison in Table 4.1 illustrates that not all sensor types are equally

Table 4.1: Comparison between variables for the monitoring of machining processes under single-part production conditions.
(○: Not satisfied, ◐: Partly satisfied, ●: Satisfied).

Distance to Process ↓

Monitoring Variable	Process Independence	Permanence	Generalizability
Force	○	○	●
Temperature	○	◐	●
Vibration	●	●	●
Active Drive Power	●	●	◐
NC Signals	●	●	◐

suitable for machining process monitoring under the requirements of single-part production. The cutting force is measured according to Section 2.3.1 via stationary or rotating dynamometers. These require integration into the tool holder or the workpiece clamping system and can only be used close to the process. The sensor integration is thus process-dependent. They are directly affected by process reconfigurations which prevents permanent process integration. The temperature is measured either by thermoelectric or radiation-based sensors. Due to the limited thermal conductivity of the machine tool structure, thermoelectric sensors must also be integrated directly into the tool or workpiece close to the process. Radiation-based sensors allow measurement from a greater distance and thus a permanent application. However, they require an unrestricted view of the contact zone, which is not always possible, especially for complex component geometries and in multi-axis machining. With respect to generalizability and machine independence, both cutting force and temperature are good indicators of the tool and process condition.

Vibration sensors meet all the requirements specified in Table 4.1. Due to vibration propagation through the machine structure and components, direct sensor integration into the directly process-related components is not required. Considering the sensors' sufficient sensitivity and frequency range, their integration based onto process-independent machine components such as the spindle housing or the machine table represents a feasible trade-off between process proximity, ease of integration and flexibility.

In addition, Table 4.1 evaluates the drive-related monitoring variables, including the active drive power and the acquisition of digital controller signals, i.e.,

drive torque, load or current signals, and axis position signals. The drive-related variables allow effortless and permanent sensor integration since they can be acquired non-invasively outside the machine tool. However, the specification of the drives and, thus, the related signals are dependent on the design of the tool machine. In addition, the acquisition of controller signals is complicated due to manufacturer-dependent communication interfaces and availability of signals. In conclusion, the generalizability of monitoring using drive-related process variables is limited.

Based on the evaluation of sensor types shown in Table 4.1, vibration sensors are used as the primary data source for further investigation in this work and as the basis for remaining tool life modeling.

4.1.2 Vibration Sources in the Milling Process

In order to use mechanical vibrations as a basis for monitoring and modeling in the context of machining, it is first necessary to characterize the vibrations occurring during the machining process. In general, the causes of vibrations are the deflection of bodies or particles from their equilibrium position. According to Figure 4.1, this distinction is also applied to the vibrations occurring during machining. The mass-dependent vibrations of the machine components (machine vibrations) and the propagation of sound waves within the machine structure (structure-borne sound, ultrasound) are differentiated.

Figure 4.1 shows the typical frequency range of the considered vibration types. Mass-dependent machine vibrations range from particularly low frequencies ($<$ 0.1 Hz) to the single-digit kHz range. The relevant sound wave-based vibrations can be further differentiated into structure-borne sound in the audible frequency range (16 Hz – 20 kHz) and ultrasound ($>$ 20 kHz). In addition, Figure 4.1 illustrates the physical vibration quantities (displacement, velocity, acceleration). The quantities are essential for detecting vibrations using sensors and thus for the sensor selection. The vibration quantities can be transferred into each other by the time derivative or integration and are thus quasi-equivalent. However, the displacement and velocity amplitude decreases as a function of the vibration frequency compared to the acceleration. Accordingly, acceleration is particularly suitable for recording vibrations relevant to machining.

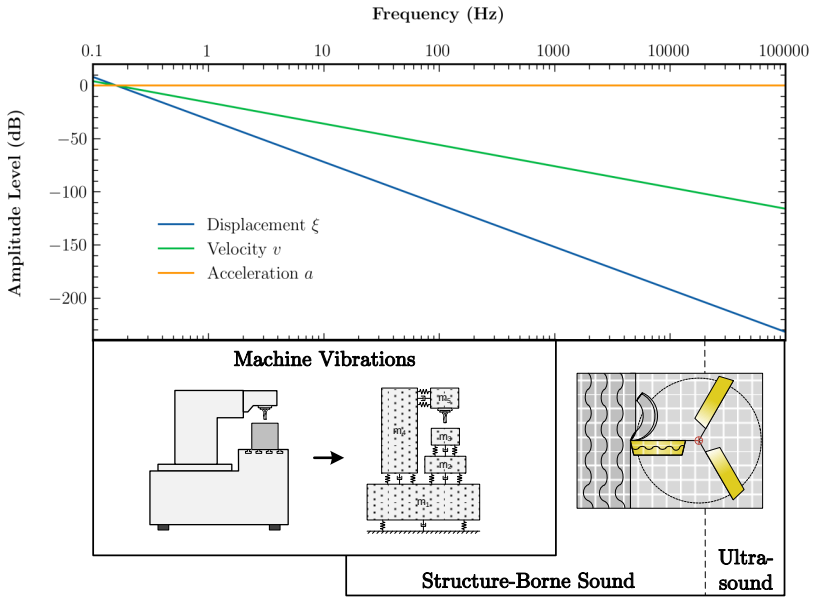

Figure 4.1: Types of mechanical vibrations in the milling process and relationship with physical vibration quantities.

The physical modeling of machine vibrations is based on mass-spring-damper systems. It aims at the dynamic machine behavior under process-induced excitations, i.e., forces generated by the machine drives and the cutting process. An example are chatter models focusing on the dynamic relative displacement between the cutting tool and workpiece during machining [98]. Furthermore, the detection of machine faults is performed based on the measurement and evaluation of machine vibrations. The standard series ISO 10816 [221] is particularly decisive for the fault detection of machine tools. Structure-borne sound in machining is subject to the physical principles of wave generation and propagation in solids, as presented in Section 2.3.1. According to this, the mechanical processes in a system are always associated with losses, e.g., due to friction. The relevant loss energy is mainly divided into thermal and acoustic energy. In machining, the relevant sound sources are the cutting process, i.e., the contact between tool and workpiece, and the mechanical components of the axis and spindle drive trains.

The information about the machine tool dynamics and the machining process contained in the vibrations can serve as a foundation for data-based modeling. However, the complexity of information extraction from resulting sensor signals is high due to the large number of components involved in the machining process and

thus the vibration sources acting simultaneously. To account for this, Figure 4.2 introduces a phase model of the machining process based on logical units of inseparable vibration sources.

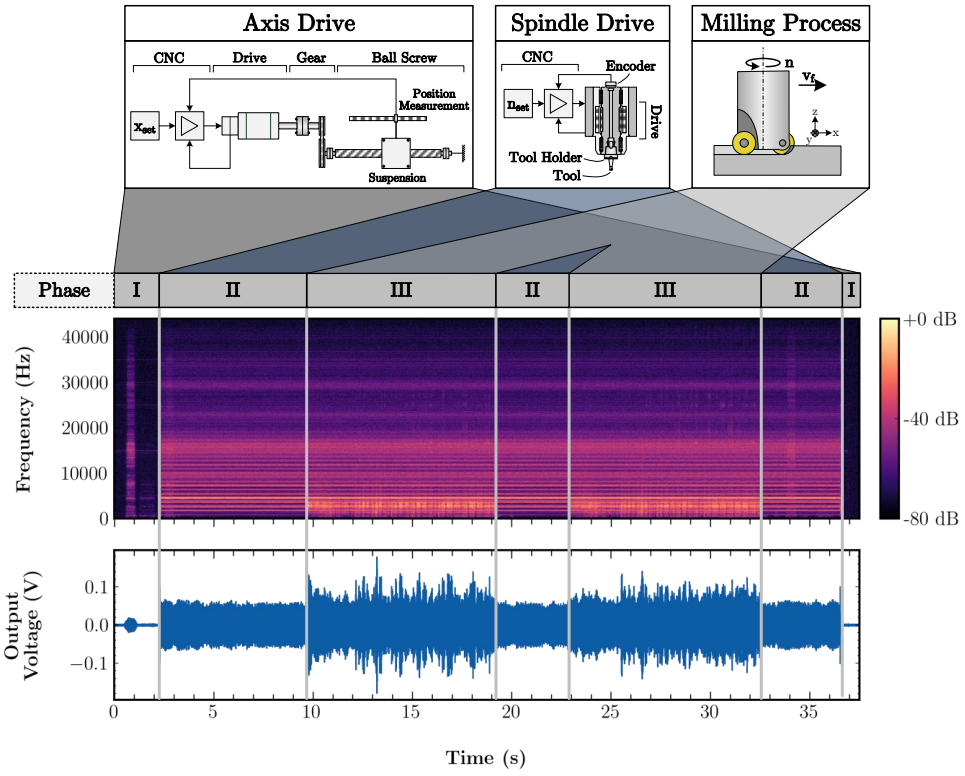

Figure 4.2: Phase model of the milling process in dependence of the vibration-generating machine tool and process components.

The logical units included are the axis drive trains, the spindle drive train and the machining process. Depending on their states, three phases can be derived. The states of the logical units are differentiated into active and inactive. All logical units are inactive during phase I except for the axis drive trains. The movement of the axes does not require the continuous and simultaneous activity of all drives. Therefore, the axis drive trains can also be temporarily inactive. Machining processes typically start and end with phase I. During phase II, the spindle drive is also active. Thus, phase II describes intervals during which there is no contact between the tool and workpiece, but the spindle is still active. Phase III describes the machining process during which all logical components are active. The contact between the tool and the workpiece initiates the machining process.

To link with Figure 4.1, Figure 4.2 includes an exemplary acceleration signal

and the derived amplitude spectrogram during a milling process. Section 4.2 provides detailed information on the used sensor. The described process phases can be distinguished based on the spectrogram. In the case of simultaneous activity of several logical units, i.e., phases II and III, separating the frequency responses is possible. Therefore, the vibration can be a foundation for extracting information about the machining process and the machine tool.

4.1.3 Process Information in Mechanical Vibrations

The previous section has shown that the differentiation of process phases during machining based on mechanical vibrations is possible. However, the focus of this work is on the modeling of the remaining tool life. Therefore, in addition to the semantic process phase detection, the information extraction about the process quality and the states of the primary process components, i.e., tool and workpiece, must be possible. To understand the process information encoded in the sensor signals, Figure 4.3 illustrates the generation of machine vibrations and structure-borne sound due to machining for the milling process.

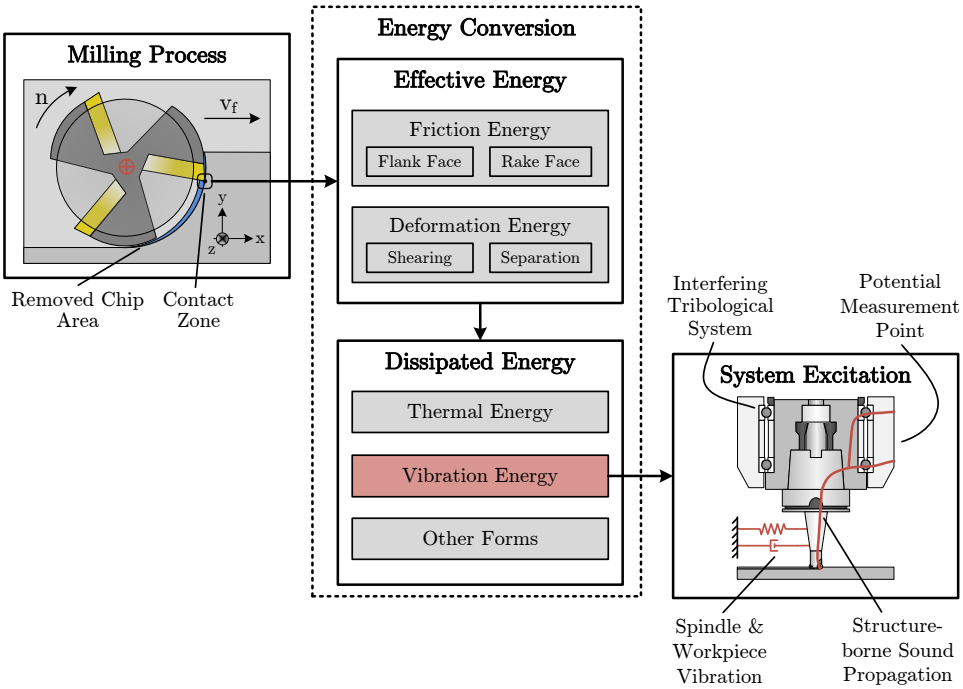

Figure 4.3: Energy dissipation and resulting vibration excitation during milling.

The excitation of the machine tool structure originates from the contact zone.

In the contact zone, the tool's cutting edge engages the workpiece to separate the chip from the material, resulting in a conversion of the effective energy introduced by the feed and rotary motion of the tool and its contact with the workpiece during the cut. The effective energy is divided into frictional energy at the flank and rake faces of the cutting tool and deformation energy during the shearing and separation processes for chip formation. The energy dissipated during chip formation consists mainly of thermal and mechanical vibration energy. The dissipated mechanical vibration energy is introduced into the machine structure and propagates in the form of structure-borne sound as well as spindle and workpiece vibrations. Other effects such as energy absorption or triboluminescence are negligible and irrelevant to this work. Equations 4.1a, 4.1b and 4.1c describe the model shown in Figure 4.3 based on the effective cutting power P_e introduced in Section 2.2.1 as milling is a dynamic, time-dependent process.

$$P_e(t) = P_c(t) + P_f(t) = F_c(t) \cdot v_c + F_f(t) \cdot v_f \tag{4.1a}$$

$$P_e(t) = P_{diss}(t) = P_{th}(t) + P_{vib}(t) + P_{others}(t) \tag{4.1b}$$

$$P_{vib}(t) = P_{vib}^{L}(t) + P_{vib}^{T} \tag{4.1c}$$

P_{diss} is the dissipated power which splits into thermal power P_{th}, vibration power P_{vib} and other forms P_{others}. According to Equation 4.1c, P_{vib} splits into two theoretical components when being measured: The power loss P_{vib}^{L} due to damping of the vibrations as well as the transmitted power P_{vib}^{T} that is potentially detectable by a sensor. The amplitudes of both components depend on the transmission path.

Equation 4.1a shows that the cutting force components F_c and F_f define the effective power P_e. F_c and F_f depend on the instantaneous engagement angle $\varphi(t)$ of the tool cutting edges according to the cutting force model [75] presented in Section 2.2.3. The periodic cutting edge engagement with the tooth engagement frequency Ω_z according to Equation 2.3 thus forms the main part of the frequency response of the cutting process. Due to the finite stiffness of the machine tool, its harmonics are also included in the response. In addition to the process, the excitation of the machine tool structure by the spindle rotation also leads to superimposed vibrations. The frequency response of the machine tool structure is composed of a finite measurable number of natural frequencies f_N

and component-related frequencies f_C, e.g., due to imbalances or bearing errors. Equation 4.2 describes the ideally expected frequency response as the positive amplitude spectrum $|\underline{X}(f)|$ of a stationary milling process:

$$|\underline{X}(f)| = \underbrace{\sum_{h=1}^{L} a_h \cdot \delta(f - h \cdot \Omega_z)}_{\substack{\text{Machining} \\ \text{Process}}} + \underbrace{\sum_{i=1}^{M} b_i \cdot \delta\big(f - f_N^i\big)}_{\substack{\text{Machine} \\ \text{Structure}}} + \underbrace{\sum_{j=1}^{N} c_j \cdot \delta\big(f - f_C^j\big)}_{\substack{\text{Machine} \\ \text{Components}}} \tag{4.2}$$

a_h, b_i and c_j are the amplitudes of the respective frequency responses ideally represented as a series of Dirac delta functions.

Based on the general description of the frequency response during milling, the connection with wear and quality-related variables can be established in the following. Since the primary process components, i.e., cutting tool and workpiece, form a tribological system, wear inevitably occurs during milling. As described in Section 2.3.1, tool wear is a gradual process. The change in the tool's cutting edge geometry due to wear affects the resulting surface of the workpiece. Figure 4.4 illustrates the relationship between tool wear and the workpiece surface in the tribological cutting system.

The surface of the workpiece is characterized by its roughness as described in Section 2.3.1. Three roughness influences are associated with the machining process: kinematic roughness, cutting surface roughness and chatter roughness. The kinematic roughness results from the cutting edge's geometry and the kinematic process parameters (axial depth of cut a_p, feed per tooth f_z). The resulting ideal surface profile P is therefore known a priori. Due to its dependence on the tool's cutting edge, the edge wear mainly influences the kinematic roughness.

The cutting surface roughness refers to the cutting surface facing the workpiece surface, i.e., the flank face. Flank face friction and wear are directly related and the wear profile of the flank face affects the surface of the workpiece. Cutting edge and flank wear occur together and cannot be separated. According to Section 2.3.1, the measurement is performed jointly using the flank wear mark width VB. The tool's rake face has only a minor influence on the surface roughness.

Chatter roughness occurs due to relative movements between the tool and workpiece caused by spindle and workpiece vibrations. These mass-dependent machine vibrations are based on the external excitation, which is mainly caused by

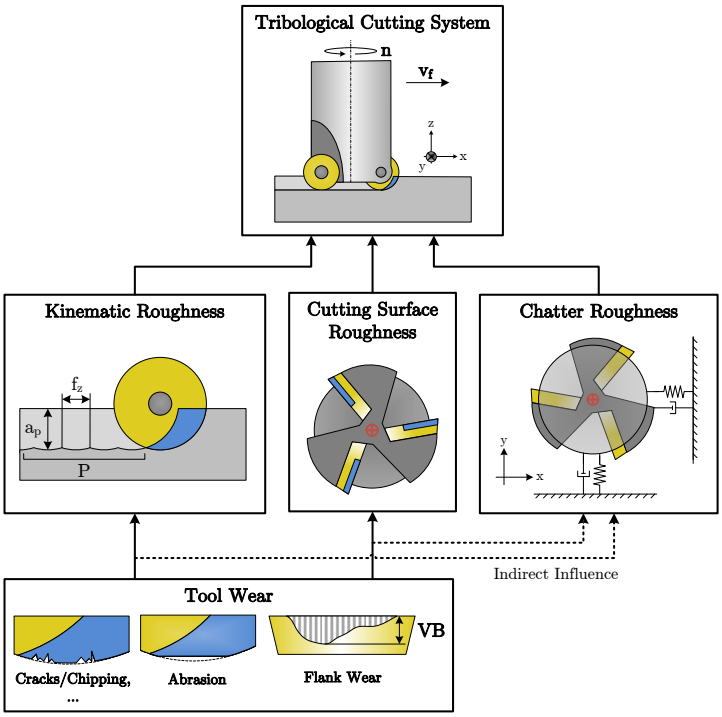

Figure 4.4: Relationship between workpiece surface quality and tool wear in the milling process.

the dynamic cutting forces and the process-induced self-excitation of the machine structure. The chatter roughness is initially independent of wear and can be caused solely by corresponding cutting parameters or workpiece shapes, due to the process instability. However, since wear influences friction effects and cutting forces, chatter roughness is also indirectly influenced.

Overall, the altered cutting edge geometry due to wear thus affects the surface roughness of the workpieces. Furthermore, the cutting forces depend on the cutting edge geometry according to the milling force model in Section 2.2.3. Therefore, Equations 4.1a to 4.1c indicate that tool wear is also represented in the vibration response during machining.

4.1.4 Signal Processing

According to the previous sections, the mechanical vibration generated during the milling process represents a suitable process monitoring variable. The mass-dependent machine vibrations and the structure-borne sound carry process and

tool life information. In addition, the sensor technology for signal acquisition has desirable properties for use in flexible and rapidly changing machining systems, e.g., required for free-form surface milling and single-part production. However, in order to make the information contained in the sensor signals usable, signal processing is essential. The conditions of single-part production pose challenges for signal processing. Due to the variability of workpieces and cutting parameters, the processing time of individual workpieces also varies. In order to record the duration a tool has been under load so far, the cutting time t_c must therefore be tracked. At the same time, this also provides the basis for the unambiguous and process-independent quantification of the remaining tool life. Furthermore, data reduction must occur to limit the volume of data that accumulates during permanent process monitoring. Data reduction enables data to be stored under constrained memory resources and information to be transferred via network with reduced bandwidth requirements. Figure 4.5 shows this work's overall approach to sensor signal processing.

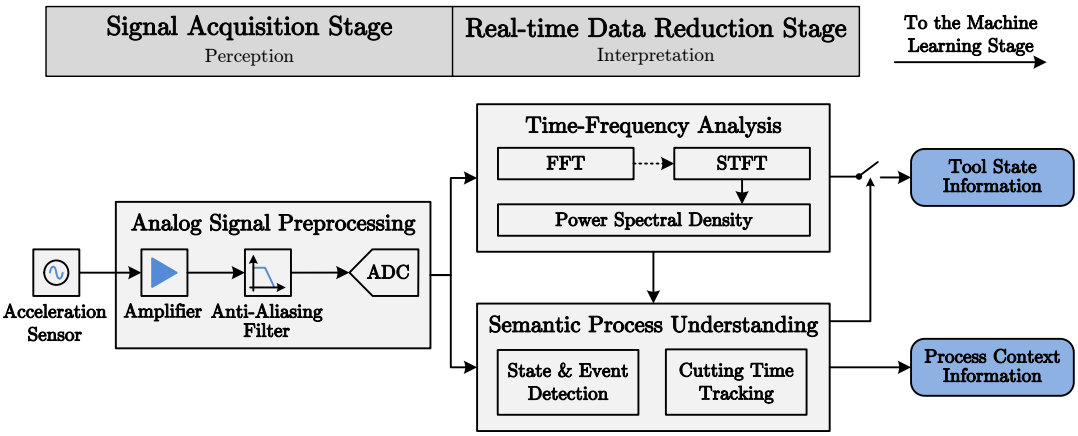

Figure 4.5: Signal processing methodology for the analysis and extraction of tool state and process context information.

According to Figure 4.5, sensor signal processing comprises two stages derived from the specification of the autonomous system components (perception and interpretation) presented in Section 2.1.1. In the signal acquisition stage, the vibration acceleration acting on the sensor integrated into the milling process is first converted into an electrical signal. A signal acquisition circuit performs the analog preprocessing and digitization of the acceleration sensor signal, i.e., the sampling with a sampling frequency f_s. Typically, signal acquisition circuits

for acceleration signals consist of analog amplifiers, filters, and an analog-to-digital converter (ADC). The ADC samples the continuous accelerometer signal $a(t)$ equidistantly after every time period $T = \frac{1}{f_s}$ to obtain the digital signal $\hat{a}(n) = a(nT)$.

After the signal acquisition stage, the digital signals are processed in real-time for information retrieval and data reduction. Free-form surface milling is a highly dynamic process, and the machine tool system comprises multiple vibration sources covering a wide frequency bandwidth. Hence, the resulting acceleration sensor signals are non-stationary, necessitating their analysis in the time and frequency domains. Time-frequency analysis enables the resolution and visualization of frequency responses related to the respective vibration sources. Thus, it is the foundation for extracting milling process-related spectral components, considering the rapidly changing conditions of the free-form surface milling process over time. The core of the time-frequency analysis is the FFT-based STFT of the discrete acceleration signal $\hat{a}(n)$. In addition to the non-stationarity of the signals when milling free-form surfaces, workpiece variations caused by single-part production lead to variable tool loads, randomly influencing the frequency response and causing different signal lengths. Comparing the random acceleration signals, which is essential for extracting information regarding the tool state and development of tool life criteria over time, ultimately requires estimating the PSD, as described in Section 4.1.4.

Only sensor signal segments are relevant for the tool life in which milling operations occur. Based on the semantic process understanding, the decision about which signal segments to pass on to the next stage of machine learning is made. The automated generation of the semantic process understanding relies on basic prior knowledge about the vibration sources of the machine tool system, according to Section 4.1.2. Its core is a signal-based model to describe the states and events during the operation of the machine tool. Based on the model, the different phases of the milling process can be identified and differentiated. Hence, the tool state and process context information can be prefiltered to pass on only the relevant data. The process understanding also includes the tracking of the cutting time t_c. For simplification, the cutting time per workpiece k is denoted by Δt_c^k in the following. If this value is available for all preceding workpieces up

to a workpiece N, the instantaneous cutting time T_c results to:

$$T_c = \sum_{k=1}^{N} \Delta t_c^k \tag{4.3}$$

Equation 4.3 can also be applied independently of the notion of workpieces using k to denote arbitrary contiguous machining operations.

4.2 Sensor System for Monitoring Flexible Machining Systems

The following sections describe the implementation of a vibration sensor system conforming to the requirements discussed in Section 4.1.1. The sensor system aims to be integrable and retrofittable into arbitrary CNC machines ensuring process-independent sensor integration while still applicable as close to the process as possible. Based on these prerequisites, it should enable the milling process analysis based on the approach introduced in Section 4.1.4, as well as the prediction of the remaining milling tool life.

4.2.1 Acceleration Sensor Selection

The first step in designing a vibration sensor system is selecting the sensor to be used. The two main types of acceleration sensors are piezoelectric and capacitive sensors. Piezoelectric acceleration sensors can cover high bandwidths up to the two-digit-MHz range. On the other hand, their suitability for embedded applications is restricted due to their size and power consumption [222]. Free-form milling, performed using three- or five-axis CNC milling centers with multiple moving components, requires the compact or even wireless design of a vibration sensor system for process monitoring. Therefore, capacitive acceleration sensors are more suitable, as they can be implemented as micro-electro-mechanical system (MEMS). MEMS acceleration sensors offer a trade-off between compact size, ease of installation, cost, energy efficiency and key specification parameters compared to piezoelectric acceleration sensors.

Table 4.2 compares multiple state-of-the-art MEMS acceleration sensors available in the market as a foundation for the selection. The comparison is based on

the frequency characteristic of the sensors defined by the 3 dB bandwidth, the resonance frequency, the noise density, and the sensitivity. Furthermore, despite the required process independence of the sensor integration, the installation in minimal process proximity is a central goal. Therefore, sensor integration inside the CNC machine may be required, exposing it to harsh ambient conditions. This results in further requirements regarding the permissible temperature and acceleration range.

Table 4.2: Comparison of state-of-the-art MEMS acceleration sensors concerning key specification parameters (parameters not provided in the documentation are indicated with -).

Specification Parameters	**MEMS Acceleration Sensors**				
	Spindle Monitoring		**Industrial Condition Monitoring**		
	Marposs VA-3D MEMS [223]	Montronix PulseNG MEMS [224]	TE Connectivity 830M1 [225]	Analog Devices ADXL1002 [226]	Analog Devices ADXL1005 [227]
3 dB Bandwidth (kHz)	2.2/2.8	1.6	15	11	23
Resonance Frequency (kHz)	5.5	-	30	21	41
Noise Density $\left(\frac{\mu g}{\sqrt{Hz}}\right)$	20	-	50/90	25	75
Sensitivity $\left(\frac{mV}{g}\right)$	100	-	20/12.5	40	20
Temperature Range ($^{\circ}C$)	0 - 60	0 - 70	-40 - 125	-40 - 125	-40 - 125
Acceleration Range (g)	± 8	± 6	$\pm 50/\pm 100$	± 50	± 100
Channels	3	3	3	1	1

The preselection shown in Table 4.2 includes acceleration sensors already applied in the context of CNC machine spindle monitoring and generally designed for industrial condition monitoring. The MEMS acceleration sensors designed for the spindle monitoring have 3 dB bandwidths below 3 kHz. A reason for this is their primary purpose, the component and machine vibration acquisition that indicate spindle problems such as bearing wear or imbalance. The other sensors generally designed for industrial condition monitoring also cover the frequency range of structure-borne sound above 3 kHz. According to Section 4.1.2, the machining process is a major structure-borne sound source. With respect to the noise density and sensitivity, the two sensors VA-3D MEMS for the spindle monitoring category and the ADXL1002 by Analog Devices for the industrial

condition monitoring category are particularly noteworthy. Both sensors have the minimum noise density at maximum sensitivity in their respective category.

Overall, the ADXL1002 MEMS acceleration sensor is selected to implement the sensor system in this work. Although the sensitivity of the VA-3D MEMS is 2.5× higher, the ADXL1002 offers a better trade-off between the three key parameters bandwidth, noise density, and sensitivity. The high 3 dB bandwidth covering the whole frequency range from component vibrations to structure-borne sound and comparably low noise density at high sensitivity for sensing low-energy vibrations offer a solid foundation for the milling process analysis. The specification parameters of the ADXL1002 are comparable to common piezoelectric acceleration sensors. Additionally, the maximum permissible temperature and acceleration ranges of the ADXL1002 acceleration sensor minimize the risk of sensor malfunctions due to the harsh ambient conditions in the CNC machine.

Besides the positive aspects, one disadvantage of the ADXL1002 is that it is a single-channel sensor. This point will be addressed in Section 4.2.3, introducing the mechanical sensor integration concept for the sensor system.

4.2.2 Sensor System Setup

After selecting an appropriate MEMS acceleration sensor, the next step is designing the overall sensor system. Other required components of the sensor system include the signal acquisition circuit for digitizing the analog sensor signal and the signal processing hardware. For the ADXL1002 MEMS sensor, the rapid prototyping platform CN-0549 is provided by Analog Devices [228]. The platform will be used in this work to enable fast and robust integration into a CNC machine, providing the foundation for the milling process analysis and remaining tool life prediction. The two main components of the CN-0549 platforms are an Integrated Electronics Piezo-Electric (IEPE)-compatible circuit (CN-0532 [229]) embedding the ADXL1002 acceleration sensor and the corresponding signal chain (CN-0540 [230]) for the conditioning and digitization of signals from IEPE sensors. Using the IEPE standard enables robust signal transmission from the sensor to the signal chain under the harsh ambient conditions inside the CNC machine, eliminating the influence of cable length on the signal quality. Further details on the CN-0532 and CN-0540 systems are summarized in Appendix A.

The ADC of the CN-0540 signal acquisition system can sample the acceleration signal with a maximum sampling rate of 256 $\frac{kS}{s}$ and includes a serial peripheral interface (SPI) for transmitting the digitized data. The third component of the CN-0549 platform and counterpart to the SPI interface of the ADC is the Cora Z7-07S FPGA-system-on-chip (SoC) [231]. The FPGA-SoC including a CPU and an FPGA fabric on a single die allows the distribution of tasks among these two main submodules. The CN-0549 platform offloads the SPI communication to the FPGA module of the SoC, hence enabling the CPU to perform other tasks, such as the transmission of the data over Ethernet. Figure 4.6 shows an overview of the sensor system architecture developed in this work.

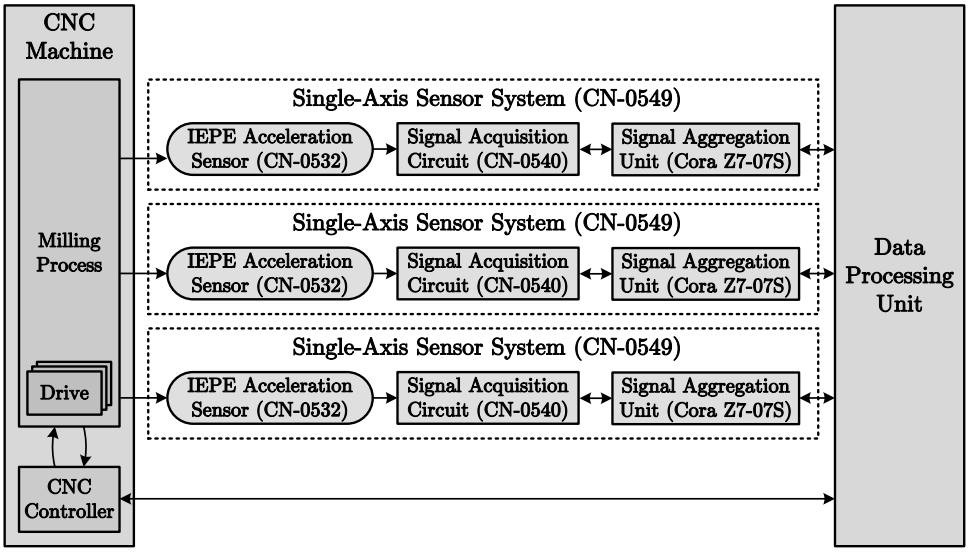

Figure 4.6: Architecture of the acceleration sensor system as a foundation for the milling process analysis and remaining tool life prediction.

The system architecture includes three single-axis CN-0549 subsystems covering the spatial axes. Capturing acceleration on the three spatial axes facilitates the process state and event detection introduced in Section 4.1.4. All translational movements can thus be detected. Furthermore, three-dimensional free-form machining processes using multi-axis milling machines can be arbitrarily supported. The processing of the sensor signals has to be performed centrally to enable a holistic overview of the milling process. Therefore, the CN-0549 subsystems are connected to a central data processing unit. The CN-0549 subsystems with a sampling rate of 256 $\frac{kS}{s}$ and a 24-bit ADC resolution generate a data stream of

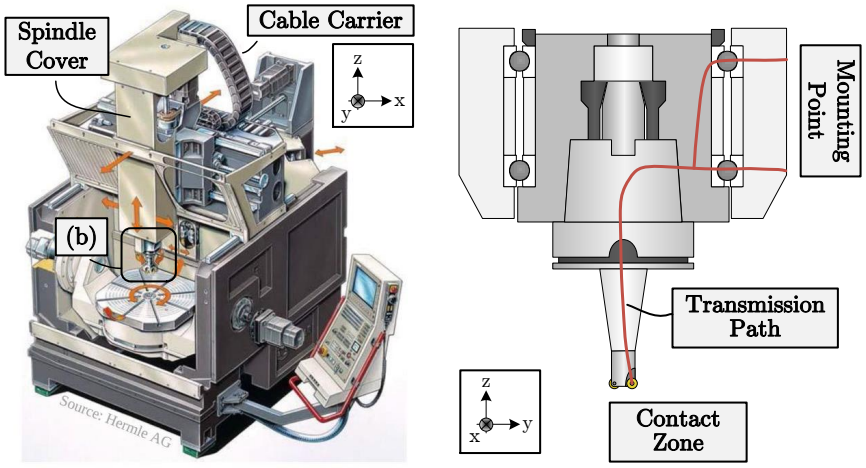

(a) Hermle C 30 U **(b)** Sensor mounting location

Figure 4.7: Overview of the Hermle C 30 U 5-axis CNC milling center [234] and the mounting location of the three-axis acceleration sensors.

2.3 $\frac{MB}{s}$. An Intel NUC8i5BEK SBC [232] is used as a data processing unit with an Intel Core i5-8259U processor and 32 GB of random-access memory (RAM). However, the data processing unit is exchangeable since the CN-0549 subsystems are connected to it via Ethernet. The overall sensor system setup is modular.

For evaluation purposes, the data processing unit is additionally connected to the CNC controller of the machine tool, which is a Heidenhain iTNC530 [233]. By using a Raspberry 4B+ as a gateway, controller signals and data can be acquired. Details on the accessible data can be found in Section 4.2.4.

4.2.3 CNC Machine Integration

In order to enable the use of the sensor system setup introduced in the previous section for the intended free-form milling process analysis, it is required to integrate the system into a CNC machine. The selection of a state-of-the-art CNC machine used in the field of free-form machining contributes to ensuring the validity and significance of the evaluations performed in this work. Therefore, the Hermle C 30 U 5-axis CNC milling center [234] shown in Figure 4.7a is chosen. The Hermle C 30 U CNC milling center is well established in industrial and scientific practice [235, 236].

Figure 4.7b shows the installation location of the CN-0532 IEPE circuits car-

rying the MEMS acceleration sensors. The sensors are placed on the spindle housing to acquire data in minimum process proximity while being independent of the directly process-related components. Apart from the permanent mounting and adaptability to arbitrary processes, this approach prevents that the sensor integration influences the process, e.g., by introducing an imbalance of the spindle. According to Section 4.2.2, the sensors cover all three spatial axes. To ensure the correct orientation of the CN-0532 subsystems and thus the single-axis ADXL1002 sensors, a mounting cube optimized for the vibration transmission from industrial equipment provided by Analog Devices is used [237]. The mechanical coupling between the spindle housing and the mounting block is established via a screw connection based on threads provided in the spindle housing by default. The vibration transmission capability of the developed mounting solution is evaluated in Section 4.3.1. A sensor enclosure is installed to protect the sensors inside the CNC machine against cooling lubricant as well as flying chips and ensure their permanent operation.

The CN-0532 IEPE circuits are connected via coaxial cables to the CN-0540 signal acquisition systems and Cora Z7-07S boards placed underneath the spindle cover. Power-over-ethernet (PoE)-capable cables are routed to the Cora Z7-07S boards through the cable carrier of the machine to provide the sensor systems with power and enable communication with the data processing unit. The data processing unit is located outside the CNC machine. It represents the programming and interaction interface of the sensor system. The system integration approach requires only the explicit protection of the acceleration sensors and allows the use of COTS systems. The mechanical integration of the subcomponents into the Hermle C 30 U CNC milling center is detailed in Appendix C.

4.2.4 System Software

The acceleration sensor system introduced in the previous sections provides the foundation for the software-defined machining process monitoring and analysis. The following sections introduce the required algorithms and software modules implemented using the data processing unit of the sensor system. The developed software modules are consolidated into a library that can be used on embedded and edge computing systems like the data processing unit and on general-purpose computers or servers. Throughout this work, Python 3.8 is used. A summary

and specification of all involved computing systems can be found in Appendix B.

Data Acquisition

The initial step required for the software-based sensor signal analysis is the centralized acquisition of the data from the three acceleration sensors by the data processing unit. The implementation of the sensor data acquisition in this work is based on LibIIO, a software library developed by Analog Devices for standardized communication with industrial I/O (IIO) devices [238]. IIO devices are digital-to-analog converter (DAC)- or ADC-based systems such as the CN-0540 signal acquisition circuit used in the sensor system architecture of this work. The data acquisition on the data processing unit is developed using the PyADI-IIO library [239], mapping the high-level application programming interface (API) of the C-based LibIIO library to Python. Appendix B provides a detailed overview of the interaction between the hardware and software components of the acceleration sensor system based on the LibIIO library. Figure 4.8 shows the structure of the computational processes the data processing unit executes to perform the parallel data acquisition from the CN-0549 subsystems.

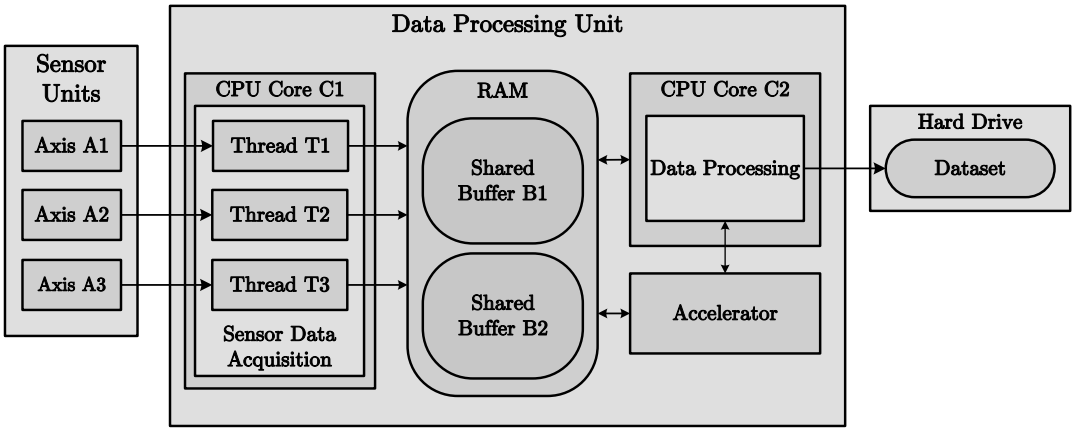

Figure 4.8: Computational process model for the parallel and real-time data acquisition from the three-axis CN-0549 sensor systems.

PyADI-IIO represents IIO devices like the CN-0540 as Python objects. The member functions and variables of the underlying class are based on the Python bindings of LibIIO and enable communication with the IIO device. The sensor data is continuously provided by the CN-0540 systems in memory buffers of adjustable size. However, the software must initially trigger the buffer transfer from

the Cora Z7-07S to the data processing unit and continuously read out the data. As the buffer transfer is a blocking process by default, multiple asynchronous threads are required on the data processing unit to enable parallel data acquisition from all three sensors. The buffer sampling is performed by a sensor data acquisition process executed by a CPU core $C1$, as shown in Figure 4.8. As core $C1$ has to continue immediately with the data sampling from the next sensor, it stores the already received data buffer in a shared memory area of the RAM. Using inter-process communication, a second CPU core $C2$ is notified by core $C1$ when a shared buffer has been written. The process executed by core $C2$ directly processes the raw data or stores it on a hard drive.

The alternating use of multiple shared buffers ($B1$ and $B2$ in Figure 4.8) prevents data from being overwritten. This is essential for the real-time processing of the incoming sensor data as sampling the next data buffer starts immediately after the previous data has been stored in RAM. There are two fundamental cases depending on the worst-case execution times (WCETs) T_1 and T_2 of the two processes running on cores $C1$ and $C2$, respectively. Real-time data processing based on the setup shown in Figure 4.8 with two CPU cores is possible if the processing of the previously sampled buffer completes before the end of the sampling of the next buffer, i.e., $T_1 \geqslant T_2$.

The second case becomes relevant when the data processing of a particular buffer takes longer than the sampling of the next buffer, i.e., $T_1 < T_2$. In order to perform the real-time processing in this case, the number of cores performing the data processing and hence also the number of shared buffers has to be increased. As for the first case, the real-time constraint requires that a shared buffer Bi must not be overwritten until its processing has been completed. The number of required cores and buffers n can be determined according Equation 4.4b which was derived from Equation 4.4a:

$$\frac{n \cdot T_1}{T_1 + T_2} \leqslant 1 \tag{4.4a}$$

$$n \geqslant 1 + \left\lceil \frac{T_2}{T_1} \right\rceil \tag{4.4b}$$

Since Python is an interpreter-based programming language, the estimation of the WCET of Python programs is difficult. Additionally, the underlying operating system (OS) influences the program execution time as well. To trade off the

required effort and dependability of the WCET estimation, a measurement-based approach is combined with an additional safety margin in this work. Furthermore, due to the modularity of the sensor system architecture, data processing units with additional accelerators for signal processing, such as FPGAs or GPUs, can be used. These enable the offloading of data processing and reduce the processing time.

In addition to the acceleration data, the iTNC530 machine tool controller data is acquired using the pyLSV2 software library. The data processing unit can read the spindle speed, axis drive positions, and relative axis drive power divided by the maximum power in percent with a sampling frequency of 110 Hz.

Data Processing

After the sensor data acquisition, the next step is data processing. For this purpose, the signal processing concept introduced in Section 4.1.4 is implemented in the following, which aims to extract tool condition and process context information for the subsequent remaining tool life prediction. The gradual progression of tool wear, which is a decisive tool state indicator, is a long-running process over an operating time of up to several hours. Therefore, the data processing should extract the long-term dependency between sensor data and tool wear as a basis for subsequent modeling and limit the amount of generated data. Data reduction allows local data caching or transferring to external systems for further processing considering limited storage capacity and transmission bandwidth. Since this work focuses on sequences of arbitrary milling processes (single-part production) with possibly different effects on tool wear, their identification is necessary. Only the contact phases between the milling tool and the workpiece affect the tool wear.

The behavioral Petri net model of the milling process shown in Figure 4.9 serves as the basis for the automated identification of these process phases and the mapping to interrelated, higher-level milling operations. The fundamentals of Petri nets underlying the model can be found in the literature [240].

Figure 4.9 represents the behavior of the machine tool and the milling process iusing the Petri nets N_{AD} (axes drives), N_{SD} (spindle drive) and N_{MP} (milling process), assigned to the vibration-generating components described in Section 4.1.2. The Petri nets model the inherently parallel operation of the com-

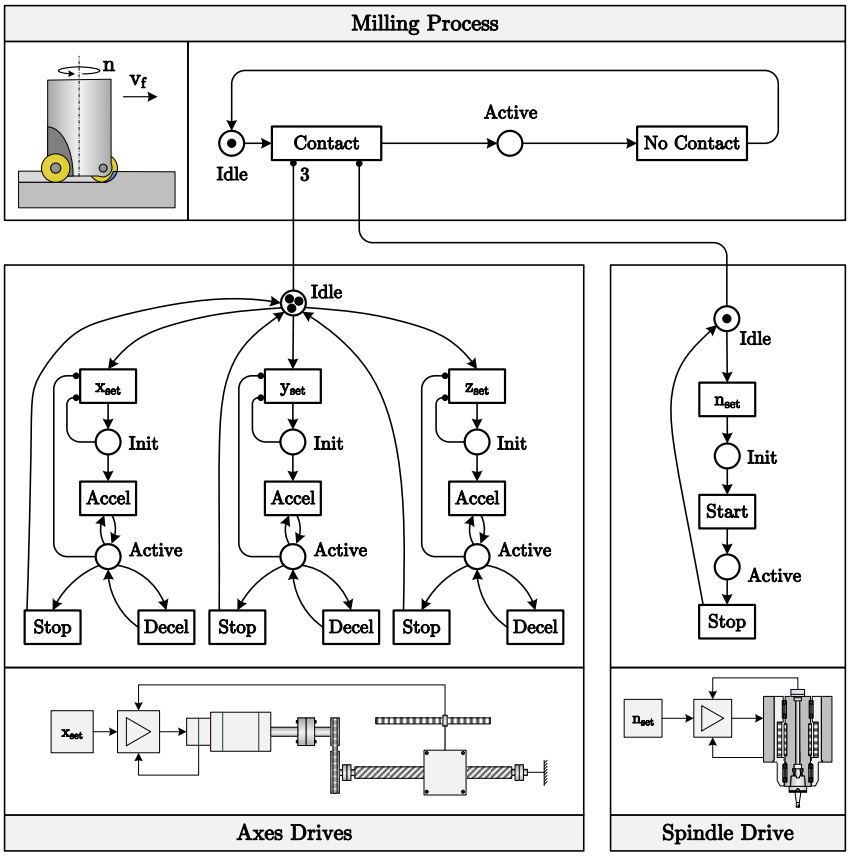

Figure 4.9: Behavioral Petri net model of the milling process based on the machine tool components operating in parallel.

ponents. Each component-level Petri net $N_C \in [N_{AD}, N_{SD}, N_{MP}]$ is defined as a 5-tuple $N_C = \left(P_C, T_C, F_C, W_C^F, M_C^0\right)$ with P_C being a finite set of component states (places), T_C being a finite set of component events (transitions), $F_C \subseteq (P_C \times T_C) \cup (T_C \times P_C)$ being a set of arcs connecting the states and events, $W_C^F : F_C \to \mathbb{N}$ being a weight function indicating the number of tokens required to activate the events T_C and M_C^0 being the initial marking of the states P_C.

The Petri net N_{AD} representing the behavior of the axes drives is furthermore embedded into a triple $N_{AD}^I = (N_{AD}, I_{AD}, W_{AD}^I)$ with $I_{AD} \subseteq (P_{AD} \times T_{AD})$ being a set of inhibitor arcs and $W_{AD}^I : F_{AD} \to \mathbb{N}$ being a weight function. An event t connected to a state p by an inhibitor arc i is inactive as long as p holds at least $w_i(t, p)$ tokens. The inhibitor arcs enable the deterministic modeling of the axes drives operating in parallel. For simplification, only the translational axes drives covering the spatial axes are represented in the model. Other axes drives, e.g.,

for tilting or rotating the machine table, can be added accordingly.

The overall model forms a triple $N^I = (N, I, W_I)$ with $N = (N_{AD}, N_{SD}, N_{MP})$ being the set of component-level Petri nets, $I \subseteq (P \times T)$ being a set of inhibitor arcs connecting states and events across the component-level Petri nets and $W_I : F \to \mathbb{N}$ being the corresponding weight function. The inhibitor arcs $I \subseteq (P \times T)$ connect the *Idle* states of the axes and spindle drives to the *Contact* event of the milling process. The inhibitor arcs model that the milling process can only be active when there is both a feed generated by the translational axes drives and a rotational movement of the tool generated by the spindle.

In order to use the model shown in Figure 4.9 for process monitoring, an algorithm is required to detect the depicted states and events. Therefore, Figure 4.10 shows the procedure for processing the acceleration sensor streams in real-time. As already described in Section 4.1.4, the time-frequency analysis using the STFT forms the basis of the signal processing algorithm.

Only the segments of the data streams during which the tool and workpiece are in contact are relevant for wear and hence remaining tool life modeling. Segmentation of the data streams is thus necessary to input relevant information to the machine learning models. The basis for the segmentation is the event and state detection, enabling the automated generation of a semantic process understanding based on the sensor signals. The semantic process understanding describes the assignment of patterns detectable in the sensor signals to operations of the vibration-generating components involved in the milling process. It is thus possible to differentiate states and events of the axis drives, the spindle drive, and the milling process itself. Furthermore, coherent signal segments can be identified even for interrupted cutting processes. State and event detection is performed separately for translational and rotational movements of the tool machine. Figure 4.11 shows both procedures applied to a sensor signal in detail.

The spindle drive generates rotational movements. The spindle rotation is the basis of the periodic engagement of the tool's cutting edges and, thus, the milling process. As shown in the spectrogram of the example process in Figure 4.10, the spindle rotation and milling process affect a broad frequency range up to approximately 6 kHz. The state change of the milling process results in significant signal power variations. Therefore, the signal power in the relevant frequency band is used as the state and event signal for the spindle drive and milling process.

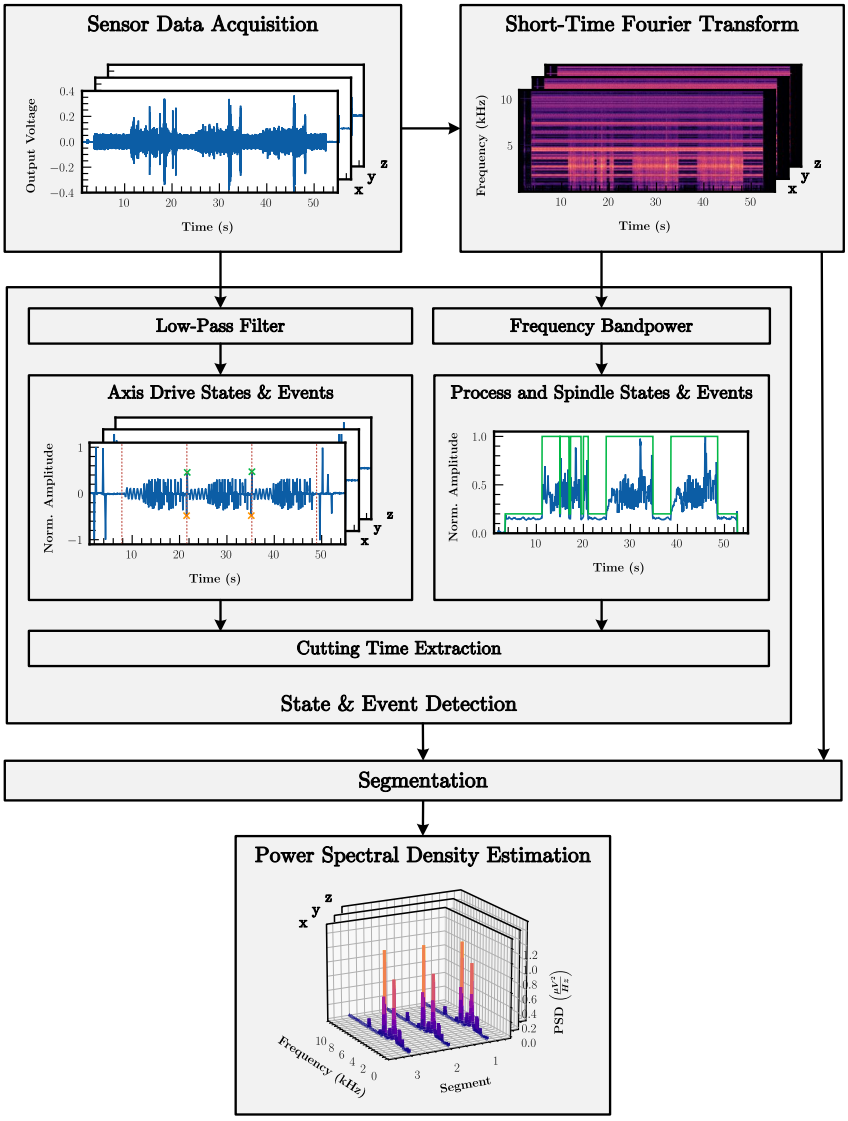

Figure 4.10: Procedure for the acceleration sensor signal-based analysis of the milling process to extract tool state and process context information.

The frequency band power is estimated based on numerical integration of the STFT spectrogram scaled to PSD. As shown in Figure 4.11a, the signal band power is approximately step-shaped, allowing the state differentiation by applying edge detection (green curve). The state of the milling process can then be used to determine the cutting time Δt_c^k of contiguous milling operations. According to Equation 4.3, Δt_c^k is the basis to determine the instantaneous cutting time $T_c(k)$.

The axis drives generate translational movements along the spatial axes. As highlighted above, the algorithm does not consider the movements of additional

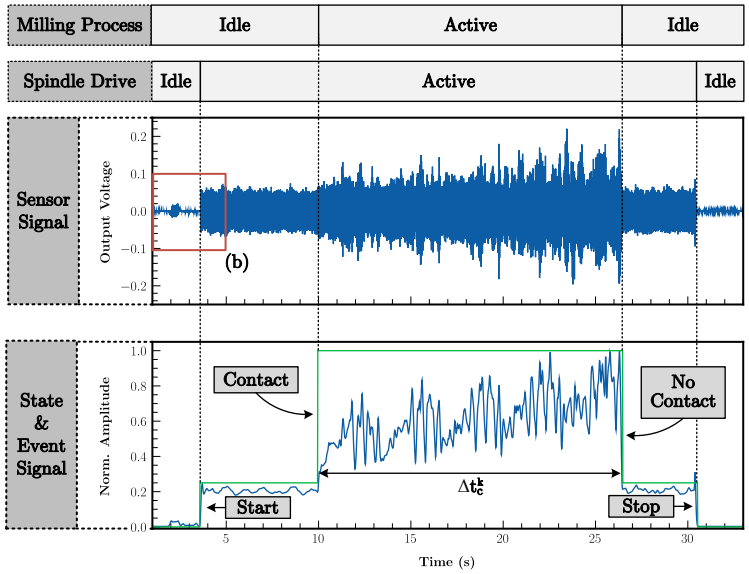

(a) Spindle drive and milling process

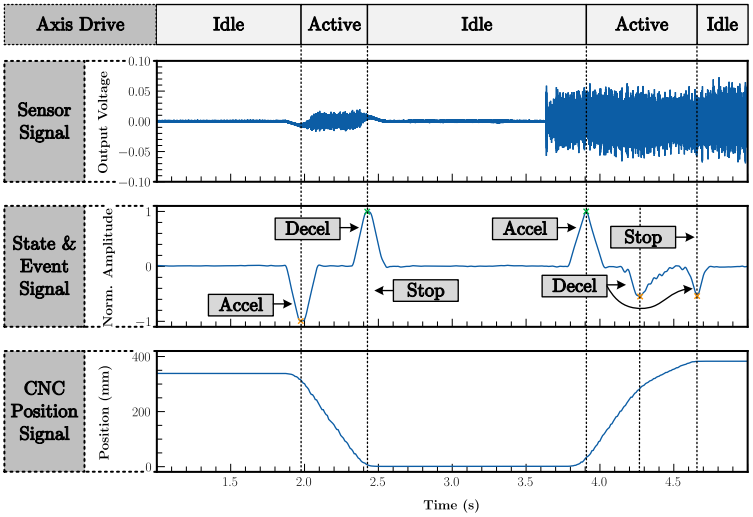

(b) Axes drives

Figure 4.11: State and event detection for rotational (spindle and milling process) and translational (axes drives) movements of the machine tool components.

axis drives, e.g., for tilting or rotating the machine table. When acquired at the moving spindle, the sensor signals inevitably include its acceleration. Low-pass filtering of the broadband acceleration sensor signals enables the extraction of the low-frequency acceleration events as shown in Figure 4.11b. Based on the filtered acceleration signal, the velocity curve of the drives can be reconstructed, assuming a given initial velocity of v_0. Thus, it is also possible to detect the

stopping of a drive. Figure 4.11b shows the position signal of the considered drive from the machine tool controller to illustrate the feasibility.

Event sequences of the drives, the tool engagement patterns, or both combined can be used as characteristic patterns for the automated detection of related milling operations. Based on their differentiation in the sensor signal, the segmentation and subsequent estimation of the PSD per segment k is performed, as shown in Figure 4.10. The PSD-estimating periodogram per segment k and sensor channel $i \in \{x, y, z\}$ is a vector $\vec{P}_{xx}^{i,k}(n)$ with n being the frequency bins.

Optimization for Energy-constrained Systems

The sensor system for cutting process monitoring introduced in the previous sections is based on the edge computing paradigm and targets integration into machine tools. Through local signal processing, the approach enables the direct availability of information on the cutting tool and process. Furthermore, an inherent and real-time data reduction is performed, accounting for the limited bandwidth when transmitting the information e.g. to server systems. Especially for multi-axis machine tools, the wireless sensor system design allows easy installation on moving machine parts like the spindle. It increases the robustness by avoiding cables inside the machine, which are prone to faults under stress. At the same time, miniaturization of the system is fostered, simplifying retrofittability. However, since a wireless system design entails limited energy availability as explained in the context of component-integrated sensor system architectures in Section 2.3.2, optimizing the local signal processing with respect to energy consumption is necessary.

The signal processing methodology for extracting information about the cutting process and the tool condition as shown in Figure 4.10 relies on the time-frequency analysis of the sensor signals. The core of the time-frequency analysis is the DFT and particularly the FFT introduced in Section 4.1.4, which is continuously calculated in permanent process monitoring. The investigation of the optimization potential of the FFT concerning computational complexity and energy consumption thus is the basis for applying the sensor system concept introduced in this chapter using wireless embedded systems.

The derivation of the FFT is based on the representation of the DFT as the matrix-vector product according to Equation 4.5a between the complex DFT

matrix $\underline{\mathbf{W}}$ and the input signal $\vec{x}$ represented as a vector with N samples:

$$\vec{\underline{y}} = \underline{\mathbf{W}}\vec{x} \tag{4.5a}$$

$$\underline{\mathbf{W}} = \left(\left(e^{-j2\pi\frac{nm}{N}}\right)_{m,n}\right) \tag{4.5b}$$

The Cooley-Tukey algorithm [145] divides the matrix-vector product into sub-operations denoted as butterfly units. The resulting butterfly graph is composed of multiple subsequent butterfly stages. The following derivations are based on radix-*2* butterfly units, but can be extended to arbitrary butterfly graphs without loss of generality. The output $\vec{\underline{b}}$ of a radix-*2* butterfly is calculated according to Equation 4.6 based on its input $\vec{\underline{a}}$:

$$\vec{\underline{b}} = \begin{pmatrix}\underline{b}_1\\ \underline{b}_2\end{pmatrix} = \begin{pmatrix}1 & \underline{w}_N^m\\ 1 & -\underline{w}_N^m\end{pmatrix}\begin{pmatrix}\underline{a}_1\\ \underline{a}_2\end{pmatrix} \tag{4.6}$$

The twiddle factors $\underline{w}_N^m$ are complex constants determined according to:

$$\underline{w}_N^m = e^{-j2\pi\frac{m}{N}} = w_{N,r}^m - jw_{N,i}^m = \cos\left(2\pi\frac{m}{N}\right) - j\sin\left(2\pi\frac{m}{N}\right) \tag{4.7}$$

The complex butterfly calculations can be expanded using only real operations according to Equation 4.8 where indices r and i denote the real and imaginary components of the respective inputs and outputs:

$$\begin{pmatrix}b_{1,r}\\ b_{1,i}\\ b_{2,r}\\ b_{2,i}\end{pmatrix} = \begin{pmatrix}1 & 0 & w_{N,r}^m & w_{N,i}^m\\ 0 & 1 & -w_{N,i}^m & w_{N,r}^m\\ 1 & 0 & -w_{N,r}^m & w_{N,i}^m\\ 0 & 1 & -w_{N,i}^m & -w_{N,r}^m\end{pmatrix}\begin{pmatrix}a_{1,r}\\ a_{1,i}\\ a_{2,r}\\ a_{2,i}\end{pmatrix} \tag{4.8}$$

A butterfly unit requires four multiplications and six additions since the products of the real and imaginary parts of the input $\underline{a}_2$ and the twiddle factors in Equation 4.8 occur twice each. For a complete butterfly graph calculating the FFT of an input signal of length N, this results in $4N\log N$ additions and $2N\log N$ multiplications. The goal is to reduce this computational complexity and thus minimize the energy requirements of the FFT. Approximate computing has emerged as a feasible method to achieve this. Approximate computing is based on reducing computational accuracy to reduce computational complexity at the same time while maintaining a minimal computation error. In particular, with computations using fixed parameters like the twiddle factors of the FFT

quantizing them is the key to apply approximate computing [241]. In addition to the reduced calculation complexity, the quantization leads to a lower memory requirement of the parameters and an associated reduction of memory accesses. Based on a ternary quantization scheme and an error reduction mechanism using a correction factor α, the twiddle factors are approximated according to:

$$\begin{aligned} w_N^m &\approx \alpha (w_N^m)_T \\ w_{N,r}^m - j w_{N,i}^m &\approx \alpha \Big(\big(w_{N,r}^m\big)_T - j \big(w_{N,i}^m\big) \Big) \end{aligned} \tag{4.9}$$

Due to the ternary quantization, the approximate twiddle factor components $(w)_T \in \left\{ \left(w_{r,N}^m\right)_T, \left(w_{i,N}^m\right)_T \right\}$ can have the values $\{-1, 0, 1\}$. Generally, the cases for $\alpha = 1$ with minimal computational complexity and $\alpha = \alpha_{opt}$ with minimal approximation error are distinguished. In the following, the ternary-quantized (TQ) FFT variants with $\alpha = 1$ and $\alpha = \alpha_{opt}$ are denoted as TQ-FFT and α-TQ-FFT, respectively. The FFT in full precision (FP), without quantization, is called FP-FFT. Appendix D includes the detailed derivation of the TQ-FFT variants. Table 4.3 provides an overview of the resulting computational and memory complexity. Since the quantized twiddle factors are represented using three values, they require two bits for their digital representation.

Table 4.3: Theoretical computational and memory complexity of FP-, TQ- and α-TQ-FFT for input signals with N samples. Computational complexity is based on additions and multiplications and memory complexity is based on the required storage for the twiddle factors assuming 32-bit floating point numbers in full precision.

FFT Variant	Additions	Multiplications	Memory (Bits)
FP-FFT	$4N \log N$	$2N \log N$	$N \cdot 32$
TQ-FFT	$4N \log N$	0	$N \cdot 2$
α-TQ-FFT	$4N \log N$	$N \log N$	$\frac{N}{2} \cdot 32 + N \cdot 2$

4.3 Evaluation

The objective of the evaluation described in the following is to validate the model of process information encoded in the mechanical vibrations of the milling process as introduced in the previous Sections 4.1.1 to 4.1.4. The evaluation results form

the basis for modeling the remaining tool life using machine learning in the following Chapter 5. The acceleration sensor system for flexible manufacturing systems described in Section 4.2 is first characterized and examined in Section 4.3.1. Next, the milling process analysis based on the sensor signals and an analysis of the long-term dependency between the sensor signals and tool life criteria are performed in Sections 4.3.2 and 4.3.3. Section 4.3.4 investigates the optimization potential of the real-time data preprocessing introduced in Section 4.1.4 for resource-constrained and ultra-low-power embedded systems.

4.3.1 System Characterization

The first step in evaluating the vibration-based sensor system is its characterization in conjunction with the machine tool regarding frequency response and sensitivity. Since the interaction between the milling tool and the workpiece is the primary source of structure-borne sound, an analysis of the transmission path between the contact zone and the structure-borne sound transducer is necessary. Despite the proximity of the accelerometers to the process due to their mounting on the spindle housing, the properties of the machine structure along the transmission path affect the structure-borne sound waves through attenuation and refraction. Therefore, it has to be ensured that the sensitivity of the sensor system is sufficient to detect excitations at the cutting edge of the tool. In addition, the knowledge about the natural frequencies of the machine structure enables the evaluation of the vibrations generated during excitation by the milling process. The investigation of the natural frequencies of the system requires an impulse-like excitation to generate free vibrations. Therefore, the breakage of a pencil lead [242] is performed at the tool's cutting edge, as shown in Figure 4.12. A pencil lead with a diameter of 2.8 mm is used.

Figure 4.12b shows the vibration response of the system to the pencil lead breakage in the time and frequency domain. With a maximum peak-to-peak output voltage of 10 mV, the pencil lead breakage is clearly visible in the time-domain signal. In the amplitude spectrum of the vibration response, the natural frequencies of the machine structure under impulse-like excitation at the tool cutting edge are visible. The dominant amplitudes occur up to 6 kHz with a dominant peak at 2.8 kHz. Furthermore, several smaller peaks are visible around 15 kHz.

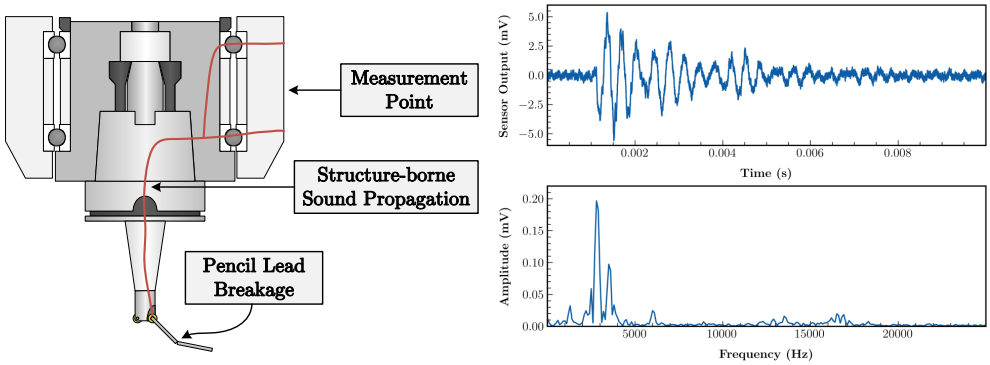

(a) Experimental setup **(b)** Measured frequency response

Figure 4.12: Pencil lead breakage experiment at the tool cutting edge to investigate the transmission path of structure-borne sound.

In the following step, the vibration excitation of the machine tool system due to spindle rotation is investigated. Since the spindle inevitably rotates during the milling process, the resulting frequency components must be identified to distinguish them from milling process-related components. Therefore, the spindle is operated with the tool holder and tool installed in idle mode, i.e., without cutting operation, at different speeds from 2710 rpm to 3175 rpm. Figure 4.13 visualizes the resulting Campbell diagram over increasing rotation speed.

The Campbell diagram shows the machine spindle's excitation- and resonance-induced vibrations. The spindle drive is the source of excitation. The components of the machine spindle, i.e., the shaft, the tool clamping system, the bearings, the tool holder, and the tool, rotate and thus contribute to the vibration response. The excitation-related components of the vibration response change with the drive's speed and result from imbalances of the rotating components (shaft, clamping system, tool holder, tool) and wear of the bearings. The dominant excitation-induced vibrations of the machine tool considered in Figure 4.13 are between 1 and 6 kHz. Dominant resonance frequencies are found at 4, 4.7 and 5.3 kHz. The resonance-induced vibrations of the machine spindle are independent of the rotation speed and depend only on the mechanical system design.

4.3.2 Analysis of the Milling Process

The previous section describes the analysis of the structure-borne sound transmission path between the tool cutting edge and the structure-borne sound transducer.

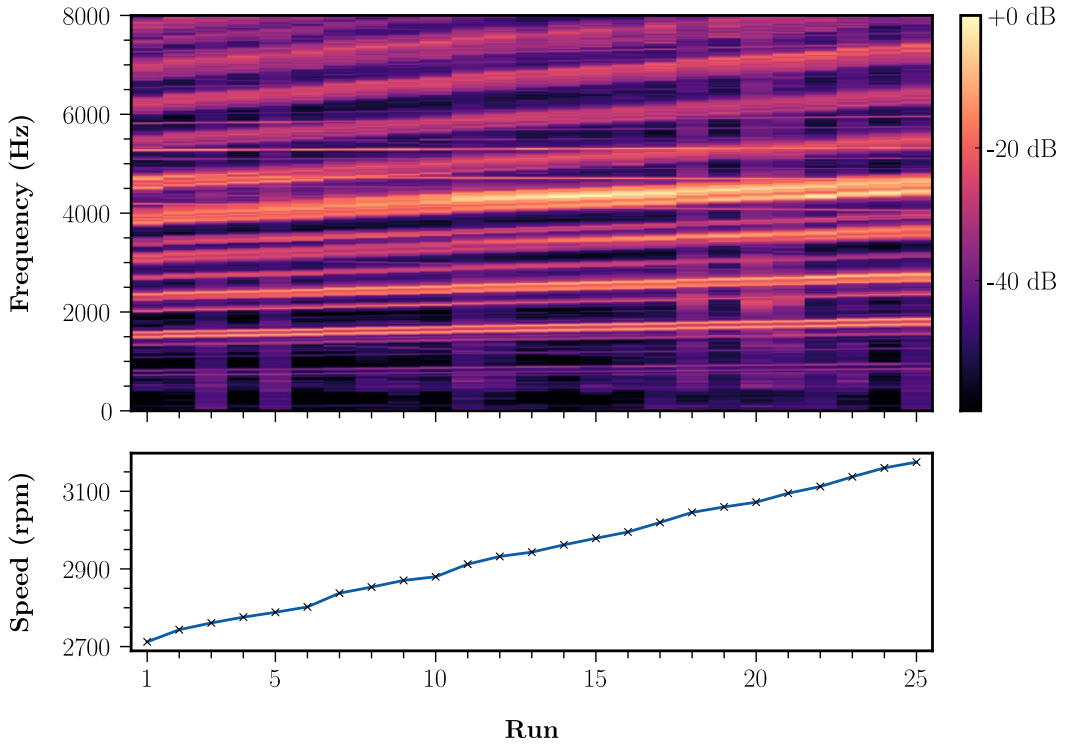

Figure 4.13: Campbell diagram of the spindle rotation with installed tool holder and tool in idle mode without cutting operation.

Furthermore, it presents the characterization of the system behavior under excitation by the spindle rotation in idle mode. Based on this, the system behavior under milling process excitation is investigated in the following. Figure 4.14a shows the experimental conditions applied in this section and the following Section 4.3.3.

The material of a workpiece is removed layer-wise based on the zig-zag face milling strategy characterized by alternating up- and down-milling. A toroidal milling tool with circular inserts and three cutting edges is used. The process parameters of the feed per tooth f_z, cutting speed v_c, axial depth of cut a_p, and radial depth of cut a_e can be varied. After removing a defined number of material layers, the wear mark width of the tool cutting edges and the surface roughness of the workpiece are measured. Details regarding the measurement are included in Appendix C. The measurement step is relevant for investigating the tool life criteria in the next Section 4.3.3. Figure 4.14b shows an example of the resulting frequency response over time for four successive milling paths. In the range of up

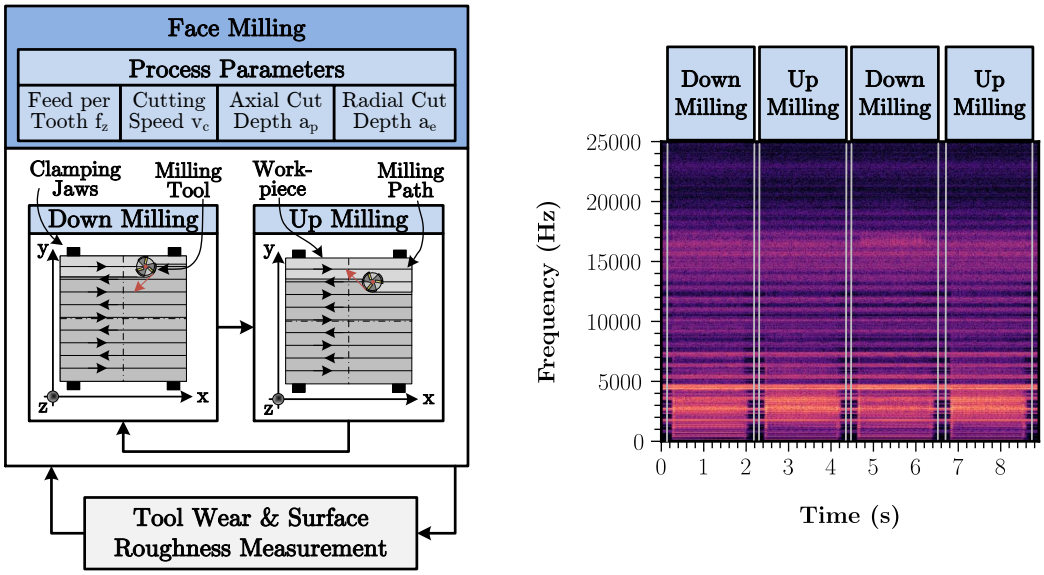

(a) Experimental setup **(b)** Time-frequency response

Figure 4.14: Face milling experiment as a foundation for the milling process and tool life criteria analysis.

to 6 kHz, it can be seen that the vibration intensity is lower for down-milling than for up-milling. The reason for this is the difference in the chip removal process. Since feed and cutting forces act in opposite directions during up-milling, the tool and workpiece repel each other during chip formation, leading to stronger vibration excitation.

In order to analyze the influence of the milling process on the system's vibration response compared to the excitation due to spindle rotation in idle mode, the Campbell diagram for individual milling paths is shown in Figure 4.13. The spindle rotation speed n is increased from 2710 rpm to 3175 rpm as described in the previous Section 4.3.1.

Figure 4.15 shows the excitation caused by the periodic engagement of the cutting edges of the milling tool, especially in the range below 1.5 kHz. In comparison, in the case of the idle mode of the spindle shown in Figure 4.13, no major vibration components are evident in this frequency range. Due to the milling tool with three cutting edges, engagement frequencies Ω_z are found at three times the spindle rotation frequency $f_n = \frac{60}{n}$. Hence, engagement frequencies between 136 and 160 Hz are obtained for the used interval of spindle speeds. Due to the finite stiffness of the machine tool, the harmonics of the engagement frequencies

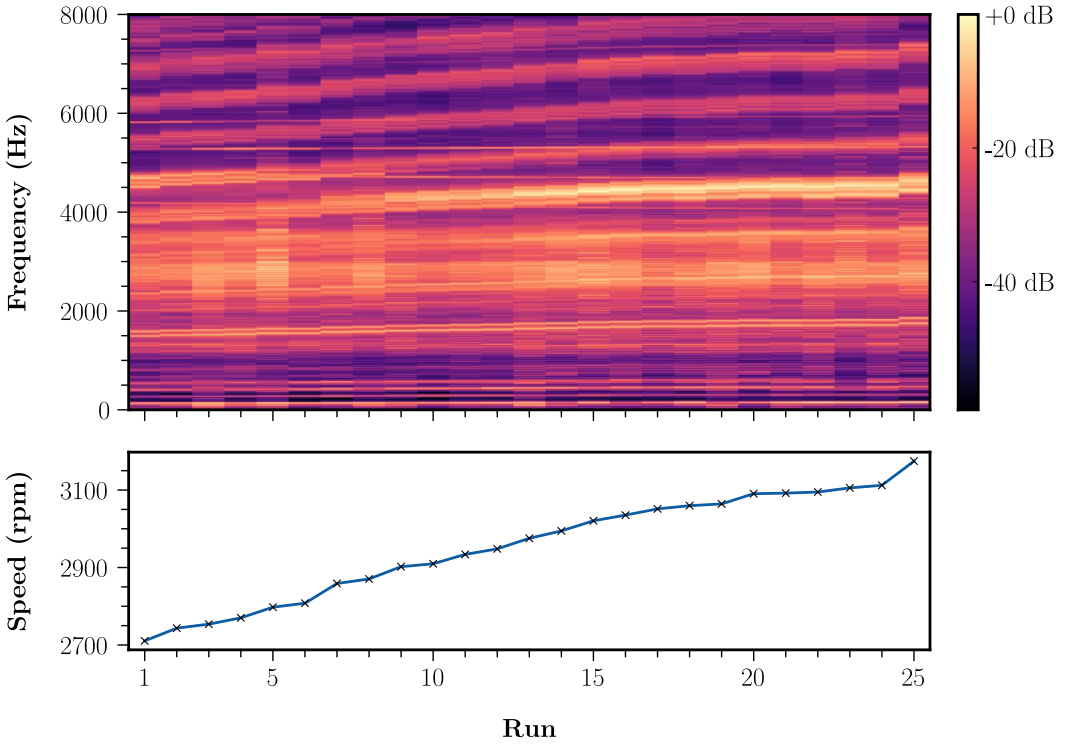

Figure 4.15: Campbell diagram of the active milling process.

$\Omega_z^h = h \cdot \Omega_z$ with $h \in \mathbb{N}$ are visible as well.

Furthermore, the high signal power distributed over the frequency band between 2 and 4 kHz is noticeable compared to Figure 4.13. It overlays the excitation-dependent vibration components influenced by the rotating machine components in this range, but appears independent of the excitation. Compared with the frequency response to the impulsive excitation of the pencil lead break in Figure 4.12, it becomes clear that the increased signal power in the frequency band results from the excitation of the dominant natural frequencies of the structure-borne sound transmission path. Other excitation-dependent frequency components above 4 kHz influenced by the rotating machine components and resonance-dependent frequency components influenced by the machine structure are the same as in the idle mode of the spindle.

4.3.3 Analysis of Tool Life Criteria

The basis for predicting the remaining tool life is the correlation analysis between the sensor signals and the tool life criteria. The correlation analysis aims to show

the dependency between the variables usable for modeling. In this work, the tool life criteria of wear and surface roughness are used, which influence each other and primarily determine the quality of the workpieces according to Section 4.1.3. In addition, the tool life criteria influence the vibration power dissipated into the machine tool structure during milling and thus the acceleration sensor signals.

The wear and surface roughness analysis is performed using the experimental setup shown in Figure 4.14a based on the face milling process. The static cutting parameters $f_z = 0.7$ mm, $v_c = 200\ \frac{\text{mm}}{\text{min}}$, $a_p = 0.8$ mm, and $a_e = 10.4$ mm are selected. After removing 1 cm of material, the wear mark width VB of the three tool cutting edges is measured with a video measuring microscope. The ten-point height of irregularities R_z is measured with a roughness probe on three down-milling paths of the workpiece at equally spaced intervals according to Appendix C. The mean wear mark width $\bar{VB}$ is calculated for the three cutting edges and the mean ten-point height of irregularities $\bar{R}_z$ is determined for three milling paths. Furthermore, the PSD-estimating periodograms $P_{xx}(n)$ of the sensor signals per milling path are determined. Figure 4.16 shows the correlation analysis for the down-milling paths.

The linear Pearson correlation $\rho(\bar{VB}, \bar{R}_z)$ between the mean tool wear and the mean absolute workpiece surface roughness, $\left|\rho(P_{xx}, \bar{VB})\right|$ between the periodograms and the mean tool wear per frequency bin n and $\left|\rho(P_{xx}, \bar{R}_z)\right|$ between the periodograms and the mean workpiece surface per frequency bin n are displayed. There is a high correlation between $\bar{VB}$ and $\bar{R}_z$ with a correlation coefficient of 0.94. This confirms the assumption in Section 4.1.3 that tool wear and surface roughness are directly related. It can be seen that initially $\bar{R}_z$ slightly decreases with a slight increase in wear. The images of the cutting inserts taken with the video measuring microscope suggest that the initial moderate wear sharpens the cutting edges, explaining the increasing surface quality. From milling path 468, $\bar{R}_z$ and $\bar{VB}$ increase sharply. The images of the cutting edges show a pronounced wear mark from this point on. While the kinematic and chatter roughness components were decisive before, the cutting surface roughness now dominates, leading to a deterioration of the workpiece surface.

The PSD-based spectrogram in Figure 4.16 shows that the vibration intensity increases with increasing wear and roughness in the frequency range between 2 and 4 kHz. This is the frequency range of the dominant natural frequencies of the

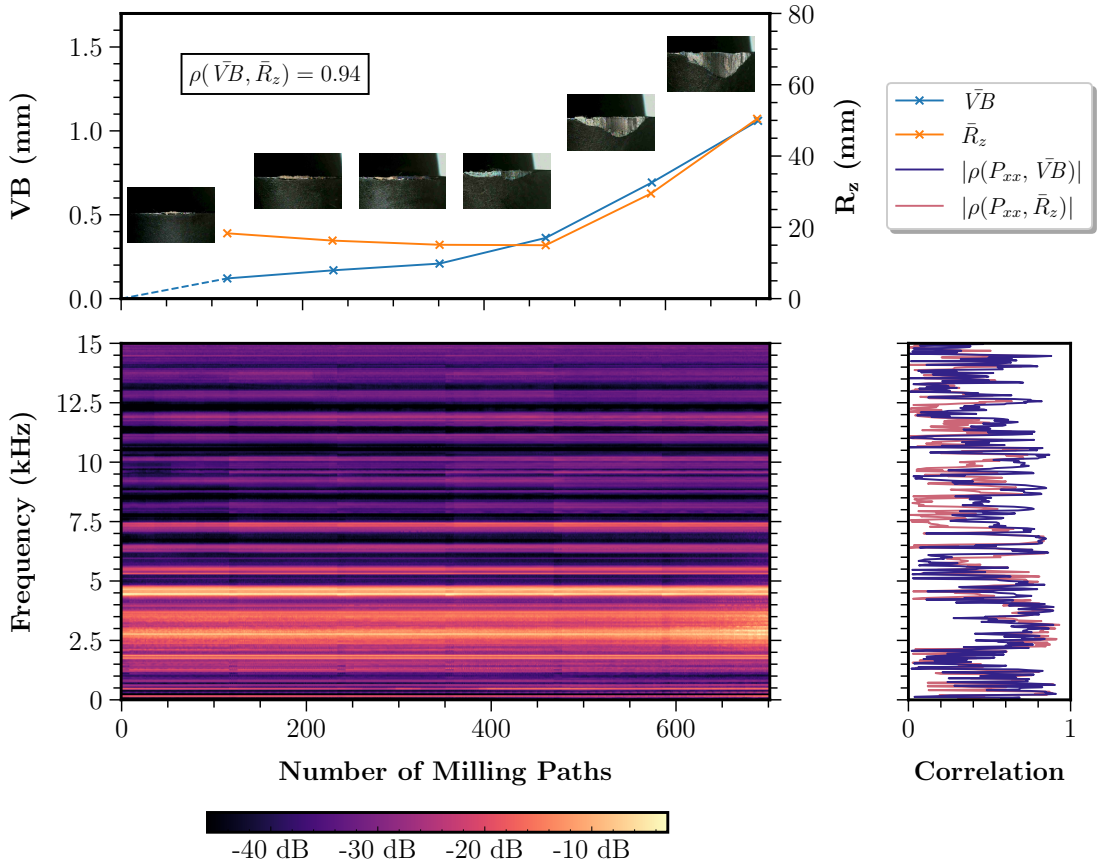

Figure 4.16: Correlation analysis between the mean flank wear mark width $\bar{VB}$, the mean ten-point height of irregularities $\bar{R}_z$ and the periodograms $P_{xx}(n)$ for PSD estimation acquired over the complete lifecycle of a tool.

spindle structure under impulsive excitation at the tool cutting edge as identified based on the pencil lead breakage response according to Figure 4.12. The relationship also becomes evident in the absolute correlation coefficients per frequency bin, with maxima of 0.9 for $\bar{VB}$ and 0.93 for $\bar{R}_z$ between 2 and 4 kHz. Between 0 and 1.5 kHz, correlation coefficients of similar magnitude occur with maxima of 0.91 for $\bar{VB}$ and 0.89 for $\bar{R}_z$. The frequency components of this frequency range are, as identified in Section 4.1.3, purely due to the excitation by the periodic engagement of the cutting edges and thus due to the milling process. Hence, the sensor signals contain information on wear and surface roughness independent of the machine structure. Modeling based on these frequency components thus allows transferability to other machines with different mechanical designs. Furthermore, frequency bins with correlations up to 0.87 for $\bar{VB}$ and 0.85 for $\bar{R}_z$ are found in the frequency range between 4 and 15 kHz. The comparison with

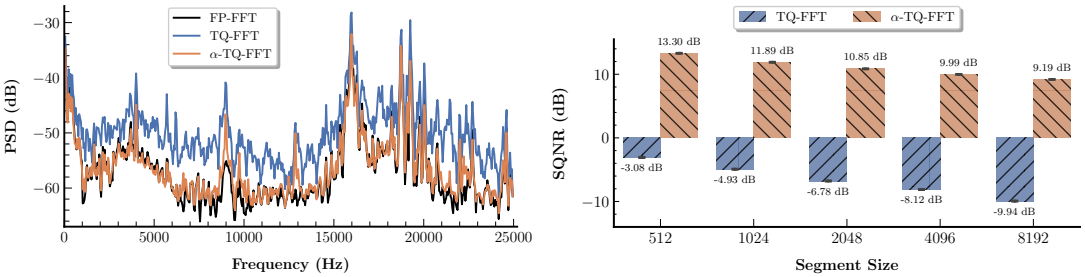

(a) Qualitative Evaluation **(b)** Quantitative Evaluation

Figure 4.17: Qualitative and quantitative accuracy evaluation of the TQ- and α-TQ-FFT compared to the FP-FFT based on the PSD calculation using the Welch method.

the Campbell diagrams in Figures 4.13 and 4.15 shows that these are excitation-dependent frequency components affected by the rotating machine components and resonance-dependent frequency components affected by the machine structure. Above 15 kHz, the correlation coefficients decrease for $\bar{VB}$ and $\bar{R}_z$, making this frequency range less suitable for modeling.

4.3.4 Optimization for Energy-constrained Systems

In the previous sections, the working principle of the sensor system and signal processing for machining process monitoring has been validated. In the last step, the approximate computing method described in Section 4.2.4 to optimize the FFT-based time-frequency signal analysis in terms of energy requirements has to be investigated. It aims to enable signal analysis and process monitoring using energy-constrained systems, e.g., wireless sensor nodes. In the following, the influence of the TQ- and α-TQ-FFT on the accuracy of the PSD calculation according to Figure 4.10 for determining the tool state is analyzed. The analysis is based on acceleration sensor signal segments acquired during milling operations as shown in Figure 4.14a. Figure 4.17a shows the PSD-estimating periodogram for a stationary signal segment calculated using the Welch method, which is based on the STFT.

Although TQ- and α-TQ-FFT introduce noise to the periodogram estimating the PSD, its rough shape is preserved in both cases. The noise results in increased total magnitudes of the periodogram, especially in the case of the TQ-FFT. It can be shown that the correction factor used in case of the α-TQ FFT compensates

the magnitude offset of the TQ-FFT. In addition to the qualitative analysis, the accuracy reduction due to the quantized FFT is evaluated quantitatively using the signal-to-quantization noise ratio (SQNR). The SQNR is calculated between the PSDs based on the FP-FFT and the TQ-FFT as well as the α-TQ-FFT, respectively. A total of 5670 segments of acceleration sensor signals from milling operations are used and the mean and standard deviation of the resulting SQNR values are evaluated. The FFT window size of the STFT as introduced in Section 4.1.4, which is the basis for the PSD calculation, is varied between 512 and 8192 samples.

Figure 4.17b shows that both quantized FFT variants are sensitive to the signal length. The SQNR of the α-TQ-FFT exceeds that of the TQ-FFT by a factor of three on average. The error reduction is achieved due to the correction factor α. In addition to the accuracy evaluation of the quantized FFT, the impact on computational complexity and energy consumption is analyzed. FP-, TQ-, and α-TQ-FFT are evaluated using the ARM Cortex-M4-based nRF52840 SoC to show the suitability of the signal processing for use in energy-constrained systems. The nRF52840 is a Bluetooth-enabled SoC based on an ultra-low power microcontroller, which can thus serve as a foundation for wireless sensor nodes. Computational complexity is determined by execution time using the Digilent Discovery logic analyzer, and power consumption is measured using the Texas Instruments INA219 power monitor. Table 4.4 compares execution time and energy consumption with the FFT implementation of the state-of-the-art CMSIS library version 5.9.0. All implementations use the floating-point data type. The C code of the CMSIS-based FFT implementations is compiled using the GCC compiler with optimization level -O3. Only the FFT functions for real-valued input signals (`arm_rfft_fast_f32`) are used.

Table 4.4: Execution time and energy consumption per FFT using nRF52840 SoC

Input Samples	Execution Time (μs)				Energy Consumption (μJ)			
	TQ-FFT	**α-TQ-FFT**	**FP-FFT**	**CMSIS**	**TQ-FFT**	**α-TQ-FFT**	**FP-FFT**	**CMSIS**
32	14.4	17.0	19.3	34.4	0.3	0.4	0.4	0.8
64	30.8	38.0	43.5	74.3	0.7	0.8	1.0	1.6
128	65.5	86.8	97.7	133.7	1.4	1.9	2.1	2.9
256	154.3	200.0	229.4	328.7	3.4	4.4	5.0	7.2
512	324.5	426.1	499.5	705.4	7.1	9.4	11.0	15.5
1024	675.1	899.5	1076.9	1271.9	14.8	19.8	23.7	28.0
2048	1513.7	2007.9	2411.6	3071.2	33.3	44.2	53.0	67.6

Table 4.4 demonstrates that both TQ- and α-TQ-FFT described in Section 4.2.4 outperform the CMSIS FFT implementation for all the evaluated numbers of input samples. The FP-FFT is 1.4× faster than the CMSIS FFT on average. The TQ-FFT enables a mean speed-up by a factor of 2.2 compared to the CMSIS FFT and by a factor of 1.5 compared to the FP-FFT. The α-TQ-FFT enables a mean speed-up by factors of 1.7 and 1.2 compared to the CMSIS FFT and the FP-FFT, respectively.

4.4 Discussion

The main objective of this chapter is to investigate the monitoring of multi-axis milling processes based on flexible machine tools in single-part manufacturing scenarios using process-integrated sensors. It should be shown that machine-transferable process monitoring of the target parameters tool wear and workpiece surface roughness with process-independent, permanent sensor integration is possible. The process monitoring should be the foundation for investigating the machine learning-based prediction of the remaining tool life.

Based on a requirements analysis of the targeted manufacturing processes, mechanical vibrations within the machining process are first identified as a suitable process monitoring variable. The main reason for this is their propagation characteristic in terms of mass-dependent machine vibrations and structure-borne sound, which makes it possible to capture machining process emissions at a certain distance from the contact zone between the workpiece and the tool. Thus, permanent sensor integration is possible independent of the components frequently changing during single-part production, i.e., tool, tool holder, workpiece, or workpiece clamping. The digital signals of the machine tool controller also meet these requirements. However, the accessibility of the signals depends on the specific controller and the machine tool. This limitation does not affect the mechanical vibrations acquired using external, retrofittable sensors that enable a higher resolution of the cutting process at the same time. Nevertheless, digital control signals can complement vibration-based process monitoring if accessible, since they directly provide contextual information, such as the axis positions of the machine tool.

The vibration-based process monitoring is subsequently investigated concerning

its machine tool dependence. The results of vibration excitation tests on a five-axis milling center in Sections 4.3.1 and 4.3.2 show that machine structure and component-dependent vibrations are separable from milling process-dependent vibrations and that the decisive frequency ranges can be identified. The correlation analysis in Section 4.3.3 between the vibration signals and the target parameters tool wear and surface roughness indicates a significant correlation in the milling process-dependent frequency range. Consequently, the vibration signals contain information about the target parameters independent of the machine tool structure, design or components. Hence, the transferability of the vibration-based process monitoring method and the use of the sensor data for machine learning-based remaining tool life prediction is plausible.

Finally, to further improve the transferability by simplified sensor integration into machine tools, the FFT-based signal processing underlying the process monitoring method is optimized concerning applicability in energy-constrained wireless systems. The investigation of the approximate ternary-quantized FFT in Section 4.3.4 confirms that the reduction in computational accuracy is controllable and that the machining process monitoring is applicable using ultra-low power microcontrollers. Compared to state-of-the-art implementations, the computational complexity and energy consumption can be reduced by a factor of 2.2 on average using the approximate FFT.

Compared to previous sensor systems for monitoring the production of complex single parts as summarized in Section 2.3.2, the approach investigated in this chapter is not based on the component-integrated architecture concept. Thus, no sensor integration into process-related components such as tools, tool holders, or workpiece clamping systems is necessary. In contrast to the state-of-the-art, this enables the application for process monitoring in flexible manufacturing systems with multiple degrees of freedom and single-part production characterized by frequent process adaptations. Previously, sensor systems and process monitoring were only designed for one manufacturing system and process configuration. The analysis results above prove the machine independence and hence the transferability of the vibration-based process monitoring approach.

5. Machine Learning-based Remaining Tool Life Prediction

In machining process monitoring, the tool life prediction is the basis for maintaining the required process quality, ensuring process reliability and increasing productivity. The objective is to provide information on the tool condition and its effects on process quality and to estimate how the tool condition will develop in the future. The information serves as input for predictive tasks of manufacturing automation, e.g., planning of future tool changes, optimization of cutting parameters or feedback for continuous process simulations.

5.1 Prediction Methodology

The previous chapter shows that in the milling process under stable conditions, the tool life criteria (wear of the tool cutting edge, surface roughness of the workpiece) and the information contained in the mechanical vibrations are correlated. However, already small changes of the load during milling lead to significant influences on the mechanical vibrations. Even for allegedly simple engagement conditions, like during face milling, process-related factors such as the milling strategy can be decisive in analyzing tool life criteria. Especially in the context of free-form surface milling of complex component shapes, the influences due to varying engagement conditions are not negligible. The general increase in single-part production in manufacturing and associated variability of the workpieces and process conditions intensify this. In order to manage the resulting complexity in modeling the remaining tool life, machine learning methodologies for prediction are investigated in the following.

5.1.1 Objective Function

The task of machine learning in the remaining tool life prediction is the approximation of a tool life function depending on information about the tool life criterion from the sensor-based process monitoring. Figure 5.1 shows the overall approach followed in this work.

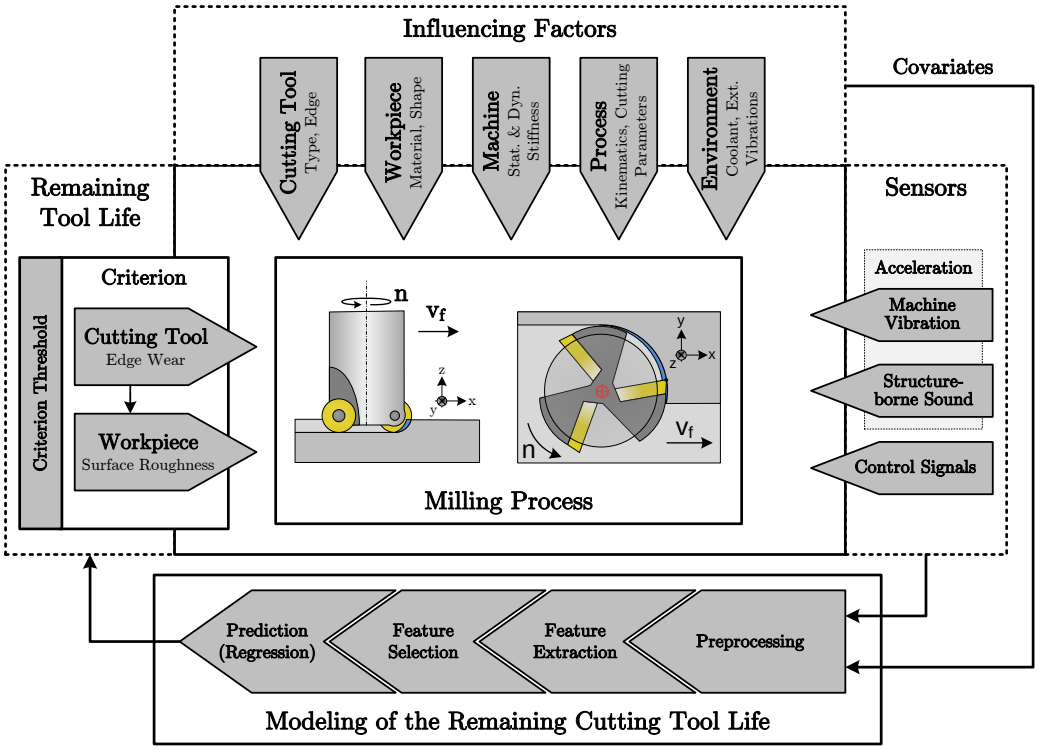

Figure 5.1: Overview of the methodology for remaining tool life modeling developed and investigated in this work.

Compared to the state-of-the-art, this work focuses on including contextual information about the specific milling process (covariates) in the remaining tool life modeling. The covariates complement the in-process sensor data from acceleration sensors, measuring machine vibrations and structure-borne sound, and the digital signals of the machine tool controller, as investigated in Chapter 4. Considering process influencing factors in the remaining tool life prediction through the covariates aims to increase the prediction accuracy and enable its applicability even in the case of their variation, such as in free-form surface milling and single-part production. The process influencing factors are critical since they

affect both the tool life and the process monitoring variables. Five influencing factors are distinguished:

- **Cutting Tool**: The tool influences the milling process through its shape and the design of its cutting edges. The chip formation process and the associated cutting forces (mechanical load) depend on this. In addition, the coating of the cutting edges influences the tool life.
- **Workpiece**: The workpiece influences the milling process mainly by its shape and material. Especially the workpiece shapes are not trivial in the context of free-form surface milling, affecting the load on the tool in the process.
- **Machine**: The machine influences the milling process through its finite stiffness. The excitation of the machine structure due to the cutting process generates vibrations affecting the process retroactively.
- **Process**: The process kinematics and the cutting parameters, mainly derived from the shape of the workpiece, represent significant influencing factors of the milling process. Together, they define its engagement conditions, varying during workpiece manufacturing due to its shape (free-form surface milling) or between workpieces (single-part production).
- **Environment**: Environmental influences include all external factors affecting the process. In addition to their effect on the tool life, they mainly represent disturbance variables for the in-process sensors.

The variation of process influencing factors occurs between different tool instances (inter-tool life) and during the life of individual tool instances (intra-tool life). All influencing factors above can be subject to inter-tool life variation in any production scenario, from series to single-part production. Intra-tool life variation occurs primarily in single-part production and free-form surface machining, where workpiece and process-related influencing factors can change abruptly. Therefore, this work focuses on the investigation of varying workpieces, cutting parameters, process kinematics, engagement conditions and thus tool load.

Since the remaining tool life as a target parameter and the associated tool life criteria are continuous variables, machine learning-based modeling is performed using regression. The prerequisite for regression is the derivation of the objective function which the machine learning models approximate. As shown in Fig-

ure 5.1, the remaining tool life objective function depends on the particular tool life criterion and the criterion threshold. Since the workpiece surface roughness is influenced by the flank wear of the tool as shown in Chapter 4, the wear mark width VB is considered the primary tool life criterion in the following. Due to the correlation of the tool life criteria, the methodology is transferable without loss of generality.

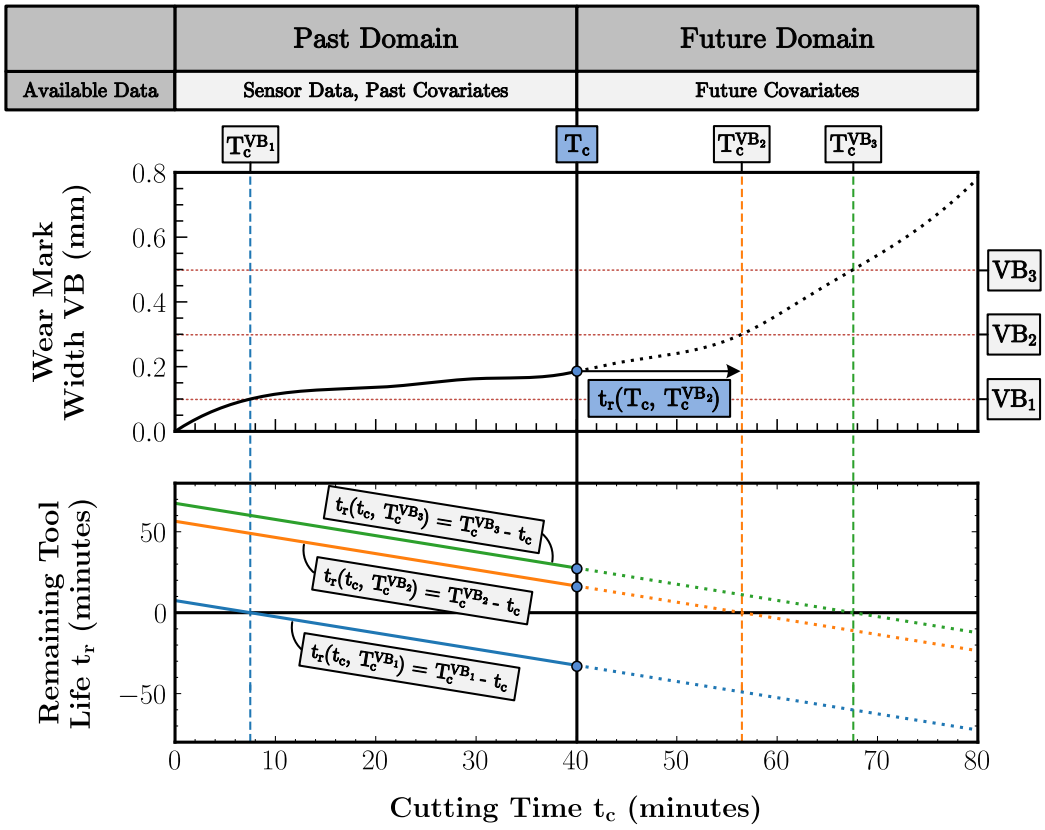

Figure 5.2: Objective function for predicting the remaining tool life, exemplarily shown for multiple wear mark threshold values VB_i.

Figure 5.2 illustrates the relationship between the remaining tool life and the wear mark width VB. The wear threshold value VB_t with $t = 1, \ldots, K$ applied to the wear curve $f_{VB}(t_c)$ depending on the cutting time t_c is the core of the remaining tool life determination. A wear threshold VB_t is defined based on the application requirements as well as expert and domain knowledge. Multiple wear thresholds can also be set, while the maximum threshold VB_K is denoted as the end-of-life criterion. The contact duration $T_c^{VB_t}$ associated with a wear threshold value VB_t is determined by evaluating the inverse wear curve f_{VB}^{-1} at the

wear threshold value. The remaining tool life function according to Equation 5.1 describes the remaining time t_r until a wear threshold value VB_t is reached:

$$t_r\left(t_c, T_c^{VB_t}\right) = T_c^{VB_t} - t_c = f_{VB}^{-1}(VB_t) - t_c \tag{5.1}$$

Therefore, Equation 5.1 is a linear function with a slope of 1 and the y-axis intercept of $T_c^{VB_t}$ over t_c. Since the non-linear wear curve f_{VB} inherently defines the y-axis intercept, f_{VB} has to be part of modeling t_r.

The task of remaining tool life prediction at an instantaneous cutting time $t_c = T_c$ divides the time axis into a past and a future domain. At T_c, the sensor data and covariates of the past cutting time are available. In the future domain, covariates may already be known, e.g., due to known workpieces to be subsequently produced. The past and future domain information available at T_c is the foundation for predicting the remaining time $t_r\left(t_c, T_c^{VB_t}\right)$ until a wear threshold VB_t is reached. Since the wear measurement using manufacturing metrology is to be replaced by the in-process sensor-based monitoring in this work, the actual wear values are available only in the context of the model training. During the inference time of the models, there is no permanent measurement and feedback of the wear values, i.e., f_{VB} up to T_c, according to Figure 5.2, is not directly known.

5.1.2 Dataset Generation

The basis for machine learning-driven prediction is the availability of a representative dataset to train and validate the underlying models. The dataset must reflect the application-specific characteristics and contain the desired input and output variables for modeling. This work focuses on the application of free-form surface milling under single-part production. Inter- and intra-tool life variation of cutting parameters and engagement conditions characterize the single-part production. The complexity of workpieces with free-form surfaces results in varying engagement conditions along contiguous tool paths. Cutting parameters and engagement conditions affect the tool load and thus the sensor data (model input) and the tool life (model output). Therefore, workpiece- and process-related influencing factors are particularly relevant for modeling. A dataset incorporating these application-specific characteristics does not yet exist as the literature review

in Section 2.4.3 suggests. The dataset generation requires the analysis of the respective influencing factors to investigate them in a controlled manner within the machine learning-based modeling. Figure 5.3 shows the underlying relationships along the milling process chain as a basis for the analysis under the assumption of a general five-axis milling model and arbitrary free-form surfaces.

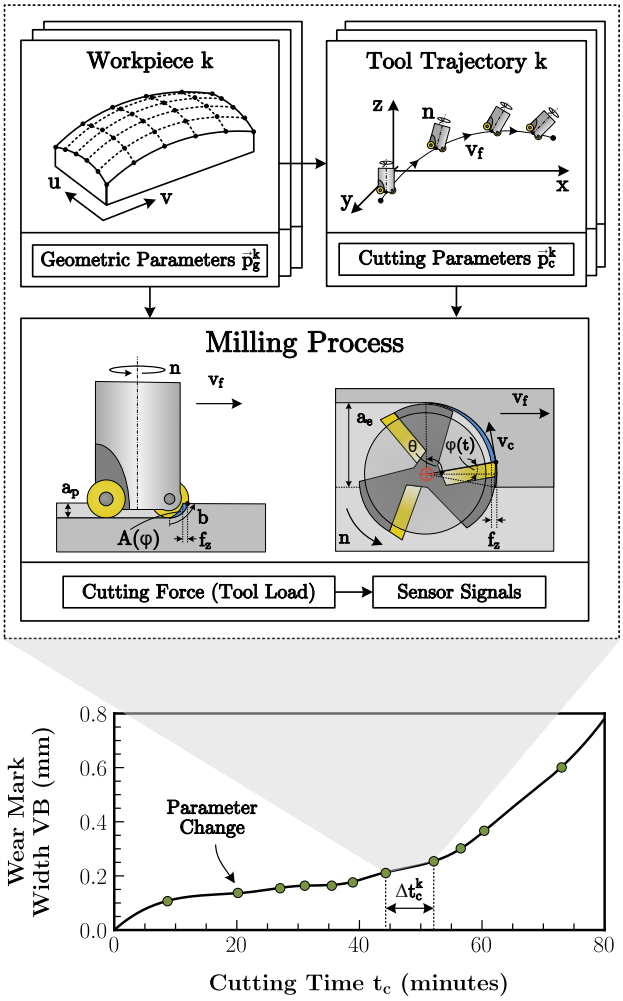

Figure 5.3: Dependencies of the milling process from workpiece- and trajectory-related covariates as a foundation for the dataset generation.

A sequence of customized free-form surface workpieces k with $k = 1, \ldots, N$ to be manufactured is considered. A free-form surface has several geometrical parameters derived from its NURBS-based definition according to Section 2.2.2. The geometric parameters defining the shape of the surface are the control point tensor $\mathbf{P}$, the orders p and q of the B-spline basis functions and the weight

matrix $\mathbf{W}$. For simplification, the geometric parameters of a workpiece k can be vectorized into a general vector $\vec{p}_g^k$.

Based on the surface definition, the trajectory of the milling tool is derived in the next step of the milling process chain, as described in Section 2.2.4. The trajectory is a time-dependent function representing the position of the tool in Cartesian coordinates, the inclination of the tool axis in the feed direction as lead angle α_L and orthogonally to it as tilt angle β_T. The tool trajectory depends on $\vec{p}_g^k$ and the cutting parameters of the particular workpiece. The cutting parameters can be expressed as a vector $\vec{p}_c^k$ and consist of the cutting speed v_c, the feed per tooth f_z, the axial depth of cut a_p, and the radial depth of cut a_e. They are either set manually by the operator or process planner or automatically based on process simulation.

On the execution of the tool trajectory, the spatiotemporal cutting force $\vec{F}(t)$ according to Section 2.2.3 acts on the engaged cutting edges of the tool. The cutting force consists of periodic and non-periodic components. According to the milling force model by Altintas [75], the periodic cutting force components result from the rotation of the tool (instantaneous engagement angle $\varphi(t)$) and corresponding periodic variation of the cross-sectional area of cut $A(\varphi)$. In the case of free-form surface milling based on five-axis machine tools, it has been shown that the inclination of the tool axis and the curvature of the machined surface mainly influence the engagement angle θ [72, 73]. θ defines the duration of the cutting edge engagement during tool rotation, affecting the course of the cutting force. Hence, if the engagement angle $\theta(t)$ changes over time, it causes non-periodic variations of the cutting force.

The machining of a tool trajectory of a workpiece k leads to a progression of the cutting time by the value Δt_c^k. The mechanical load on the tool's cutting edges in this interval, influenced by the workpiece geometry, the cutting parameters, and the tool trajectory, contributes to the increase in tool wear. Cutting time progression and wear contribution vary depending on the current tool condition and the parameters $\vec{p}_g^k$ and $\vec{p}_c^k$.

5.1.3 Machine Learning Model

Based on the procedure described in the previous Section 5.1.2, a dataset $\mathcal{D}$ can be generated representing the tool wear under single-part production of free-form surfaces. $\mathcal{D}$ can include the data of multiple tool instances up to their respective end-of-life point $T_c^{VB_K}$. Modeling the remaining tool life based on tool wear is thus a multi-series forecasting task [172], where the data over the lifetime of a tool instance represents a series. As described in Section 2.4.3, the forecasting-based remaining tool life prediction is advantageous over the direct and criterion-based methods because it retains the relationship to the tool life criterion. Therefore, it enables an overall explainable methodology. Figure 5.4 shows an overview of the machine learning-based modeling approach of this work.

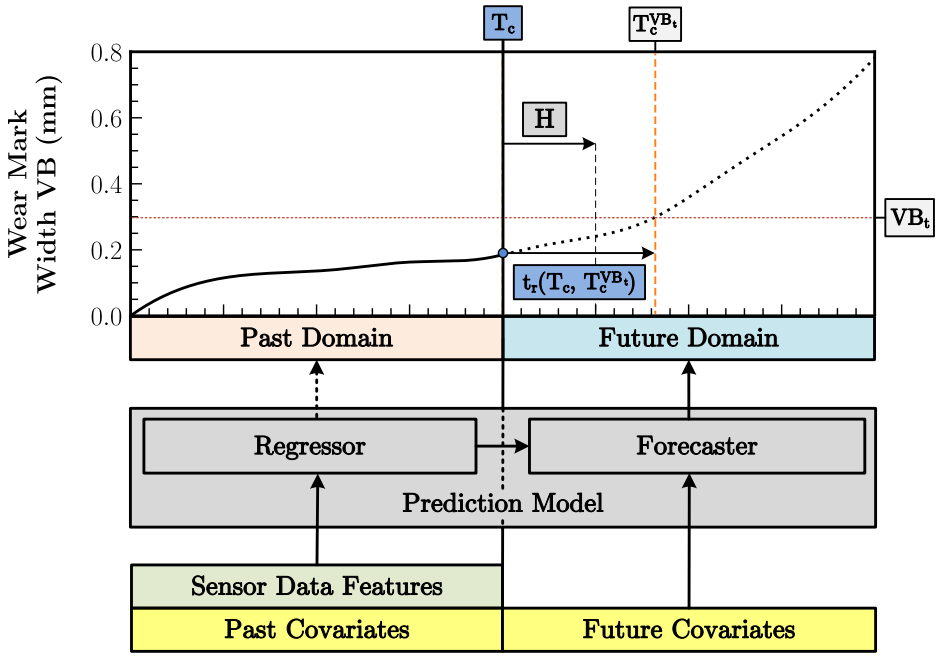

Figure 5.4: Overview of the machine learning-based remaining tool life modeling approach formulated as a combined regression and forecasting task. The approach uses features extracted from the sensor data as well as covariates representing contextual process information.

The dataset $\mathcal{D}$ containing N tool instance series is defined as $\mathcal{D} = \{\mathcal{D}_i\}_{i=1}^{N}$. The samples of $\mathcal{D}_i$ are defined as $\mathcal{D}_i = \left\{\mathbf{x}_{\mathbf{i},1:T_c}^{(p)}, \mathbf{x}_{\mathbf{i},T_c+1:T_c+H}^{(f)}, \mathbf{y}_{\mathbf{i},1:T_c}, \mathbf{y}_{\mathbf{i},T_c+1:T_c+H}\right\}$ with T_c being the instantaneous cutting time step beyond which the wear curve f_{VB} is to be forecasted and H being the forecasting horizon, i.e., the cutting time steps

over which a model predicts f_{VB}. A cutting time step is defined as the cutting duration of a continuous tool trajectory during which the tool is not lifted from the workpiece surface, i.e., moved along the normal vector perpendicular to the workpiece surface. It is assumed that the manufacturing of a workpiece k according to Figure 5.3 represents a cutting time step of length Δt_c^k. The tensors $\mathbf{x}_{\mathbf{i},1:T_c}^{(p)}$, $\mathbf{x}_{\mathbf{i},T_c+1:T_c+H}^{(f)}$, $\mathbf{y}_{\mathbf{i},1:T_c}$ and $\mathbf{y}_{\mathbf{i},T_c+1:T_c+H}$ describe the past features, known future features as well as past and future targets. The target tensors both contain a wear mark width value per cutting time step. As shown in Figure 5.4, the past features consist of the sensor-related features and the past covariates, whereas the known future features are covariates only. Covariates represent process-describing contextual information and can be elements of the geometric and cutting parameter vectors $\vec{p}_g^k$ and $\vec{p}_c^k$ or values derived from them, e.g., during simulation. Past and future covariates may differ depending on the future parameters assumed to be available before workpiece production. The general periodogram vectors $\vec{P}_{xx}^k$ estimating the PSD of a cutting time step, calculated for the acceleration sensor signals of contiguous tool trajectories according to the procedure shown in Figure 4.10, constitute the sensor-related features.

The task of modeling the wear curve f_{VB} starting from T_c over a horizon H into the future using a machine learning model can be expressed according to Equation 5.2:

$$\hat{y}_{T_c+1:T_c+H} = f\left(\mathbf{x}_{1:T_c}^{(p)}, \mathbf{x}_{T_c+1:T_c+H}^{(f)}, \theta_{\mathbf{p}}\right) \tag{5.2}$$

$\hat{y}_{T_c+1:T_c+H}$ is the forecast of the model with parameters $\theta_{\mathbf{p}}$. Model inputs are only the past and future features since this work aims to replace the wear mark width measurement with process-integrated sensors. Hence, the measured wear curves f_{VB} and thus the target tensors are only included in the training data set and are not available at inference time. The forecast requires the reconstruction of the past targets from the available sensor data features and covariates. Accordingly, the model has to perform the tasks of wear curve regression (regressor) and forecasting (forecaster), as shown in Figure 5.4. The regressor f_R and the forecaster f_F are defined according to Equations 5.3a and 5.3b, with $\theta_{\mathbf{p}}^{\mathbf{R}}$ and $\theta_{\mathbf{p}}^{\mathbf{F}}$ being the regressor and forecaster parameters.

$$\hat{y}_{1:T_c} = f_R\left(\mathbf{x}^{(p)}_{1:T_c}, \theta^{\mathbf{R}}_{\mathbf{p}}\right) \tag{5.3a}$$

$$\hat{y}_{T_c+1:T_c+H} = f_F\left(f_R, \mathbf{x}^{(f)}_{T_c+1:T_c+H}, \theta^{\mathbf{F}}_{\mathbf{p}}\right) \tag{5.3b}$$

The regressor thus replaces the input of past targets in the forecaster. It is problematic when the forecasting horizon H of the forecaster is smaller than the remaining interval until the end-of-life criterion $T_c^{VB_K} - T_c$. In this case, the remaining tool life prediction is impossible as there is no forecasting value of the wear curve f_{VB} available at $T_c^{VB_K}$. The forecaster must be autoregressive to predict the remaining tool life at any time independently of H. An autoregressive forecaster allows predicting f_{VB} for any number of future steps $n \cdot H$ from T_c.

5.2 Implementation

In order to implement and evaluate the method for remaining tool life prediction presented in the previous section, the sensor system setup used in Chapter 4 is prepared for dataset generation in the following. Furthermore, from a software perspective, the basis for the training and evaluation of the prediction models is created.

5.2.1 Testbed for the Dataset Generation

The testbed developed in the following maps the milling process chain considering the prerequisites of dataset generation for single-part production described in Section 5.1. The testbed enables the consolidated collection of planning, in-process and post-process measurement data. Therefore, the sensor system developed in Chapter 4 for acquiring in-process data is extended by pre- and post-process stages. The resulting end-to-end data availability forms the basis for a dataset meeting the requirements of Section 5.1.1, particularly concerning available covariates and target variables for training machine learning models. Figure 5.5 provides an overview of the testbed.

In advance of the milling process, process planning is performed. As highlighted in Section 5.1.2, a dataset representing single-part production scenarios has to include the variation of geometric and process parameters. Hence, these parameters must be externally adjustable. The geometric parameters are transferred via

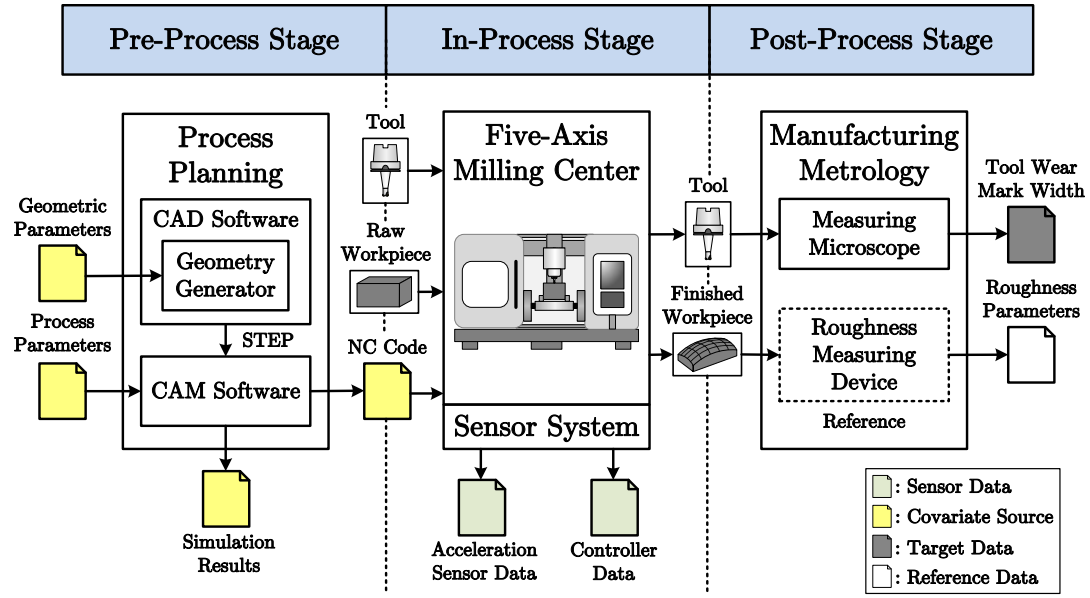

Figure 5.5: Overview of the testbed for execution of milling processes with guaranteed data availability along the milling process chain. The testbed is the basis for the dataset generation.

a software interface to the CAD software, which generates the 3D model of the workpiece automatically. In this work, the CAD software OpenSCAD [243] is used since it allows the programmatic generation of 3D models and thus the realization of corresponding geometry generators. The following Section 5.2.2 presents the parameterizable workpiece geometries used in this work in detail. From the CAD software, the 3D model of the workpiece is transferred to the CAM software. The CAM software converts the 3D model into NC code interpretable by the machine tool controller considering the adjustable process parameters (cutting speed v_c, feed per tooth f_z, axial depth of cut a_p, radial depth of cut a_e) and the geometric parameters of the used milling tool. In this work, the CAM software SolidCAM [244] is used for this purpose. The standard for the exchange of product model data (STEP) ISO 10303 [245] is the basis for transferring the 3D workpiece models from the CAD to the CAM software.

The machine tool performs the machining operation in the in-process stage using the generated NC code. The Hermle C 30 U milling center already used in the previous Chapter 4 with the installed sensor system according to Section 4.2 is used. Based on the milling tool under test monitored over its entire lifetime,

a raw workpiece is brought into the shape defined by its 3D model. During machining, the sensor system acquires both the acceleration sensor data and the sensor data used by the machine tool controller, i.e., current spindle speed, axes positions and drive loads.

After the machining of the workpiece, the measurement of the tool and workpiece is performed in the post-process stage using manufacturing metrology devices. The tool wear mark width of the cutting edges is measured using a microscope, and the surface roughness of the workpiece is determined with a roughness probe. The Garant MM1 [246] video measuring microscope and the MarSurf PS 10 [247] roughness measuring device are used. Section 5.1.1 describes the wear mark width as the primary tool life criterion considered in this work. The roughness measurement is performed for reference only to ensure the correlation between the surface roughness and the wear mark width.

5.2.2 Reference Process Design

The previously introduced testbed enables continuous collection of sensor, covariate and target data during milling. However, the testbed requires process boundary conditions to generate representative datasets. The process boundary conditions include the geometric parameters of the workpieces, the cutting parameters, the geometric and material properties of the used tools, and the material properties of the workpieces. The reference process is a process template for the parameterizable generation of the process boundary conditions within specified limits. Based on the reference process, the process planning steps can be performed according to Figure 5.5.

As described in Section 5.1.2, single-part production is characterized by the intra-tool life variability of the geometric and cutting parameters. The geometric and cutting parameters primarily influence the engagement conditions, i.e., the relative orientation of tool and workpiece surface. Furthermore, the complex shape of free-form workpieces leads to the intra-workpiece variability of the engagement conditions along contiguous tool paths. Since the engagement conditions directly influence the cutting force, they also affect the sensor signals. The objective of the reference process is to map this relationship.

Section 5.1.2 derives the parameters influencing the cutting force from a general

NURBS-based workpiece description and the five-axis milling model. The intra-tool life variability of the engagement conditions results primarily from the tool inclination and the surface curvature of the workpiece. Therefore, the engagement angle $\theta(t)$ represents the varying engagement conditions. In order to constrain the complexity of the reference process and facilitate the data analysis, a workpiece shape produced by three-axis milling can be selected, given the variation of $\theta(t)$ along contiguous tool trajectories.

Pocket geometry milling enables the abstraction from the five-axis to the three-axis milling model while maintaining the engagement angle variation. The variation of $\theta(t)$ along a contiguous tool path occurs as the milling tool enters the corners of a pocket. Figure 5.6 illustrates this based on a pocket geometry with four corners.

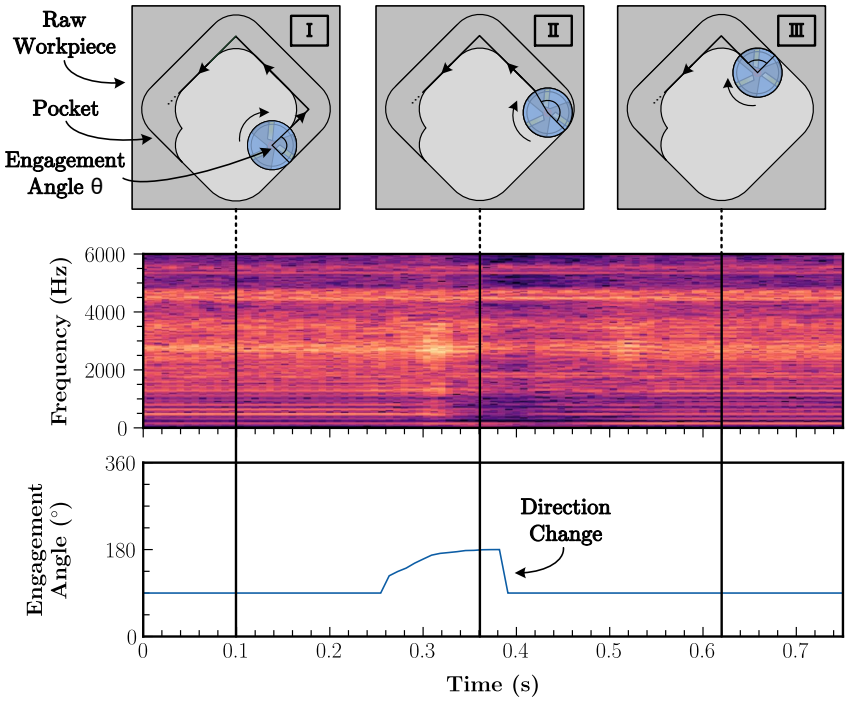

Figure 5.6: Engagement angle variation during pocket milling using the example of a square pocket geometry.

The straight-line movement with a path stepover of 50 % corresponding to a radial cut depth of $a_e = R$, with R being the tool radius, results in an engagement angle of 90° (I). When the tool enters the corner of the pocket, the engagement angle increases due to the corner angle of the geometry (II). The increased en-

gagement angle increases the chip volume and causes an extended load on the cutting edge. This is visible in the spectrogram of the acceleration sensor signal by an increased intensity, approximately between 0.26 s and 0.36 s. Once the cutter has reached the corner, the engagement angle approaches 180°. Since the movement direction changes in the corner, no feed motion and thus no cutting process occurs for a short time interval, approximately between 0.36 s and 0.42 s, leading to a drop of the vibration intensity. Subsequently, the cutting process continues in the new direction with an engagement angle of 90° (III). Adjusting the number of corners of the pockets changes the corner angle, which simultaneously influences the course of $\theta(t)$ during milling. This relationship is exploited in the following for the design of the reference process depicted in Figure 5.7.

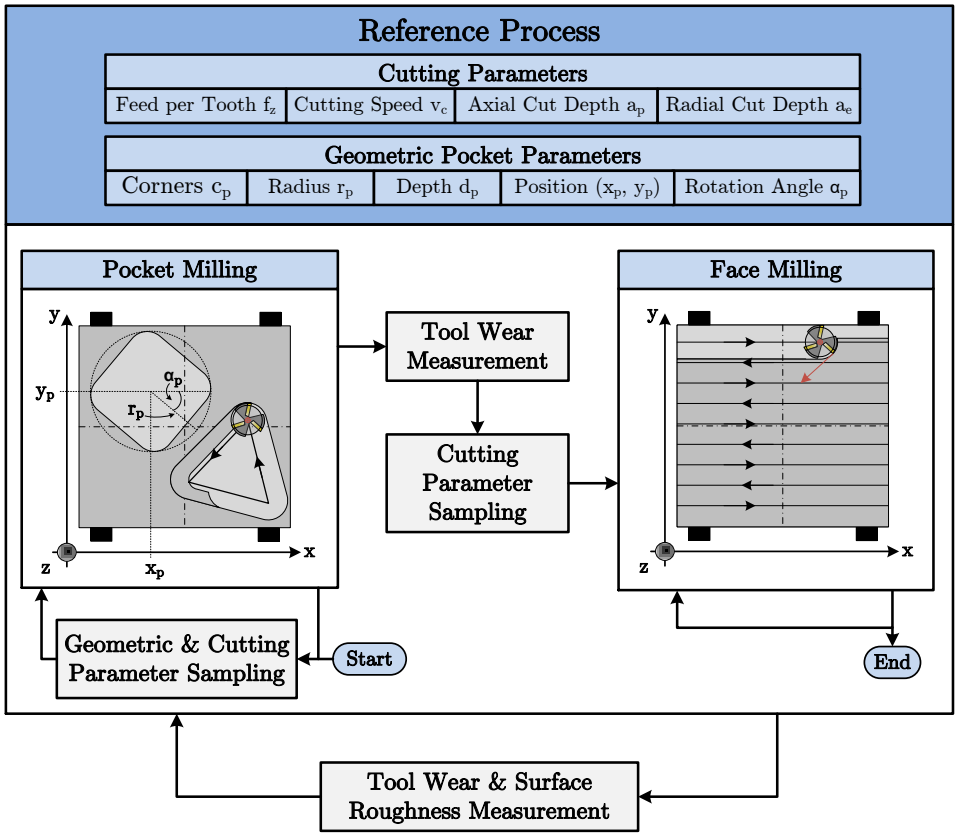

Figure 5.7: Experimental setup and procedure for the dataset generation using the pocket geometry-based reference process.

The pocket geometries aim to generate variable load patterns of the tool and thus simulate manufacturing of free-form surfaces. The cutting parameters of the reference process are the same as those already used for face milling in Chap-

ter 4. In addition, the reference process includes the geometric parameters of the pockets. The geometric parameters are the number of corners c_p varying the engagement angle, the radius r_p varying the pocket area, the depth d_p, the position of the pocket center point (x_p, y_p), and the rotation angle α_p. All parameters have a predefined range of values and thus form a multivariate distribution from which random combinations can be sampled to generate intra-tool life parameter variations.

At the beginning of the reference process, a defined number N_p of pockets are parameterized and then manufactured. After the completion of the manufacturing, the wear mark width VB of the tool cutting edges is measured. In addition, the cutting parameter sampling for the following face milling is performed. The face milling removes the pockets and resets the raw workpiece for the next process iteration. The face milling has to be repeated until the maximum pocket depth is reached. After face milling, the wear mark width and the surface roughness are measured. The reference process is repeated until the maximum tool life criterion VB_K has been reached. Table 5.1 provides a detailed overview of the reference process boundary conditions.

Table 5.1: Fixed and variable parameters of the reference milling process for the dataset generation.

Category	Parameter	Unit	Range / Value
Cutting Process	Feed per Tooth (f_z)	mm	$[0.4, 0.7]$
	Cutting Speed (v_c)	$\frac{mm}{s}$	$[170, 200]$
	Axial Cut Depth (a_p)	mm	$[0.5, 0.8]$
	Radial Cut Depth (a_e)	mm	R
Pocket Geometry	Corners (c_p)	-	$[3, 9]$
	Radius (r_p)	mm	$[30, 100]$
	Depth (d_p)	mm	$[1, 10]$
	Position (x_p, y_p)	mm	$[50, 150]$, $[50, 150]$
	Rotation Angle (α_p)	$^\circ$	$[0, 360]$
Milling Tool	Type	-	Indexable
	Tool Shape	-	Toroidal
	Edge Shape	-	Circular
	Number of Teeth (z_c)	-	3
	Max. Radius (R)	mm	10
	Edge Radius (r)	mm	4
	Max. Criterion (VB_K)	mm	0.8
Workpiece	Dimensions (l, w, h)	mm	200, 200, 200
	Material	-	X155CrVMo12-1 (DIN 1.2379)
	Consecutive Pockets (N_p)	-	4

Since the workpiece shapes are assumed arbitrary in single-part production and

can change randomly, sampling of the pocket geometry parameters has to be also random. In order to optimally cover the space of cutting process parameters, Latin hypercube sampling [248] is used. The varying cutting parameters must be statistically independent of the wear. Since the wear curve is known to be monotonically increasing, it is estimated in advance as a linear function with a slope of 1. The Latin hypercube sampling is repeated until the magnitude of the Pearson correlation coefficients between the points of the approximated wear curve and the samples of all cutting process parameters is less than 0.1. The number of samples and thus of reference process iterations is selected based on expert knowledge such that the tool life criterion is exceeded. The radial cut depth a_e is fixed at a constant value since it changes automatically due to the pocket geometries.

The used tool and workpiece material are motivated by the industrial practice of mold and die manufacturing. Toroidal tools with circular cutting edges are extensively used in multi-axis machining of free-form workpieces [72] for roughing and finishing operations and are therefore of particular relevance. The maximum tool life criterion is based on the manufacturer's recommendation. The steel X155CrVMo12-1 is characterized by moderate to poor machinability. Due to the high temperatures of the tool cutting edges when machining the steel, no cooling lubricant is used in practice. Omitting the cooling lubricant is adopted in the reference process.

5.2.3 Remaining Tool Life Modeling Framework

The remaining tool life prediction according to Section 5.1.3 requires a regressor and a forecaster model. Implementing these machine learning models requires a software framework that enables their training and validation based on a dataset representing the lifetime of multiple tool instances. A core objective of the machine learning-based method for remaining tool life prediction according to Section 5.1 is the holistic explainability of the final model decision. As highlighted in Section 2.5, previous sensor-driven approaches lack the explainability and interpretability of the tool life criterion regression using sensor-related features. However, this is crucial for flexible machine tools, which are subject to frequent adaptations and for the general transferability of a prediction method based on sensor-driven process monitoring. Without the explainability of the model deci-

sions, it is impossible to ensure that the model is based purely on process-related features that can be extracted in any machine configuration or across machines. Thus, an explainable remaining tool life prediction methodology significantly increases the robustness. In order to keep the effort for feature engineering low, an automated machine learning-based methodology is developed in this work according to Figure 5.8.

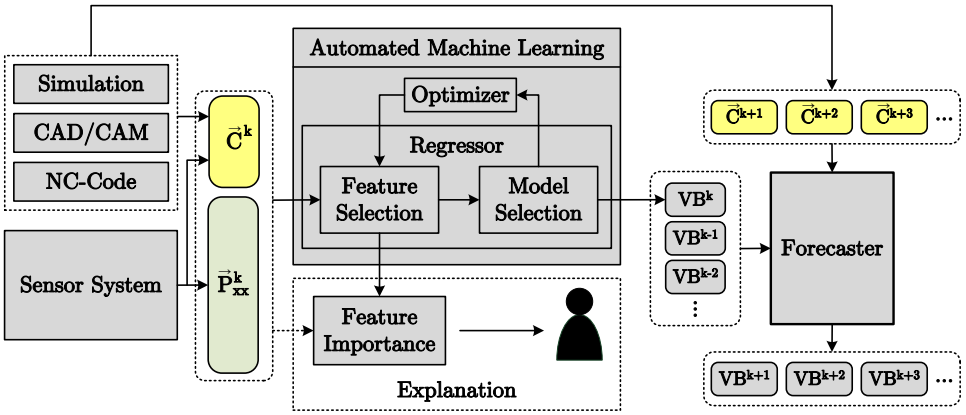

Figure 5.8: Methodology for automated and explainable feature selection from the sensor-based periodograms $\vec{P}^k_{xx}$ and the past and future covariates $\{\vec{C}^k, \vec{C}^{k+1}, \dots\}$ embedded into the remaining tool life prediction.

A regressor based on a feature selection component and a machine learning model is explicitly chosen. As described in Section 2.4.1, most feature selection methods internally apply a mechanism to determine feature importance. The feature importance is exploited with the automated machine learning mechanism, which performs a joint search for optimal hyperparameters and optimal pairing of feature selection and model. A heatmap is generated from the feature weighting for the best regressor, which visualizes the decisive features. Based on the heatmap, an expert can evaluate the model's transferability and robustness and optimize it if necessary. The heatmap is particularly important for the periodograms of the acceleration sensors $\vec{P}^k_{xx}$ since the frequency ranges the model relies on determine its machine dependence, as shown in Section 4.3. Based on the wear regression and the future covariates, the forecaster model performs the wear forecast and the prediction of the remaining tool life.

Sources of covariates are process simulations, CAD/CAM software tools, the NC code, and the sensor system itself. In particular, the sensor system developed

in this work can track the cutting time t_c of the milling tool based on the acceleration sensor signals, as described in Section 4.2.4. However, only past covariates usable by the regressor can be provided by the sensor system as it only targets the current process. If information about future machining operations is to be generated for the forecaster, the other covariate sources must be used. Below, the covariates used in the following sections for evaluation are listed and described. They can all be potential past and future covariates.

- **Cutting Time $\mathbf{t_c}$**: The sensor system can track the cutting time per workpiece Δt_c^k based on the acceleration sensor signals. The absolute cutting time can then be calculated by accumulation of Δt_c^k according to Equation 4.3. In addition, state-of-the-art CAM software tools also offer the possibility of estimating Δt_c^k as part of process simulations [87].
- **Removed Material Volume V**: Similar to the cutting time, the volume of material removed contains information about the load on the tool during machining. The determination of the removed volume is also part of state-of-the-art CAM software tools [84].
- **Material Removal Rate Q**: The material removal rate is the quotient of V and t_c and is the measure of the productivity of a process. Since it is a central optimization parameter, it is also part of state-of-the-art CAM software tools [81].
- **Cutting Process Parameters**: The varying cutting parameters v_c, f_z and a_p according to Table 5.1 are used.
- **Pocket Geometry Parameters**: The varying pocket geometry parameters c_p, r_p, d_p, x_p, y_p and α_p according to Table 5.1 are used.

Figure 5.9 shows the test strategy for the regressor and forecaster models aiming to ensure the robustness of the models and their evaluation with a limited number of available tools and their data.

The data from N tools is divided into training and testing regions for the training and evaluation of regressor and forecaster models. The data of a particular tool is selected for testing and not used for model training. Each tool is used once for testing to ensure that the prediction methodology is functional for arbitrary permutations and that its performance is not just based on the random selection of individual test tools. The procedure is referred to in the following as

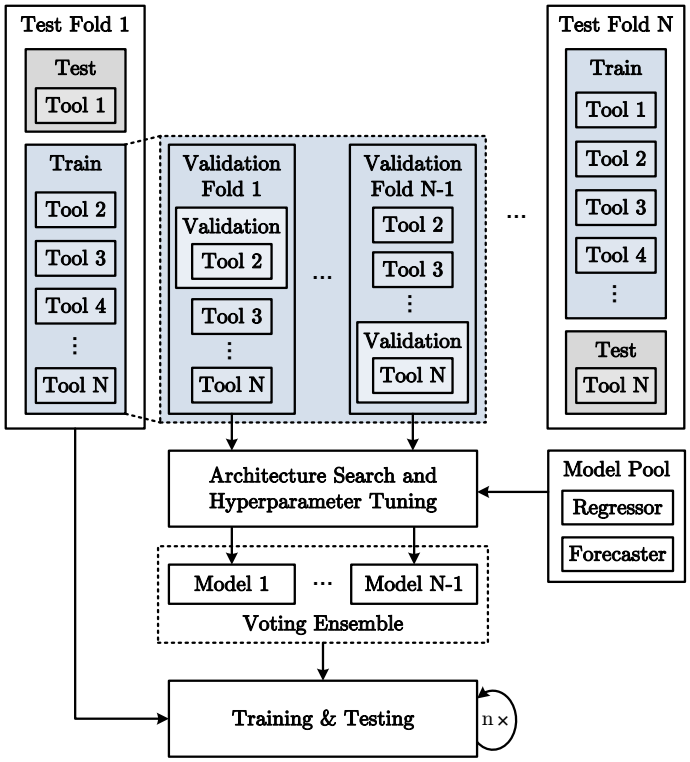

Figure 5.9: Test strategy of the remaining tool life prediction methodology based on a dataset with a limited number of represented tools.

leave-one-tool-out (LOTO) testing.

Based on the training segment with $N-1$ tools, the model architecture and hyperparameter search are then performed. For this purpose, model architecture and hyperparameter configurations are sampled from a model pool. When searching for the best configuration, a search criterion is required, enabling the evaluation of the configurations and their optimization. As with training, the prediction error can be used for this purpose. However, an additional validation tool has to be kept out of the training segment. The evaluation of a model using the data of the validation tool guides the search.

Problematic is that selecting a single random validation tool can overfit the models thus misleading the architecture and hyperparameter search. Hence, each tool is used once for validation to generate an overall model robust to the test tool data. The resulting models of the $N-1$ validation folds are combined into a voting ensemble. The outputs of the models are averaged to compensate for overfitted models. The procedure is referred to as LOTO cross-validation.

After the model architecture and hyperparameter search is complete, the voting ensemble models are trained using the data from all training tools. Subsequently, its evaluation is performed based on the data of the test tool. The stochastic nature of parameter initialization and optimization of machine learning models may lead to different model outputs for multiple training runs. To allow for a reliable statement regarding the model quality, the training and testing step is repeated n times.

The regressor and forecaster are models with different objectives, structures and inputs. While the procedure for training and evaluating the models according to Figure 5.9 is the same, the underlying implementation differs. The regressor is implemented based on the Auto-sklearn [177] library since it supports the methodology according to Figure 5.8. Auto-sklearn offers various importance-based feature selection methods and is based on the joint optimization of feature selection and machine learning model. The forecaster is implemented based on the Darts library [173]. Since Darts does not natively support automated machine learning like Auto-sklearn, an additional wrapper based on the Tune library [249] is implemented for automated architecture and hyperparameter search. In combination with Bayesian optimization, the asynchronous successive halving algorithm (ASHA) is used for the architecture and hyperparameter search of the forecaster models [178].

5.3 Evaluation

The following sections present the evaluation of the components of the remaining tool life prediction methodology developed in this work. The evaluation is based on a dataset generated using the testbed and the reference process according to Section 5.2. Besides the regressor and forecaster models, the explainability of the methodology is analyzed.

5.3.1 Dataset Exploration

Before evaluating the machine learning models, the generated dataset has to be examined. The dataset includes data from seven tools of the type specified in Table 5.1 over their entire lifetime. Since a cutter head with indexable inserts

is used, the term tool is synonymous with a set of three indexable inserts in the following. The data was generated based on resampling the cutting process and pocket geometry parameters, as shown in Figure 5.7. Figure 5.10 depicts the mean, minimum and maximum values of the measured flank wear mark widths VB and the time points of the parameter change over the cutting time t_c.

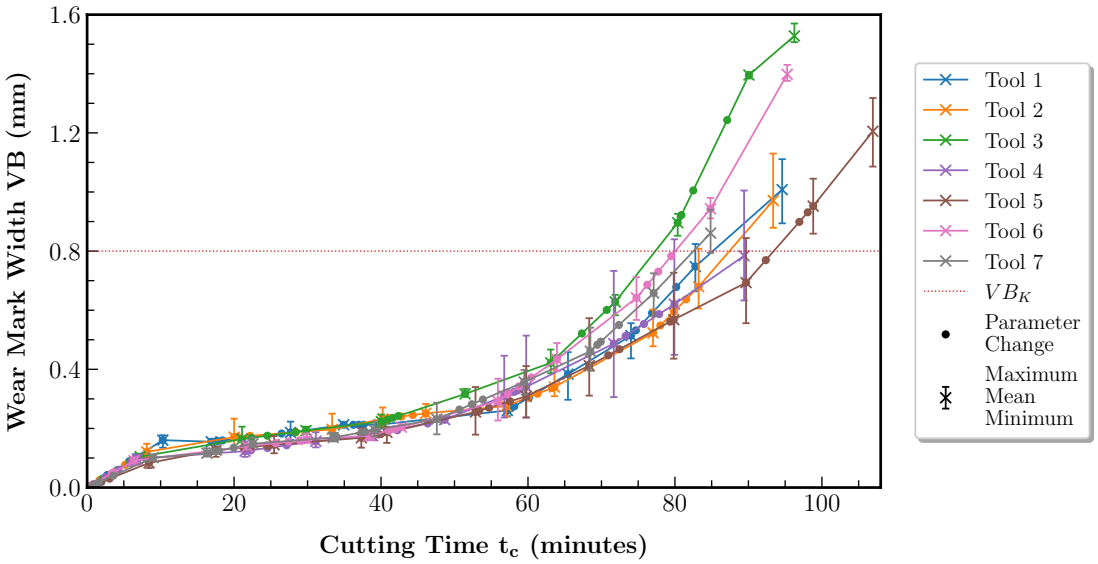

Figure 5.10: Tool wear mark width measurements and parameter resampling points for the seven tools of the dataset generated for the analysis and verification of the remaining tool life prediction methodology.

VB develops similarly for all tools up to a cutting time of approximately 60 minutes. From then on, wear progresses faster, and the scatter of the measured VB values increases. The maximum difference in cutting time $\Delta t_c^{VB=0.8mm}$ evaluated at the tool's end-of-life criterion VB_K of 0.8 mm is 16 minutes.

This chapter is based on the assumption that gradual tool wear leads to an increase in workpiece surface roughness and thus to a reduction in workpiece quality. Therefore, only the tool wear is considered for predicting the remaining tool life. Since the assumption results from the investigation of the face milling experiment according to Chapter 4, it must be ensured that it also applies to the dataset. Table 5.2 shows the Pearson correlation coefficients $\rho(\bar{VB}, \bar{R}_z)$ between the mean wear mark width and the mean workpiece surface ten-point height of irregularities for all tools in the dataset.

The tool wear and the workpiece surface roughness show an overall high correlation. Therefore, the assumption justifying the flank wear mark width as the

Table 5.2: Pearson correlation coefficients of the average workpiece surface ten-point height of irregularities $\bar{R}_z$ and the average tool wear mark width $\bar{VB}$ per tool included in the dataset.

	Tool 1	**Tool 2**	**Tool 3**	**Tool 4**	**Tool 5**	**Tool 6**	**Tool 7**
$\rho(\bar{\mathbf{VB}}, \bar{\mathbf{R}}_\mathbf{z})$	0.51	0.81	0.99	0.99	0.99	0.90	0.71

primary tool life criterion can be confirmed.

In addition to process quality, the manufacturing time and hence the process productivity are crucial factors. Process quality and productivity both influence the economic efficiency of production. For the tools in the dataset, the average material removal rate $\bar{Q}$ is determined as a measure of process productivity on the basis of the volume removed during machining and the cutting time. Table 5.3 shows $\bar{Q}$ for all tools.

Table 5.3: Average material removal rate $\bar{Q}$ and standard deviation over all manufactured workpieces per tool included in the dataset.

	Tool 1	**Tool 2**	**Tool 3**	**Tool 4**	**Tool 5**	**Tool 6**	**Tool 7**
$\bar{Q}$ ($\frac{mm^3}{min}$)	367.7 (±17.5)	343.7 (±9.9)	328.8 (±11.2)	350.1 (±23.0)	375.27 ±(9.9)	343.5 (±19.2)	401.9 (±11.3)

Tool 7 has the highest material removal rate and Tool 3 has the lowest. Comparing the wear curves of the two tools, it becomes evident that Tool 7 reaches the wear threshold VB_K later than Tool 3 despite the higher material removal rate. Tool 5 with the highest tool life has only the second-highest material removal rate. A trade-off between productivity, wear progress, and product quality must be found.

5.3.2 Analysis of the Feature Importance

The implementation of the remaining tool life prediction, according to Section 5.2.3, has the goal of automated and explainable feature selection based on which the tool life criterion VB and subsequently the remaining tool life is determined. In this section, the methodology developed for this purpose, according to Figure 5.8, is examined first. The focus is on the automated machine learning-based regressor model and the integrated mechanism for explaining the feature selection. For validating the methodology, a feature space is defined as a basis for the selection. It consists of the periodograms of the three-axis acceleration sensor system

introduced in Chapter 4 and all process covariates according to Section 5.2.3.

The periodograms are determined according to Section 4.1.4 by applying the Welch method to the signal segments of contiguous tool trajectories k per sensor channel i. The STFT on which the Welch method is based is parameterized with a window size of 8192 samples and a window overlap of 75 %. Hence, a periodogram vector per sensor channel $\vec{P}_{xx}^{i,k}$ has 4096 elements with $i = \{x, y, z\}$. The periodogram vectors of the three sensor channels constitute the tensor $\mathbf{P}_{xx}^{k}$ and the global tensor $\mathbf{P}_{xx}^{xl}$ summarizes the acceleration sensor-based periodogram tensors for all tool trajectories over the lifetime of a tool instance. The tensor $\mathbf{C}$ summarizes the covariate vectors $\vec{C}^{k}$ over the lifetime of a tool instance.

Chapter 4 shows that the frequency range of 0 to 6 kHz contains a high degree of process information. There are intervals in the frequency range that can be assigned to the process, the machine (natural frequencies), and its state (excitation-induced vibration response during idling). The signal power in all frequency intervals may correlate with the tool life criteria, thus serving as a basis for regression-based modeling. The evaluation in this section first aims to show that the relevant intervals can be found automatically by the automated machine learning-based regression methodology. Model optimization can subsequently be performed, applying the feature importance-based explanation of the methodology, e.g., to obtain machine-independent models.

Before validation, the Auto-sklearn [177] environment is first configured for the automated machine learning-based training. Both the meta-learning and ensembling capabilities of Auto-sklearn are enabled. The maximum time budgets are set to 10 minutes for the entire training and 30 seconds for training a single model configuration with a memory limit of 20 GB. The R^2 score function is used as a metric for training. The training and testing are repeated five times according to the LOTO strategy shown in Figure 5.9. An input feature vector per contiguous tool trajectory based on the periodogram tensors $\mathbf{P}_{xx}^{k}$ between 0 and 6 kHz and the covariates $\vec{C}^{k}$ has 588 elements. Since the regression is only required up to the end-of-life criterion VB_K to enable the forecast, the range of VB for prediction and evaluation is limited to 0.8 mm. Figure 5.11 shows the regression results. For a comprehensive error analysis, the prediction errors in terms of RMSE and MAE over the dataset are summarized in Table 5.4. The error metrics are calculated for the mean prediction and the mean measurement

values of *VB*.

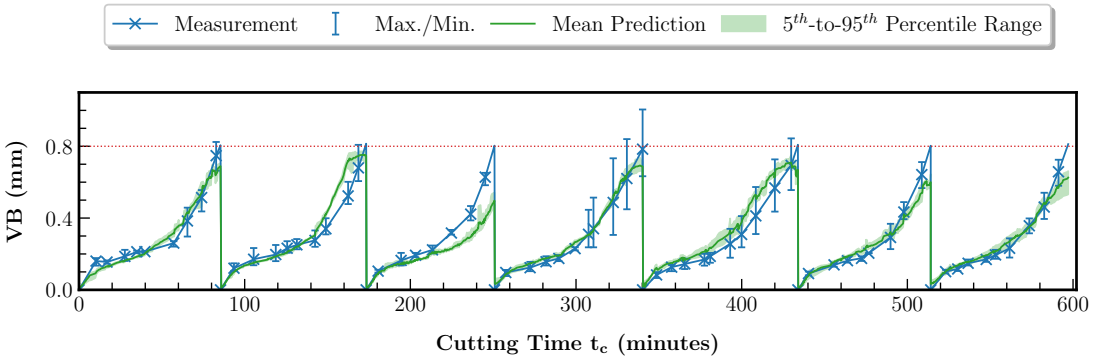

Figure 5.11: Prediction results of the automated machine learning-based tool wear regression to investigate the feature importance. The input features of the model are the acceleration sensor periodogram vectors $\mathbf{P}_{xx}^{xl}$ in a range of $[0, 6000]$ Hz and the past covariate vectors $\mathbf{C}$ with all covariates. The results for Tools 1 to 7 are shown from left to right.

Table 5.4: Prediction errors of the tool wear regression to investigate the feature importance. The input features of the model are the acceleration sensor periodogram vectors $\mathbf{P}_{xx}^{xl}$ in a range of $[0, 6000]$ Hz and the past covariate vectors $\mathbf{C}$ with all covariates.

Metric	Prediction Errors per Tool (mm)							
	Tool 1	Tool 2	Tool 3	Tool 4	Tool 5	Tool 6	Tool 7	Mean
RMSE	0.038	0.068	0.107	0.026	0.066	0.065	0.041	0.059 (±0.025)
MAE	0.031	0.046	0.070	0.021	0.055	0.045	0.028	0.042 (±0.016)

Figure 5.11 and Table 5.4 show that the regression of the flank wear mark width *VB* is possible for all tools using the sensor data-based features and covariates. Overall, the mean RMSE across the dataset is 0.059 mm and the mean MAE is 0.042 mm.

Based on the regression, the feature importance is determined. For this purpose, the feature scores and feature selection masks of the feature selection modules are extracted from all model configurations found by the Auto-sklearn environment. Per tool, i.e., per modeling run, the feature selection mask is superimposed on the feature scores to set the scores of unselected features to 0. Subsequently, the feature scores are normalized and averaged to derive the feature importance. Figure 5.12 shows the feature importance averaged over the complete dataset and split by periodograms and covariates.

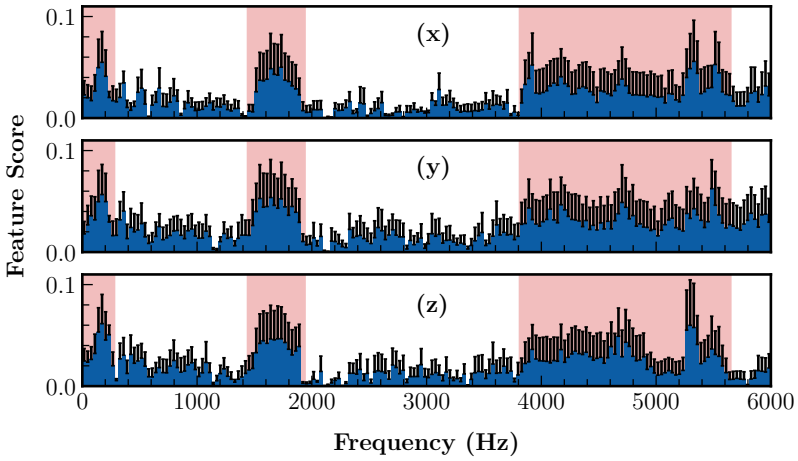

(a) Periodogram importance.

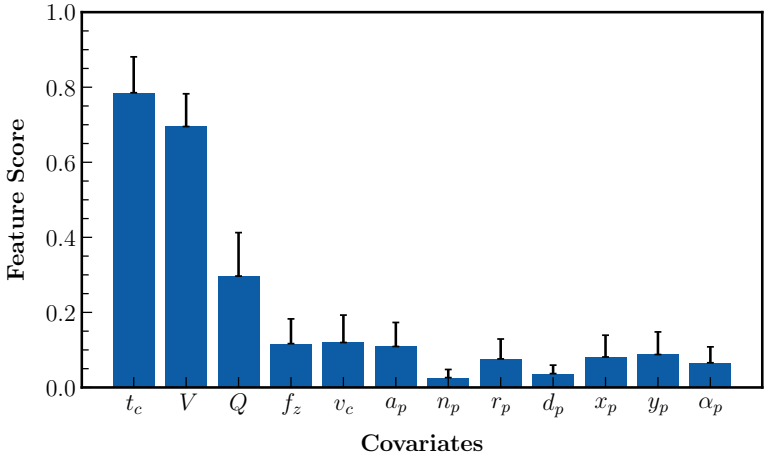

(b) Covariate importance.

Figure 5.12: Feature importance analysis of covariates and periodogram frequency bins derived from the automated machine learning-based wear regression. The mean feature scores and their standard deviation over all tools are shown.

Figure 5.12a shows three dominant frequency ranges with maximum feature importance scores. The first frequency range is approximately between 0 Hz and 280 Hz. Based on the Campbell diagrams in Sections 4.3.1 and 4.3.2, depicting the frequency response due to spindle rotation with and without machining, it can be shown that the process-related tooth engagement frequency Ω_z is located here. Based on the parameters of the reference process according to Table 5.1 underlying the dataset, the Ω_z is between 135 Hz and 159 Hz. This corresponds to the range of maximum feature scores. The second and third dominant frequency ranges from 1440 Hz to 1940 Hz and from 3810 Hz to 5650 Hz, respectively, can be assigned to the machine structure and components. They can be identified

in the Campbell diagram showing the frequency response due to spindle rotation without machining in Section 4.3.1. The response in these frequency intervals results e.g. from imbalances or bearing errors, but also natural frequencies are located here. In conclusion, the feature-importance-based method for explaining the model decisions can automatically identify the relevant frequency ranges related to the tool wear.

By looking at the feature importance scores of the covariates, it becomes clear that these are weighted more strongly and thus contribute more to the model output than the periodograms. In particular, the cutting time t_c and the removed material volume V have a significant influence with mean feature scores of 0.8 and 0.7 respectively. One possible reason for this is that, compared to the other covariates, t_c and V are accumulative variables and hence correlated with the tool wear.

5.3.3 Optimization of the Tool Wear Regression

The results of the previous feature importance analysis are used in the following to optimize the tool wear regression. This section has several objectives. First, based on the relevant frequency ranges identified in the previous section, the performance of a machine-independent model will be investigated. For this purpose, the frequency range of the periodograms $\mathbf{P}_{xx}^{xl}$ is limited to the value range between 0 and 625 Hz to use only the tooth engagement frequencies Ω_z and their first harmonics. Thus, no machine-dependent vibration components are used for modeling. In addition, the covariates $\mathbf{C}$ are restricted to the two accumulative variables with the maximum feature scores t_c and V. Besides enabling the machine independence, reducing the feature space size is expected to improve the architecture and hyperparameter search of the automated machine learning-based training and hence the model performance.

Furthermore, the significance of the covariates for modeling is verified by using only the covariates or the periodograms as input features, respectively. Lastly, the model performance is compared using the NC controller signals according to Chapter 4 in addition to the acceleration sensor signals. Therefore, the PSD-estimating periodograms $\mathbf{P}_{xx}^{nc}$ of the axis drive power signals are derived. As described in Section 2.3.1, the drive power is directly related to the cutting force

and thus also represents the tool wear. Table 5.5 shows the prediction errors of the feature configurations being compared.

Table 5.5: Prediction errors of the tool wear regression with variable input features. The covariate vectors $\mathbf{C}$ are reduced to t_c and V and the frequency range of $\mathbf{P}_{xx}^{xl}$ is $[0, 625]$ Hz. The following feature configurations are evaluated: I → ($\mathbf{P}_{xx}^{xl}$, $\mathbf{C}$), II → ($\mathbf{P}_{xx}^{xl}$), III → ($\mathbf{C}$), IV → ($\mathbf{P}_{xx}^{xl}$, $\mathbf{P}_{xx}^{nc}$, $\mathbf{C}$), → ($\mathbf{P}_{xx}^{nc}$, $\mathbf{C}$)

Tool	Prediction Errors per Input Feature Configuration (mm)									
	I		II		III		IV		V	
	RMSE	MAE	RMSE	MAE	RMSE	MAE	RMSE	MAE	RMSE	MAE
1	**0.034**	**0.029**	0.169	0.133	0.035	**0.029**	0.049	0.038	0.046	0.036
2	0.052	0.038	0.140	0.102	0.046	**0.035**	**0.045**	0.036	0.046	**0.035**
3	0.070	0.047	0.189	0.155	**0.062**	**0.042**	0.086	0.059	0.074	0.053
4	**0.028**	**0.022**	0.131	0.097	0.031	0.025	0.032	0.026	0.030	0.025
5	0.056	0.044	0.199	0.147	**0.053**	**0.042**	0.063	0.052	0.055	0.045
6	**0.054**	**0.035**	0.182	0.143	0.057	0.036	0.075	0.051	0.069	0.043
7	**0.025**	**0.019**	0.162	0.132	0.029	0.021	0.031	0.025	0.047	0.039
Mean	**0.045** (±0.016)	**0.033** (±0.010)	0.167 (±0.023)	0.130 (0.021)	**0.045** (±0.012)	**0.033** (±0.007)	0.054 (±0.020)	0.041 (±0.012)	0.052 (±0.014)	0.039 (±0.008)

The evaluation with reduced feature space (Configuration I) has a mean RMSE of 0.045 mm and an MAE of 0.033 mm. Compared to the input feature configuration in the previous section, this corresponds to an error reduction of 24 % for the RMSE and 21 % for the MAE. Machine-independent modeling is thus possible, and reducing the feature space allows a more efficient architecture and hyperparameter search while maintaining the same time budget for training. Using only the periodograms (Configuration II) exhibits the maximum error with an RMSE of 0.167 mm and an MAE of 0.130 mm. Figure 5.13 shows the prediction results of Configuration II.

Figure 5.13 shows that modeling solely based on periodograms $\mathbf{P}_{xx}^{xl}$ is not possible. The variable process conditions affect the sensor signals such that without additional process-describing information from the covariates no relationship to *VB* can be learned. In comparison, using only the covariates exhibits the same error as with Configuration I, with both RMSE and MAE being minimal for configurations I and III. However, looking at the training runs per tool of configuration 1 using $\mathbf{P}_{xx}^{xl}$ and the covariates, more minimal prediction errors occur than for Configuration III. Overall, the significance of the covariates for the tool wear regression can be confirmed.

Configurations IV and V using the drive power-based periodograms $\mathbf{P}_{xx}^{nc}$ have RMSE values of 0.054 combined with $\mathbf{P}_{xx}^{xl}$ and the covariates and 0.052 mm

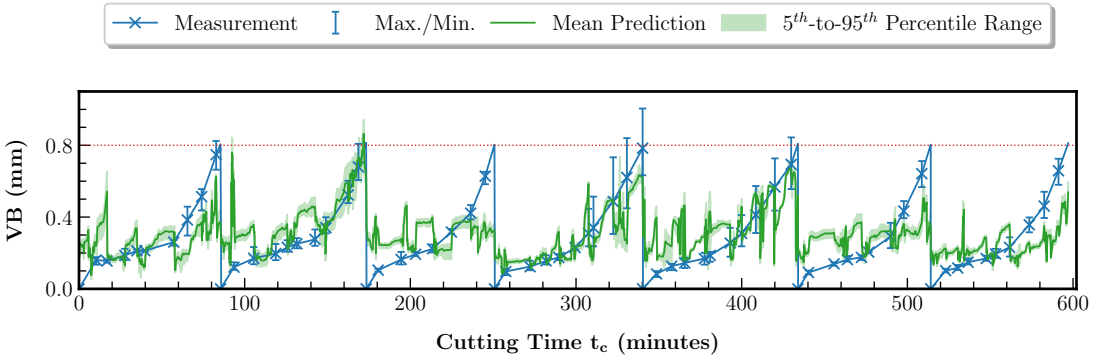

Figure 5.13: Prediction results of the automated machine learning-based tool wear regression using only the acceleration sensor periodograms $\mathbf{P}_{xx}^{xl}$ in a range of $[0, 625]$ Hz as inputs.

combined with the covariates only. The MAE values are 0.041 mm and 0.039 mm, respectively. The errors are 20 % and 16 % higher for the RMSE and 24 % and 15 % higher for the MAE than for Configuration I. Thus, modeling based on the control signals is generally possible, but with reduced performance compared to the acceleration signals or covariates. A possible reason for this may be the reduced sampling rate, which according to Chapter 4 is only 110 Hz for the control signals. In addition, the inertia of the axis drive trains can negatively affect the process information in the sensor signals.

5.3.4 Analysis of the Remaining Tool Life Prediction

Based on the feature analysis and investigation of the tool wear regression in the previous sections, the remaining tool life prediction is analyzed in the following. The remaining tool life prediction is performed using tool wear forecasting, as described in Section 5.2.3. The main objective of this section is to show that remaining tool life prediction is possible under intra-tool life variability of process conditions. Furthermore, it is investigated how the process-describing information of future machining operations, i.e., future covariates e.g. from simulations, CAD/CAM software tools, or NC code, affects the prediction. The forecaster model is implemented using the Darts [173] and Tune [249] libraries. Before evaluation, the model type of the forecaster must be determined. The model type must support the use of future covariates. Because of this property and its ability to learn complex temporal relationships, the LSTM architecture, commonly used

in forecasting problems, is chosen.

The forecaster model is first tuned and trained based on the LOTO mechanism according to Section 5.2.3. The LSTM model is characterized by a single layer and a hidden dimension, i.e. a number of hidden states, of 25. The length of the model input sequences between 12 and 60 samples and the output sequences between 1 and 36 samples is subject to the model tuning. Furthermore, the hyperparameters of batch size in the range of $[4, 32]$ and learning rate in the range of $[1e{-}5, 1e{-}2]$ are tuned. The tuning is guided by the MAE and implemented using the tree-structured Parzen estimator [250] as a search algorithm and the ASHA [178] as a scheduler. An LSTM instance can train for a maximum of 30 epochs while early stopping is employed. In total, the training and testing of the models are repeated five times, as for the regressor model.

Model inputs and outputs during training are the respective tools' past and future VB sequences. The cutting time t_c is investigated as a future covariate since it has the highest significance for wear prediction according to Section 5.3.2. The assumption that t_c is available in advance for future workpieces is valid since it can be estimated using state-of-the-art CAM and process simulation tools, as described in Section 5.2.3. For comparison, the forecast without future covariates is considered. During testing, the predictions of the tool wear regression are provided to the LSTM model as input sequences. Figure 5.14 shows the tool wear forecast at an instantaneous cutting time of $T_c = 25$ minutes.

The qualitative comparison of the forecasts in Figures 5.14a and 5.14b shows that the mean forecasts at the end-of-life criterion $VB_K = 0.8$ mm deviate further from the measured values without future covariates. In addition, the 5^{th}-to-95^{th} percentile range indicates that the dispersion of the predicted values can be reduced by using future covariates. In order to evaluate the accuracy of the remaining tool life prediction quantitatively for all instantaneous cutting times, the remaining tool life over t_c is determined from the forecasts in the following. The remaining tool life is derived based on the time the end-of-life criterion $VB_K = 0.8$ mm is reached by the forecast. Figure 5.15 shows the actual and estimated remaining tool life curves and the prediction errors are summarized in Table 5.6.

The remaining tool life prediction without future covariates has an average RMSE of 9.5 minutes and an MAE of 7.8 minutes. With t_c as a future covari-

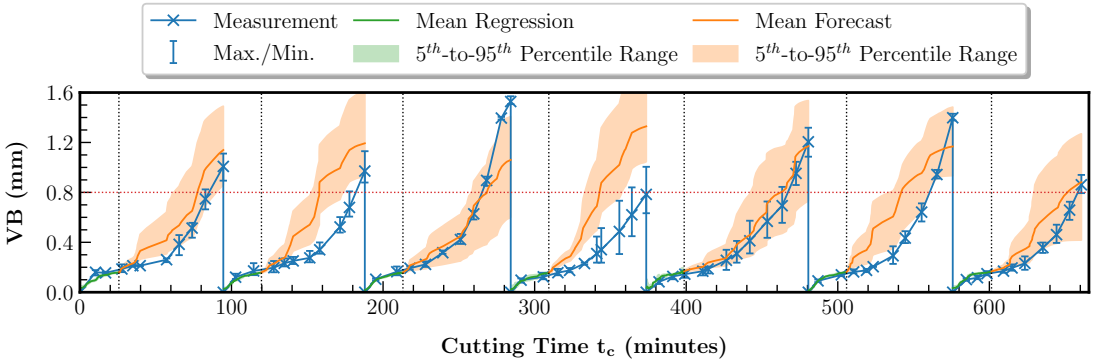

(a) No future covariates.

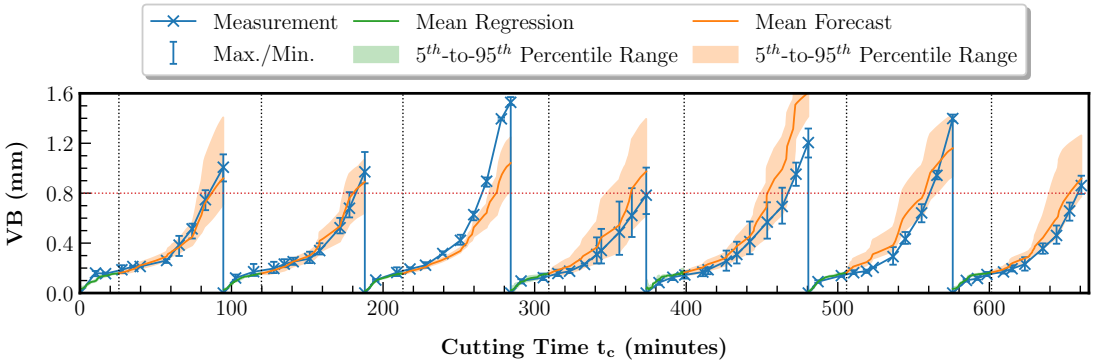

(b) Cutting time t_c as future covariate.

Figure 5.14: Tool wear forecasting results at $T_c = 25$ minutes, comparing two configurations of future covariates.

Table 5.6: Prediction errors of the remaining tool life derived from the tool wear forecast without future covariates and with cutting time t_c as future covariate.

Tool	Prediction Errors per Future Covariate Configuration (minutes)			
	None		Cutting Time t_c	
	RMSE	MAE	RMSE	MAE
1	5.7	4.7	**2.0**	**1.6**
2	12.9	10.8	**2.7**	**2.4**
3	**7.9**	**7.2**	9.9	9.9
4	16.5	14.0	**12.2**	**11.4**
5	**6.9**	**6.0**	9.8	9.4
6	7.1	4.9	**3.0**	**2.6**
7	9.6	6.5	**6.1**	**5.6**
Mean	9.5 (± 3.6)	7.8 (± 3.2)	**6.5** (± 3.8)	**6.1** (± 3.8)

ate, the RMSE is reduced by 32 % to 6.5 minutes and the MAE by 22 % to 6.1 minutes. Determining the average RMSE and MAE from all minimum errors per tool results in errors of 5.8 and 5.3 minutes, respectively. In Figure 5.15 the difference in prediction accuracy becomes evident. Without future covariates, the

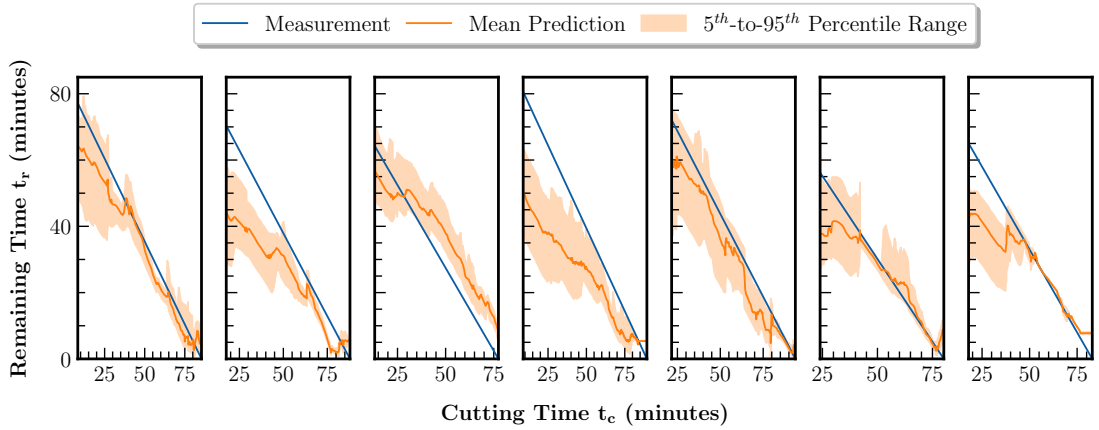

(a) No future covariates.

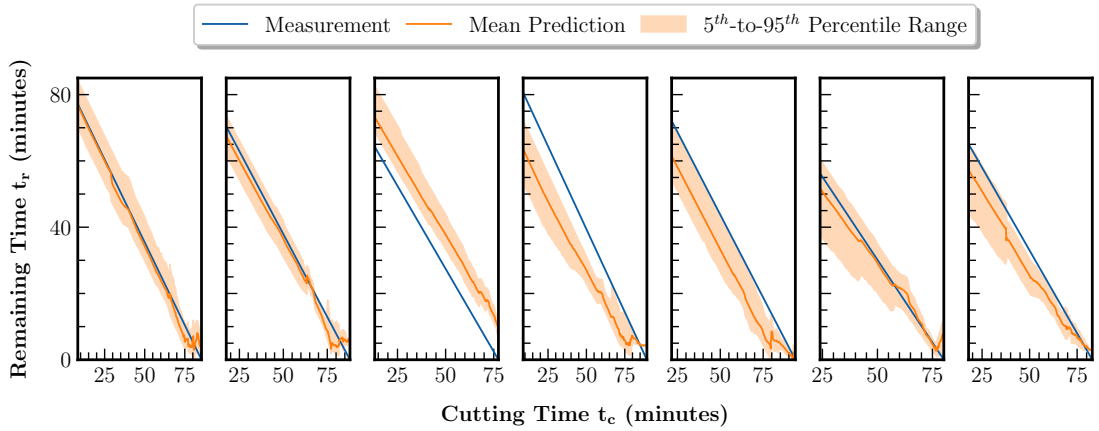

(b) Cutting time t_c as future covariate.

Figure 5.15: Remaining tool life prediction results based on the tool wear forecasts comparing two configurations of future covariates.

prediction is inaccurate, especially in the early stages of tool life, up to approximately 55 minutes for most of the tools (Tools 1, 2, 4, 6 and 7). Including the future covariates allows a mostly accurate estimation of the remaining tool life at arbitrary time points. Only Tools 3, 4, and 5 are characterized by a constant offset error. A reason for this could be the fact that their tool wear curves are the outermost, which causes that the value ranges are not represented evenly in the dataset. For Tool 2, the maximum optimization of the prediction is achieved by an error reduction of 79 % in RMSE and 78 % in MAE. In addition, the dispersion of the predicted values over the entire tool life can be reduced using future covariates, indicating a reduction in model uncertainty. Overall, it can be confirmed that the remaining tool life prediction is possible under variable

process conditions. In addition, an increase in accuracy and higher robustness of the prediction can be achieved by including process-describing information about future machining operations.

5.4 Discussion

The main objective of this chapter was to investigate the prediction of remaining tool life in single-part production. Therefore, it should be shown that prediction is possible under the intra-tool life variability of process conditions, i.e., cutting parameters, workpiece geometry, and derived tool trajectories. Furthermore, it should be investigated whether knowledge about future machining processes can be used to improve the remaining tool life prediction.

The methodology for predicting the remaining tool life consists of the regression of the tool life criterion, i.e., the flank wear mark width VB and its forecast. First, the regression of tool wear was analyzed in Sections 5.3.2 and 5.3.3. It could be shown that the automated and explainable regression approach was able to identify relevant features. Using expert knowledge, the features were then used to generate optimized and machine-independent wear regression models. Overall, it was thus shown that wear regression for intra-tool life variability of process conditions is possible. Furthermore, it was found that especially the covariates of cutting time t_c and removed material volume V are significant for the prediction quality of the models. A prediction based only on the direct sensor data-related features is not possible.

The regression methodology can automatically identify features that a human expert can also find through experiments and domain knowledge. However, since the regression method is automated machine learning-based and requires no intervention by an expert, it can replace resource-intensive feature engineering and enable the continuous adaptivity of the models. Its explainability enables targeted model optimization and enhancement of their robustness, e.g., against environmental or application-related influences thus ensuring transferability and generalizability. The high importance of the covariates, especially of the cutting time t_c and the removed material volume V, for the wear regression can be explained by the fact that the variables represent the history of the load on the tools accumulatively. t_c and V thus correlate with the tool wear but are at the

same time directly dependent on the cutting parameters and the tool trajectories. Accordingly, they allow the feasible wear prediction under the intra-tool life variation of the process parameters. On the other hand, the intra-tool life variation of the process parameters influences purely sensor signal-based features such as the periodograms, so that the dependencies on the process parameters cannot be resolved. Therefore, tool wear regression is not possible using only signal-based features. Since repetitive signal patterns occur in series production, the tool wear can be inferred by signal-based pattern recognition and their course over time. Previous methods for wear and remaining tool life prediction are limited to this. In contrast, the method developed in this work is universally applicable, independent of the production scenario. However, it becomes clear that tracking the covariates and especially the cutting time t_c, e.g., using the sensor system introduced in Chapter 4, is inevitable.

The wear forecast based on the wear regression is the second step of the methodology for predicting the remaining tool life and was investigated in Section 5.3.4. Overall, it was confirmed that the forecast and the remaining tool life prediction are possible under the intra-tool life variability of the process conditions. Furthermore, the investigation of future covariates showed that the accuracy of the forecast could be increased and the uncertainty of the forecast could be reduced. Compared to the covariate-free forecast, the prediction can be improved especially in the early stages of tool life with knowledge of the cutting time in advance, e.g., based on process simulations of future machining operations.

The inaccuracy of the covariate-free forecast in the early stages of the tool life can be explained by the fact that the course of the tool wear curves in this range is still similar for all tools. Hence, the uncertainty concerning the time point of reaching the end-of-life criterion is high, which only changes when the wear curves drift apart. However, the future course of tool wear can be estimated independently of this if the information on the future development of a wear-correlated variable such as the cutting time t_c is available. A drawback of the methodology evaluated in Section 5.3.4 is that it is based on the assumption of the availability of the optimal future cutting time. Therefore, the estimated future cutting time equals the measured cutting time. However, inaccuracies in the cutting time estimation, e.g., due to simulation errors, can influence the performance of the remaining tool life prediction in practice. The inaccuracies

can be compensated by continuously monitoring the cutting time and optimizing the simulation and cutting time estimation models.

6. Summary and Future Work

6.1 Summary and Conclusion

The main objective of this work was the investigation of the remaining tool life prediction under the variable process conditions of single-part production. The variable process conditions lead to variable tool load, affecting the tool life and sensor signals used for monitoring. Therefore, the three sub-research questions summarized below should be answered:

I. Which monitoring variables are suitable for permanent and transferable indication of quality-related tool life criteria under frequent changes in machine and process configuration?

II. What information must be extracted from sensor data or collected from other data sources to enable reliable remaining tool life prediction?

III. Can the remaining tool life prediction be optimized by incorporating a priori accessible information about future machining operations?

In order to answer the first research questions, multiple process monitoring variables were first assessed with respect to the requirements of single-part production. The assessment showed that monitoring variables requiring tight sensor integration into the process, such as force and temperature, are unsuitable because they must be adjusted with any change in the process configuration. The process-independent sensor integration at a greater distance from the process, as given for vibration or drive signals, enables permanent process monitoring. However, drive signals are always dependent on the design of the respective machine and its drives. Only vibration offers the possibility of process-independent sensor integration with simultaneous machine independence of the sensor signals. Therefore, the vibration was selected as the primary monitoring variable.

In order to confirm the machine independence of vibration as a monitoring variable and simultaneously ensure that quality-related parameters can be represented, a test setup was implemented on a five-axis milling machine. The flank wear mark width of the cutting edges was used as the primary quality-related parameter in this work since it determines both the dimensional accuracy and the surface roughness of the workpieces. A three-axis acceleration sensor system was installed on the machine spindle to acquire the machine vibrations and structure-borne sound. First, the machine tool was characterized by identifying its natural frequencies and machine component-related frequency responses. Then, face milling tests were performed. A clear correlation between tool wear, workpiece surface roughness, and multiple frequency ranges of the acceleration sensor signals could be shown. Comparing the results with the machine characterization, machine-specific frequency ranges could be separated from purely process-related vibrations. Hence, it was proven that the vibration signals contain information on the target parameters independent of the machine and its configuration.

The method proposed in this work for predicting the remaining tool life consists of tool wear regression based on vibration sensor data and subsequent wear forecast. The wear regression is based on an automated and explainable approach to identify relevant input features without feature engineering by a human expert. In order to evaluate the method, a dataset was first recorded based on the test setup described above, representing single-part production by varying workpiece geometries as well as cutting parameters and, thus, tool load throughout the tool life. The results of the initial regression evaluation indicated an MAE of the flank wear mark width of 0.042 mm with an end-of-life criterion of 0.8 mm. The significance analysis of the features showed that the variables of the cutting time and the removed material volume are particularly relevant for the prediction quality of the regression models. An explanation for this is that the variables accumulatively summarize the history of tool load. Thus, although they represent the process conditions, they are at the same time strongly correlated with the tool wear. Optimization of the regression models based on this knowledge enabled a 21 % error reduction to an MAE of 0.033 mm. Thus, the feasibility of the automated and explainable method for model optimization could be confirmed.

The cutting time can be extracted based on the vibration sensor data described

above. Therefore, wear regression is possible using only process monitoring data without additional data sources. On the other hand, cutting time and removed material volume can be estimated in the context of process simulations. Hence, a prediction based on data from CAM software systems also works in principle. In particular, however, this can be exploited for the wear forecast since the estimates are already available before the actual machining. The regression showed that the cutting time had the highest significance. Furthermore, the cutting time is available both based on process monitoring and through process simulations. Therefore, it was investigated how it affects the remaining tool life prediction. The remaining tool life was first predicted as a baseline using the wear forecast without the future cutting time. This resulted in an MAE of 7.8 minutes, which is an absolute error of 9.2 % in relation to the average lifetime of the underlying tools of 85 minutes. By adding the future cutting time, the MAE could be reduced by an average of 22 % to 6.1 minutes. The increase in accuracy and the reduction in uncertainty could be achieved mainly in the early stages of the tool life up to 55 minutes. Overall, the average minimum MAE achieved was 5.3 minutes, and the total minimum was 1.6 minutes.

In conclusion, this work shows that remaining tool life prediction is possible under the variable process conditions of single-part production. In particular, combining process simulation and monitoring is a promising way to provide robust and reliable remaining tool life prediction. The developed method opens up the possibility of process optimization and productivity increase with simultaneously guaranteed process reliability in single-part production.

6.2 Future Work

The remaining tool life prediction method proposed in this work forms the basis for application under single-part production conditions. It partly uses information from process simulations. However, the next step is to fully integrate the method into digital tool and process twins to ensure a comprehensive mutual exchange of information between process simulation and monitoring. Especially the wear forecast as feedback for process-parallel simulations offers potential for process optimization. In addition, the remaining tool life information can be used in the context of tool life-cycle management.

On the sensor system level, the architectural concept implemented in this work can also be explored in other flexible machining systems, such as industrial robots, for process monitoring and optimization. Due to its retrofittable design, it offers the possibility of easy integration. Likewise, the combined wear regression and forecasting method can be investigated in other use cases, such as predictive maintenance of machine tools, since it can be used for arbitrary target variables.

The developed sensor system focuses on local data processing even under resource constraints, e.g., by implementation using wireless sensor nodes. However, only the optimization of signal analysis and not the machine learning models have been considered so far. Since the remaining tool life prediction method is already based on the automated machine learning approach, investigating hardware-aware automated machine learning is a promising direction for further increase in resource efficiency.

List of Figures

List of Tables

Bibliography

[1] Lorenz, Markus ; Lüers, Martin ; Ludwig, Max ; Rees, Simon ; Rauen, Hartmut ; Zelinger, Matthias ; Stiller, Robert: For Machinery Makers, Green Tech Creates Green Business. (2020)

[2] Merchant, M. E.: Twentieth Century evolution of machining in the United States – An interpretative review. (2003)

[3] Abele, Eberhard ; Rumpel, Guido ; Hohenstein, Julien ; Benning, Karl-Heinz: Elektromobilität – Konsequenzen für die Zerspanung. In: *Zeitschrift für wirtschaftlichen Fabrikbetrieb* 104 (2009), Nr. 11, 993–997. http://dx.doi.org/10.3139/104.110194. – DOI 10.3139/104.110194. – ISSN 2511–0896

[4] Boos, Wolfgang ; Kelzenberg, Christoph ; Prümmer, Marcel ; Goertz, David ; Boshof, Julian ; Horstkotte, Rainer ; Ochel, Tim, Lürken, Christian: Tooling in Germany 2020. (2020)

[5] Denkena, Berend ; Krüger, Max ; Schmidt, Justin: Condition-based tool management for small batch production. In: *The International Journal of Advanced Manufacturing Technology* 74 (2014), Nr. 1-4, 471–480. http://dx.doi.org/10.1007/s00170-014-6013-2. – DOI 10.1007/s00170–014–6013–2. – ISSN 0268–3768

[6] Staufen AG: Deutscher Industrie 4.0 Index 2019. (2019)

[7] Boos, Wolfgang ; Arntz, Kristian ; Johannsen, Lars ; Prümmer, Marcel ; Horstkotte, Rainer ; Ganser, Phillipp ; Venek, Tommy ; Gerretz, Vincent: Erfolgreich Fräsen im Werkzeugbau. (2018)

[8] Plattform Industrie 4.0: Sustainable production: actively shaping the ecological transformation with Industrie 4.0. (2020)

[9] Goyal, Deepam ; Mongia, Chirag ; Sehgal, Shankar: Applications of

Digital Signal Processing in Monitoring Machining Processes and Rotary Components: A Review. In: *IEEE Sensors Journal* 21 (2021), Nr. 7, S. 8780–8804. http://dx.doi.org/10.1109/JSEN.2021.3050718. – DOI 10.1109/JSEN.2021.3050718. – ISSN 1530–437X

[10] McKinsey: Smartening up with Artificial Intelligence (AI) - What's in it for Germany and its Industrial Sector? (2017)

[11] Arntz, Christian ; Brandstätter, Tobias C. ; Dorissen, Jonas ; Frye, Maik ; Krauss, Jonathan ; Krebs, Leonie ; Holst, Carsten ; Horstkotte, Rainer ; Mende, Hendrik ; Schiller, Sven ; Stepien, Grzegorz ; Wollbrink, Moritz ; Zhen, Zhen: Künstliche Intelligenz in der Einzel- und Kleinserienfertigung. (2021)

[12] Sayyad, Sameer ; Kumar, Satish ; Bongale, Arunkumar ; Kamat, Pooja ; Patil, Shruti ; Kotecha, Ketan: Data-Driven Remaining Useful Life Estimation for Milling Process: Sensors, Algorithms, Datasets, and Future Directions. In: *IEEE Access* 9 (2021), S. 110255–110286. http://dx.doi.org/10.1109/ACCESS.2021.3101284. – DOI 10.1109/ACCESS.2021.3101284

[13] Klocke, Fritz: *Fertigungsverfahren 1*. Berlin, Heidelberg : Springer Berlin Heidelberg, 2018. http://dx.doi.org/10.1007/978-3-662-54207-1. http://dx.doi.org/10.1007/978-3-662-54207-1. – ISBN 978–3–662–54206–4

[14] Buyurgan, Nebil ; Saygin, Can ; Kilic, S.Engin: Tool allocation in flexible manufacturing systems with tool alternatives. In: *Robotics and Computer-Integrated Manufacturing* 20 (2004), Nr. 4, 341–349. http://dx.doi.org/10.1016/j.rcim.2004.01.001. – DOI 10.1016/j.rcim.2004.01.001. – ISSN 0736–5845

[15] Goswami, Mohit ; Tiwari, M. K. ; Mukhopadhyay, S. K.: An integrated approach to solve tool-part grouping, job allocation and scheduling problems in a flexible manufacturing system. In: *The International Journal of Advanced Manufacturing Technology* 35 (2008), Nr. 11-12, 1145–1155. http://dx.doi.org/10.1007/s00170-006-0796-8. – DOI 10.1007/s00170–006–0796–8. – ISSN 0268–3768

[16] Kagermann, Henning ; Wahlster, Wolfgang ; Helbig, Johannes ;

acatech – Deutsche Akademie der Technikwissenschaften e.V.: *Recommendations for implementing the strategic initiative Industrie 4.0: Final report of the Industrie 4.0 Working Group.* Frankfurt, 2013

[17] Wegener, Dieter: *Industrie 4.0 – Schritt für Schritt auf dem Weg zu innovativen Produktionsumgebungen.* Universität Passau, 2014

[18] Plattform Industrie 4.0: *Key themes of Industrie 4.0: Research and development needs for successful implementation of Industrie 4.0.* München, 2019

[19] Plattform Industrie 4.0: *Structure of the Administration Shell: Continuation of the Development of the Reference Model for the Industrie 4.0 Component.* Berlin, 2016

[20] Plattform Industrie 4.0: *Details of the Administration shell - Part 1: The exchange of information between partners in the value chain of Industrie 4.0.* Berlin, 2020

[21] Plattform Industrie 4.0: *Details of the Asset Administration Shell - Part 2: Interoperability at Runtime – Exchanging Information via Application Programming Interfaces.* Berlin, 2021

[22] Plattform Industrie 4.0: *AAS Reference Modelling: Exemplary modelling of a manufacturing plant with AASX Package Explorer based on the AAS metamodel.* Berlin, 2021

[23] DIN German Institute for Standardization e.V.: *DIN SPEC 91345 - Referenzarchitekturmodell Industrie 4.0 (RAMI4.0).* 2016

[24] Plattform Industrie 4.0: *Umsetzungsstrategie Industrie 4.0: Ergebnisbericht der Plattform Industrie 4.0.* Berlin, 2015

[25] Jacoby, Michael ; Volz, Friedrich ; Weissenbacher, Christian ; Stojanovic, Ljiljana ; Usländer, Thomas: An approach for Industrie 4.0-compliant and data-sovereign Digital Twins. In: *at - Automatisierungstechnik* 69 (2021), Nr. 12, S. 1051–1061. `http://dx.doi.org/10.1515/auto-2021-0074`. – DOI 10.1515/auto–2021–0074. – ISSN 0178–2312

[26] Plattform Industrie 4.0: *Relationships between I4.0 Components – Composite Components and Smart Production: Continuation of the Development of the Reference Model for the I4.0 SG Models and Standards.* Berlin, 2017

[27] VDI Verein Deutscher Ingenieure e.V. ; VDE Association for Electrical, Electronic & Information Technologies e.V. ; ZVEI German Electrical and Electronic Manufacturers' Association e.V.: *Status Report - Reference Architecture Model Industrie 4.0 (RAMI4.0)*. Düsseldorf, 2015

[28] IEC International Electrotechnical Commission: *IEC 62890:2020 - Industrial-process measurement, control and automation - Life-cycle-management for systems and components*. 2020

[29] IEC International Electrotechnical Commission: *IEC 62264-1:2013 - Enterprise-control system integration - Part 1: Models and terminology*. 2014

[30] IEC International Electrotechnical Commission: *IEC 61512-1:1997 - Batch control - Part 1: Models and terminology*. 1997

[31] Brettel, Malte ; Friederichsen, Niklas ; Keller, Michael ; Rosenberg, Marius: How Virtualization, Decentralization and Network Building Change the Manufacturing Landscape: An Industry 4.0 Perspective. In: *International journal of mechanical, aerospace, industrial and mechatronics engineering* 8 (2014), Nr. RWTH-2015-01642. https://publications.rwth-aachen.de/record/465283

[32] Usländer, Thomas ; Epple, Ulrich: Reference model of Industrie 4.0 service architectures. In: *at - Automatisierungstechnik* 63 (2015), Nr. 10, S. 858–866. http://dx.doi.org/10.1515/auto-2015-0017. – DOI 10.1515/auto–2015–0017. – ISSN 0178–2312

[33] Monostori, László: Cyber-physical Production Systems: Roots, Expectations and R&D Challenges. In: *Procedia CIRP* 17 (2014), 9–13. http://dx.doi.org/10.1016/j.procir.2014.03.115. – DOI 10.1016/j.procir.2014.03.115. – ISSN 22128271

[34] DIN German Institute for Standardization e.V. ; DKE German Commission for Electrical, Electronic & Information Technologies of DIN and VDE: *German Standardization Roadmap Industrie 4.0 – Version 4*. Berlin, 2020

[35] DIN German Institute for Standardization e.V. ; DKE German Commission for Electrical, Electronic & Information Tech-

nologies of DIN and VDE: *Progress Report Standardization Roadmap Industrie 4.0*. Berlin, 2022

[36] Industrial Internet Consortium: *The Industrial Internet of Things - Volume G1: Reference Architecture*. 2019

[37] O. Vermesan ; M. Eisenhauer ; M. Serrano ; Patrick Guillemin ; H. Sundmaeker ; E. Tragos ; J. Valino ; Bertrand Copigneaux ; M. Presser ; Annabeth Aagaard ; R. Bahr ; E. Darmois: The Next Generation Internet of Things – Hyperconnectivity and Embedded Intelligence at the Edge. (2018)

[38] Industrial Internet Consortium: *Introduction to Edge Computing in IIoT*. 2018

[39] Industrial Internet Consortium: *The Industrial Internet of Things - Distributed Computing in the Edge*. 2020

[40] Industrial Internet Consortium: *Architecture Alignment and Interoperability: An Industrial Internet Consortium and Plattform Industrie 4.0 Joint Whitepaper*. 2017

[41] Braunisch, Nico ; Hilbert, Frank ; Wollschlaeger, Martin: Distributed asset management in Industrie 4.0. (2021). http://dx.doi.org/10.25673/39550. – DOI 10.25673/39550

[42] Plattform Industrie 4.0: *Verwaltungsschale in der Praxis: Wie definiere ich Teilmodelle, beispielhafte Teilmodelle und Interaktion zwischen Verwaltungsschalen*. Berlin, 2020

[43] Willner, Alexander ; Gowtham, Varun: Toward a Reference Architecture Model for Industrial Edge Computing. In: *IEEE Communications Standards Magazine* 4 (2020), Nr. 4, S. 42–48. http://dx.doi.org/10.1109/MCOMSTD.001.2000007. – DOI 10.1109/MCOMSTD.001.2000007. – ISSN 2471–2825

[44] Kief, Hans B. (Hrsg.) ; Roschiwal, Helmut A. (Hrsg.) ; Schwarz, Karsten (Hrsg.): *CNC-Handbuch*. 30., überarbeitete Auflage. München : Hanser, 2017 (Hanser eLibrary). http://dx.doi.org/10.3139/9783446452657. http://dx.doi.org/10.3139/9783446452657. – ISBN 9783446452657

[45] Müller, Manuel ; Müller, Timo ; Ashtari Talkhestani, Behrang

; Marks, Philipp ; Jazdi, Nasser ; Weyrich, Michael: Industrial autonomous systems: a survey on definitions, characteristics and abilities. In: *at - Automatisierungstechnik* 69 (2021), Nr. 1, S. 3–13. http://dx.doi.org/10.1515/auto-2020-0131. – DOI 10.1515/auto–2020–0131. – ISSN 0178–2312

[46] Roman Dumitrescu, Jürgen Gausemeier, Philipp Slusallek Sarah Cieslik, Georg Demme, Tommy Falkowski, Hilko Hoffmann, Susanne Kadner, Felix Reinhart, Thorsten Westermann, Johannes Winter: Studie "Autonome Systeme": Studien zum deutschen Innovationssystem. (2018)

[47] Fachforum Autonome Systeme im Hightech-Forum: *Autonome Systeme - Chancen und Risiken für Wirtschaft, Wissenschaft und Gesellschaft (Langversion, Abschlussbericht).* Berlin, 2017

[48] Dumitrescu, Roman ; Westermann, Thorsten ; Falkowski, Tommy: Autonome Systeme in der Produktion: Planungssystematik für die Entwicklung autonomer Systeme. In: *Industrie 4.0 Management* 2018 (2018), Nr. 6, S. 17–20. http://dx.doi.org/10.30844/I40M{_}18-6{_}17-20. – DOI 10.30844/I40M _18–6_17–20. – ISSN 23649208

[49] Jürgen Gausemeier, Harald Anacker, Anja Czaja, Helene Wassmann, Roman Dumitrescu: Auf dem Weg zu intelligenten technischen Systemen. (2013)

[50] Zhu, Kunpeng: *Smart Machining Systems.* Cham : Springer International Publishing, 2022. http://dx.doi.org/10.1007/978-3-030-87878-8. http://dx.doi.org/10.1007/978-3-030-87878-8. – ISBN 978–3–030–87877–1

[51] Dumitrescu, Roman: *Entwicklungssystematik zur Integration kognitiver Funktionen in fortgeschrittene mechatronische Systeme*, Diss., 2010

[52] Bergs, Thomas ; Gierlings, Sascha ; Auerbach, Thomas ; Klink, Andreas ; Schraknepper, Daniel ; Augspurger, Thorsten: The Concept of Digital Twin and Digital Shadow in Manufacturing. In: *Procedia CIRP* 101 (2021), S. 81–84. http://dx.doi.org/10.1016/j.procir.2021.02.010. – DOI 10.1016/j.procir.2021.02.010. – ISSN 22128271

[53] ISO International Organization for Standardization: *ISO*

23247-1:2021 - Automation systems and integration — Digital twin framework for manufacturing — Part 1: Overview and general principles. 2021

[54] Liu, Chao ; Xu, Xun: Cyber-physical Machine Tool – The Era of Machine Tool 4.0. In: *Procedia CIRP* 63 (2017), S. 70–75. http://dx.doi.org/10.1016/j.procir.2017.03.078. – DOI 10.1016/j. procir.2017.03.078. – ISSN 22128271

[55] Hänel, Albrecht ; Seidel, André ; Friess, Uwe ; Teicher, Uwe ; Wiemer, Hajo ; Wang, Dongqian ; Wenkler, Eric ; Penter, Lars ; Hellmich, Arvid ; Ihlenfeldt, Steffen: Digital Twins for High-Tech Machining Applications—A Model-Based Analytics-Ready Approach. In: *Journal of Manufacturing and Materials Processing* 5 (2021), Nr. 3, S. 80. http://dx.doi.org/10.3390/jmmp5030080. – DOI 10.3390/jmmp5030080

[56] Ladj, Asma ; Wang, Zhiqiang ; Meski, Oussama ; Belkadi, Farouk ; Ritou, Mathieu ; Da Cunha, Catherine: A knowledge-based Digital Shadow for machining industry in a Digital Twin perspective. In: *Journal of Manufacturing Systems* 58 (2021), S. 168–179. http://dx.doi.org/10.1016/j.jmsy.2020.07.018. – DOI 10.1016/j. jmsy.2020.07.018. – ISSN 02786125

[57] ISO International Organization for Standardization: *ISO 13399-1:2006-02 - Cutting tool data representation and exchange - Part 1: Overview, fundamental principles and general information model*. 2006

[58] Botkina, Darya ; Hedlind, Mikael ; Olsson, Bengt ; Henser, Jannik ; Lundholm, Thomas: Digital Twin of a Cutting Tool. In: *Procedia CIRP* 72 (2018), S. 215–218. http://dx.doi.org/10.1016/j.procir.2018.03.178. – DOI 10.1016/j.procir.2018.03.178. – ISSN 22128271

[59] B. Caesar ; A. Hänel ; E. Wenkler ; C. Corinth ; S. Ihlenfeldt ; A. Fay: Information Model of a Digital Process Twin for Machining Processes. In: *25th IEEE International Conference on Emerging Technologies and Factory Automation (ETFA)* (2020), S. 1765–1772. http://dx.doi.org/10.1109/ETFA46521.2020.9212085. – DOI 10.1109/ETFA46521.2020.9212085

[60] Davim, J. P.: *Machining*. London : Springer London, 2008. http:

//dx.doi.org/10.1007/978-1-84800-213-5. http://dx.doi.org/10.1007/978-1-84800-213-5. – ISBN 978–1–84800–212–8

[61] Denkena, Berend ; Tönshoff, Hans K.: *Spanen*. Berlin, Heidelberg : Springer Berlin Heidelberg, 2011. http://dx.doi.org/10.1007/978-3-642-19772-7. http://dx.doi.org/10.1007/978-3-642-19772-7. – ISBN 978–3–642–19771–0

[62] Laperrière, Luc (Hrsg.) ; Reinhart, Gunther (Hrsg.): *CIRP Encyclopedia of Production Engineering*. Berlin, Heidelberg : Springer, 2014 (SpringerLink Bücher). http://dx.doi.org/10.1007/978-3-642-20617-7. http://dx.doi.org/10.1007/978-3-642-20617-7. – ISBN 9783642206177

[63] Dietrich, Jochen: *Praxis der Zerspantechnik*. Wiesbaden : Springer Fachmedien Wiesbaden, 2016. http://dx.doi.org/10.1007/978-3-658-14053-3. http://dx.doi.org/10.1007/978-3-658-14053-3. – ISBN 978–3–658–14052–6

[64] Choi, Byoung K. ; Jerard, Robert B.: *Sculptured Surface Machining: Theory and applications*. Boston, MA and s.l. : Springer US, 1998. http://dx.doi.org/10.1007/978-1-4615-5283-3. http://dx.doi.org/10.1007/978-1-4615-5283-3. – ISBN 9781461552833

[65] Piegl, Les: *The NURBS Book*. Berlin, Heidelberg : Springer Berlin / Heidelberg, 1995 (Monographs in Visual Communication Ser). https://ebookcentral.proquest.com/lib/kxp/detail.action?docID=6505535. – ISBN 9783642973857

[66] Cabral, Gustavo F.: *Modeling and simulation of tool engagement and prediction of process forces in milling*, Rheinisch-Westfälische Technische Hochschule Aachen, Dissertation, 2016

[67] Neugebauer, Reimund: *Werkzeugmaschinen: Aufbau, Funktion und Anwendung Von Spanenden und Abtragenden Werkzeugmaschinen*. 1st ed. Berlin, Heidelberg : Springer Berlin / Heidelberg, 2012 (VDI-Buch Ser). https://ebookcentral.proquest.com/lib/kxp/detail.action?docID=1030150. – ISBN 9783642300783

[68] Brecher, Christian ; Weck, Manfred: *Werkzeugmaschinen Fertigungssysteme 1: Maschinenarten und Anwendungsbereiche*. 9th ed. Berlin,

Heidelberg : Vieweg, 2019 (VDI-Buch Ser). https://ebookcentral.proquest.com/lib/kxp/detail.action?docID=5592896. – ISBN 9783662465653

[69] DIN German Institute for Standardization e.V.: *DIN 8589-3:2003-09 - Manufacturing processes chip removal - Part 3: Milling; Classification, subdivision, terms and definitions*. 2009

[70] DIN German Institute for Standardization e.V.: *DIN ISO 11529:2014-10 - Milling cutters - Designation - Shank-type and bore-type milling cutters of solid or tipped design or with indexable cutting edges*. 2014

[71] DIN German Institute for Standardization e.V.: *DIN 6581:1985-10 - Terminology of chip removing; reference systems and angles on the cutting part of the tool*. 1985

[72] Gdula, Michał ; Burek, Jan: Effect of the lead angle and the radius of curvature on the cutting forces in a 5-axis milling of sculptured surfaces. In: *Mechanik* 91 (2018), Nr. 1, S. 18–22. http://dx.doi.org/10.17814/mechanik.2018.1.2. – DOI 10.17814/mechanik.2018.1.2. – ISSN 0025–6552

[73] Gdula, Michal ; Burek, Jan ; Zylka, Lukasz ; Plodzien, Marcin: Five-axis milling of sculptured surfaces of the turbine blade. In: *Aircraft Engineering and Aerospace Technology* 90 (2018), Nr. 1, 146–157. http://dx.doi.org/10.1108/AEAT-11-2015-0242. – DOI 10.1108/AEAT–11–2015–0242. – ISSN 1748–8842

[74] Sai, L. ; Sai, W. B. ; Zghal, A.: Influence of the surface geometry on the material removal rate in milling. In: *International Conference Design and Modeling of Mechanical Systems* (2009)

[75] Altintaş, Y. ; Lee, P.: A General Mechanics and Dynamics Model for Helical End Mills. In: *CIRP Annals* 45 (1996), Nr. 1, 59–64. http://dx.doi.org/10.1016/S0007-8506(07)63017-0. – DOI 10.1016/S0007–8506(07)63017–0. – ISSN 00078506

[76] Budak, E. ; AltintasÂ¸, Y. ; Armarego, E. J. A.: Prediction of Milling Force Coefficients From Orthogonal Cutting Data. In: *Journal of Manufacturing Science and Engineering* 118 (1996), Nr. 2, S. 216–224. http://dx.doi.org/10.1115/1.2831014. – DOI 10.1115/1.2831014. –

ISSN 1087–1357

[77] Zhou, Xu ; Luo, Ming ; Zhang, Dinghua ; Liu, Wanzhu: Cutting Force Prediction in Four-axis Milling of Curved Surfaces with Bull-nose End Mill. In: *Procedia CIRP* 56 (2016), S. 100–104. http://dx.doi.org/10.1016/j.procir.2016.10.027. – DOI 10.1016/j. procir.2016.10.027. – ISSN 22128271

[78] Song, Qinghua ; Liu, Zhanqiang ; Ju, Ganggang ; Wan, Yi: A generalized cutting force model for five-axis milling processes. In: *Proceedings of the Institution of Mechanical Engineers, Part B: Journal of Engineering Manufacture* 233 (2019), Nr. 1, S. 3–17. http://dx.doi.org/10.1177/0954405417711970. – DOI 10.1177/0954405417711970. – ISSN 0954–4054

[79] Suh, Suk-Hwan ; Kang, Seong K. ; Chung, Dae-Hyuk ; Stroud, Ian: *Theory and Design of CNC Systems*. London : Springer London, 2008. http://dx.doi.org/10.1007/978-1-84800-336-1. http://dx.doi.org/10.1007/978-1-84800-336-1. – ISBN 978–1–84800–335–4

[80] Yeung, Chi-Ho ; Altintas, Yusuf ; Erkorkmaz, Kaan: Virtual CNC system. Part I. System architecture. In: *International Journal of Machine Tools and Manufacture* 46 (2006), Nr. 10, S. 1107–1123. http://dx.doi.org/10.1016/j.ijmachtools.2005.08.002. – DOI 10.1016/j. ijmachtools.2005.08.002. – ISSN 08906955

[81] Sun, Yuwen ; Jia, Jinjie ; Xu, Jinting ; Chen, Mansen ; Niu, Jinbo: Path, feedrate and trajectory planning for free-form surface machining: A state-of-the-art review. In: *Chinese Journal of Aeronautics* 35 (2022), Nr. 8, S. 12–29. http://dx.doi.org/10.1016/j.cja.2021.06.011. – DOI 10.1016/j. cja.2021.06.011. – ISSN 10009361

[82] Xu, Ke ; Luo, Ming ; Tang, Kai: Machine based energy-saving tool path generation for five-axis end milling of freeform surfaces. In: *Journal of Cleaner Production* 139 (2016), 1207–1223. http://dx.doi.org/10.1016/j.jclepro.2016.08.140. – DOI 10.1016/j. jclepro.2016.08.140. – ISSN 0959–6526

[83] Moodleah, S. ; Makhanov, S. S.: 5-axis machining using a curvilinear tool path aligned with the direction of the maximum removal rate. In: *The International Journal of Advanced Manufacturing Technology* 80 (2015),

Nr. 1-4, 65–90. http://dx.doi.org/10.1007/s00170-015-6958-9. – DOI 10.1007/s00170–015–6958–9. – ISSN 0268–3768

[84] Benardos, Panorios ; Vosniakos, George C.: Removed material volume calculations in CNC milling by exploiting CAD functionality. In: *International Journal of Computer Aided Engineering and Technology* 10 (2018), Nr. 5, 491. http://dx.doi.org/10.1504/IJCAET.2018.10013720. – DOI 10.1504/IJCAET.2018.10013720. – ISSN 1757–2657

[85] Kolivuso, M. ; Rajeshkannan, A. ; Jeevanantham, A. K.: Study on Computational and Conventional Method of Determining Volume of Material Removal in CNC Milling Process. In: *Materials Today: Proceedings* 22 (2020), 1360–1368. http://dx.doi.org/10.1016/j.matpr.2020.01.429. – DOI 10.1016/j.matpr.2020.01.429. – ISSN 2214–7853

[86] Souza, Adriano F. ; Camargo, Lucas G. ; Gaspar, Helton da S. ; Marin, Felipe ; Calleja Ochoa, Amaia ; López de Lacalle, Luis Norberto: New mechanistic model to predict machining time for milling free form geometries using 4-axis milling. In: *Procedia CIRP* 101 (2021), 34–37. http://dx.doi.org/10.1016/j.procir.2020.09.187. – DOI 10.1016/j.procir.2020.09.187. – ISSN 22128271

[87] Ward, Rob ; Sencer, Burak ; Jones, Bryn ; Ozturk, Erdem: Accurate prediction of machining feedrate and cycle times considering interpolator dynamics. In: *The International Journal of Advanced Manufacturing Technology* 116 (2021), Nr. 1-2, 417–438. http://dx.doi.org/10.1007/s00170-021-07211-2. – DOI 10.1007/s00170–021–07211–2. – ISSN 0268–3768

[88] DIN German Institute for Standardization e.V.: *DIN 66025-1:1983-01 - Numerical control of machines, format; general requirements.* 1983

[89] International Organization for Standardization: *ISO 6983-1:2009-12 - Automation systems and integration - Numerical control of machines - Program format and definitions of address words - Part 1: Data format for positioning, line motion and contouring control systems.* 2009

[90] Czichos, Horst: *Tribologie-Handbuch: Tribometrie, Tribomaterialien, Tribotechnik.* 3., überarbeitete und erweiterte Auflage. Wiesbaden :

Vieweg+Teubner, 2010 (Springer eBook Collection Computer Science & Engineering). http://dx.doi.org/10.1007/978-3-8348-9660-5. http://dx.doi.org/10.1007/978-3-8348-9660-5. – ISBN 9783834896605

[91] International Organization for Standardization: *ISO 3685:1993-11 - Tool-life testing with single-point turning tools*. 1993

[92] International Organization for Standardization: *ISO 21920-2:2022-12 - Geometrical product specifications (GPS) - Surface texture: Profile - Part 2: Terms, definitions and surface texture parameters*. 2022

[93] Marxer, Michael ; Bach, Carlo ; Keferstein, Claus P.: *Fertigungsmesstechnik*. Wiesbaden : Springer Fachmedien Wiesbaden, 2021. http://dx.doi.org/10.1007/978-3-658-34168-8. http://dx.doi.org/10.1007/978-3-658-34168-8. – ISBN 978–3–658–34167–1

[94] Kistler Group: *Cutting force measurements in research and development: High-precision measurement systems for metal-cutting production*. https://www.kistler.com/INT/en/cutting-force-measurements-with-dynamometers/C00000017

[95] Rudolf, Thomas M.: *Adaptierbare Parametrierung von Diagnosesystemen durch Verwendung digitaler Antriebssignale in der Prozessüberwachung*. Aachen, Rheinisch-Westfälische Technische Hochschule Aachen, Dissertation, http://nbn-resolving.de/urn:nbn:de:hbz:82-opus-50325

[96] Franke, Dieter: *Wälzlagerdiagnose an Maschinensätzen: Diagnose und Überwachung von Wälzlagerfehlern und -schäden*. 1. Aufl. 2022. Berlin, Heidelberg : Springer Berlin Heidelberg, 2022 http://nbn-resolving.org/urn:nbn:de:bsz:31-epflicht-2004275. – ISBN 9783662626207

[97] Weck, Manfred: *Werkzeugmaschinen 5: Messtechnische Untersuchung und Beurteilung, dynamische Stabilität*. 7., neu bearbeitete Auflage. Berlin, Heidelberg : Springer Berlin Heidelberg, 2006 (SpringerLink Bücher). http://dx.doi.org/10.1007/978-3-540-32951-0. http://dx.doi.org/10.1007/978-3-540-32951-0. – ISBN 9783540329510

[98] Insperger, T. ; Stépán, G. ; Bayly, P.V ; Mann, B.P: Multiple chatter frequencies in milling processes. In: *Journal of Sound and Vibration* 262 (2003), Nr. 2, 333–345. http://dx.doi.org/10.1016/S0022-460X(02)01131-8. – DOI 10.1016/S0022–460X(02)01131–8. – ISSN 0022–460X

[99] Sturm, Adolf ; Förster, Rudolf: *Maschinen- und Anlagendiagnostik: Für die zustandsbezogene Instandhaltung*. Wiesbaden and s.l. : Vieweg+Teubner Verlag, 1990 (Springer eBook Collection Computer Science and Engineering). http://dx.doi.org/10.1007/978-3-322-99814-9. http://dx.doi.org/10.1007/978-3-322-99814-9. – ISBN 9783322998149

[100] Möser, Michael: *Körperschall: Physikalische Grundlagen und technische Anwendungen*. Berlin, Heidelberg : Springer Berlin Heidelberg, 2010 (SpringerLink Bücher). http://dx.doi.org/10.1007/978-3-540-49048-7. http://dx.doi.org/10.1007/978-3-540-49048-7. – ISBN 9783540490487

[101] Möser, Michael: *Technische Akustik*. 10. Aufl. 2015. Berlin, Heidelberg : Springer Berlin Heidelberg, 2015 (VDI-Buch). http://nbn-resolving.org/urn:nbn:de:bsz:31-epflicht-1603908. – ISBN 9783662477045

[102] Bender, Beate: *Dubbel Taschenbuch Für Den Maschinenbau 1*. 26th ed. Berlin, Heidelberg : Springer Berlin / Heidelberg, 2020 https://ebookcentral.proquest.com/lib/kxp/detail.action?docID=6424342. – ISBN 9783662597118

[103] Möser, Michael: *Körperschall-Messtechnik*. Berlin, Heidelberg : Springer Berlin / Heidelberg, 2018 (Fachwissen Technische Akustik Ser). https://ebookcentral.proquest.com/lib/kxp/detail.action?docID=5387309. – ISBN 9783662566213

[104] Schorr, Sebastian: *Prozessparallele Prognose der Werkstückqualität mithilfe von NC-internen Daten und maschinellem Lernen*, Universität des Saarlandes, Dissertation, 2021

[105] Eifert, Tobias ; Eisen, Kristina ; Maiwald, Michael ; Herwig, Christoph: Current and future requirements to industrial analytical infrastructure-part 2: smart sensors. In: *Analytical and bioanalytical chemistry* 412 (2020), Nr. 9, S. 2037–2045. http://dx.doi.org/10.1007/s00216-020-02421-1. – DOI 10.1007/s00216–020–02421–1

[106] Mohamed, Ayman ; Hassan, Mahmoud ; M'Saoubi, Rachid ; Attia, Helmi: Tool Condition Monitoring for High-Performance Machining Systems-A Review. In: *Sensors (Basel, Switzerland)* 22 (2022), Nr. 6.

http://dx.doi.org/10.3390/s22062206. – DOI 10.3390/s22062206

[107] Rizal, Muhammad ; Ghani, Jaharah A. ; Nuawi, Mohd Z. ; Haron, Che Hassan C.: An embedded multi-sensor system on the rotating dynamometer for real-time condition monitoring in milling. In: *The International Journal of Advanced Manufacturing Technology* 95 (2018), Nr. 1-4, S. 811–823. http://dx.doi.org/10.1007/s00170-017-1251-8. – DOI 10.1007/s00170–017–1251–8. – ISSN 0268–3768

[108] Ostasevicius, Vytautas ; Karpavicius, Paulius ; Jurenas, Vytautas ; Cepenas, Mindaugas ; Cesnavicius, Ramunas ; Eidukynas, Darius: Development of universal wireless sensor node for tool condition monitoring in milling. In: *The International Journal of Advanced Manufacturing Technology* 110 (2020), Nr. 3-4, S. 1015–1025. http://dx.doi.org/10.1007/s00170-020-05812-x. – DOI 10.1007/s00170–0 20–05812–x. – ISSN 0268–3768

[109] Öztürk, Tuğrul ; Sarikaya, Erkut ; Weigold, Matthias: Sensor-integrated tap holder for process uncertainty detection based on tool vibration and axial length compensation sensors. In: *The International Journal of Advanced Manufacturing Technology* 117 (2021), Nr. 5-6, S. 1905–1914. http://dx.doi.org/10.1007/s00170-021-07825-6. – DOI 10.1007/s00170–021–07825–6. – ISSN 0268–3768

[110] Lu, Zhiyuan ; Wang, Meiqing ; Dai, Wei: Machined Surface Quality Monitoring Using a Wireless Sensory Tool Holder in the Machining Process. In: *Sensors (Basel, Switzerland)* 19 (2019), Nr. 8. http://dx.doi.org/10.3390/s19081847. – DOI 10.3390/s19081847

[111] Maier, W. ; Möhring, H.-C. ; Werkle, K.: Tools 4.0 – Intelligence starts on the cutting edge. In: *Procedia Manufacturing* 24 (2018), S. 299–304. http://dx.doi.org/10.1016/j.promfg.2018.06.024. – DOI 10.1016/j. promfg.2018.06.024. – ISSN 23519789

[112] Möhring, H.-C. ; Werkle, K. ; Maier, W.: Process monitoring with a cyber-physical cutting tool. In: *Procedia CIRP* 93 (2020), S. 1466–1471. http://dx.doi.org/10.1016/j.procir.2020.03.034. – DOI 10.1016/j. procir.2020.03.034. – ISSN 22128271

[113] Möhring, H.-C. ; Nguyen, Q. P. ; Kuhlmann, A. ; Lerez, C. ;

Nguyen, L. T. ; Misch, S.: Intelligent Tools for Predictive Process Control. In: *Procedia CIRP* 57 (2016), S. 539–544. http://dx.doi.org/10.1016/j.procir.2016.11.093. – DOI 10.1016/j. procir.2016.11.093. – ISSN 22128271

[114] Möhring, H.-C. ; Eschelbacher, S. ; Georgi, P.: Fundamental investigation on the correlation between surface properties and acceleration data from a sensor integrated milling tool. In: *Procedia Manufacturing* 52 (2020), S. 79–84. http://dx.doi.org/10.1016/j.promfg.2020.11.015. – DOI 10.1016/j. promfg.2020.11.015. – ISSN 23519789

[115] Wójcicki, Jeremi ; Leonesio, Marco ; Bianchi, Giacomo: Potential for smart spindles adoption as edge computing nodes in Industry 4.0. In: *Procedia CIRP* 99 (2021), S. 86–91. http://dx.doi.org/10.1016/j.procir.2021.03.015. – DOI 10.1016/j. procir.2021.03.015. – ISSN 22128271

[116] Chen, Jihong ; Hu, Pengcheng ; Zhou, Huicheng ; Yang, Jianzhong ; Xie, Jiejun ; Jiang, Yakun ; Gao, Zhiqiang ; Zhang, Chenglei: A Smart Spindle Component concept as a standalone measurement system for Industry 4.0 Machine Tools. In: *Engineering* 5 (2019), Nr. 4, S. 679–690. http://dx.doi.org/10.1016/j.eng.2019.07.018. – DOI 10.1016/j. eng.2019.07.018. – ISSN 20958099

[117] Xi, Tiandong ; Benincá, Igor M. ; Kehne, Sebastian ; Fey, Marcel ; Brecher, Christian: Tool wear monitoring in roughing and finishing processes based on machine internal data. In: *The International Journal of Advanced Manufacturing Technology* 113 (2021), Nr. 11-12, S. 3543–3554. http://dx.doi.org/10.1007/s00170-021-06748-6. – DOI 10.1007/s00170–021–06748–6. – ISSN 0268–3768

[118] Schunk GmbH & Co. KG: *iTENDO*^{2} *- der intelligente Weg zum optimalen Prozess.* https://schunk.com/de/de/tools/werkzeughalter-quickfinder/itendo2/c/PGR_6468?gclid=CjwKCAjwrJ-hBhB7EiwAuyBVXTG55SU8tU7RtLROAepQ89hmY_700bO7sb_nxWI4VpMRUxDAs4hf9BoChw0QAvD_BwE

[119] Röhm GmbH: *iJAW: Clamping force measurement during machining.* https://www.roehm.biz/downloads/kataloge-flyer/ijaw/

[120] pro-micron GmbH: *spike - Flyer.* https://www.pro-micron.de/spike/

[121] Lynn, Roby ; Wescoat, Ethan ; Han, Dongmin ; Kurfess, Thomas: Embedded fog computing for high-frequency MTConnect data analytics. In: *Manufacturing Letters* 15 (2018), S. 135–138. http://dx.doi.org/10.1016/j.mfglet.2017.11.002. – DOI 10.1016/j.mfglet.2017.11.002. – ISSN 22138463

[122] Christoph Schäfer: *Signaltechnische Voraussetzungen und Analyseverfahren zur Überwachung von Präzisions- und Ultrapräzisionsbearbeitungsverfahren.* Aachen, Rheinisch-Westfälische Technische Hochschule Aachen, Dissertation, 2013

[123] Tieng, Hao ; Yang, Haw-Ching ; Cheng, Fan-Tien: Total precision inspection of machine tools with virtual metrology. In: *2015 IEEE International Conference on Automation Science and Engineering (CASE)*, IEEE, 24.08.2015 - 28.08.2015. – ISBN 978–1–4673–8183–3, S. 1446–1447

[124] Kuo, Shu-Wei ; Raihany, Ully ; Peng, Cheng-Yu: Sound Detection of CNC Milling Machine by Embedded System. In: *2020 International Symposium on Computer, Consumer and Control (IS3C)*, IEEE, 13.11.2020 - 16.11.2020. – ISBN 978–1–7281–9362–5, S. 130–133

[125] Castaño, Fernando ; Haber, Rodolfo E. ; Mohammed, Wael M. ; Nejman, Miroslaw ; Villalonga, Alberto ; Lastra, Jose L. M.: Quality Monitoring of Complex Manufacturing Systems on the basis of Model Driven Approach. (2020)

[126] Morgan, Jeff ; O'Donnell, Garret E.: Multi-sensor process analysis and performance characterisation in CNC turning—a cyber physical system approach. In: *The International Journal of Advanced Manufacturing Technology* 92 (2017), Nr. 1-4, S. 855–868. http://dx.doi.org/10.1007/s00170-017-0113-8. – DOI 10.1007/s00170–017–0113–8. – ISSN 0268–3768

[127] Ramirez-Nunez, Juan A. ; Trejo-Hernandez, Miguel ; Romero-Troncoso, Rene J. ; Herrera-Ruiz, Gilberto ; Osornio-Rios, Roque A.: Smart-sensor for tool-breakage detection in milling process under dry and wet conditions based on infrared thermography. In: *The International Journal of Advanced Manufacturing Technology* 97 (2018), Nr. 5-8, S. 1753–1765. http://dx.doi.org/10.1007/s00170-018-2060-4. –

DOI 10.1007/s00170–018–2060–4. – ISSN 0268–3768

[128] Iliyas Ahmad, Maznah ; Yusof, Yusri ; Mustapa, Mohammad S. ; Daud, Mohd E. ; Latif, Kamran ; Kadir, Aini Zuhra A. ; Saif, Yazid ; Adam, Anbia ; Hatem, Noor: A novel integration between service-oriented IoT-based monitoring with open architecture of CNC system monitoring. In: *The International Journal of Advanced Manufacturing Technology* (2022). http://dx.doi.org/10.1007/s00170-022-08675-6. – DOI 10.1007/s00170–022–08675–6. – ISSN 0268–3768

[129] Christoph Schäfer: *Signaltechnische Voraussetzungen und Analyseverfahren zur Überwachung von Präzisions- und Ultrapräzisionsbearbeitungsverfahren*. Aachen, RWTH Aachen, Dissertation, 2013

[130] Humphreys, Ivor ; Eisenblätter, Gerrit ; O'Donnell, Garret E.: FPGA based Monitoring Platform for Condition Monitoring in Cylindrical Grinding. In: *Procedia CIRP* 14 (2014), S. 448–453. http://dx.doi.org/10.1016/j.procir.2014.03.022. – DOI 10.1016/j. procir.2014.03.022. – ISSN 22128271

[131] Chen, Ching-Han ; Lin, Ming-Yi ; Liu, Chung-Chi: Edge Computing Gateway of the Industrial Internet of Things Using Multiple Collaborative Microcontrollers. In: *IEEE Network* 32 (2018), Nr. 1, S. 24–32. http://dx.doi.org/10.1109/MNET.2018.1700146. – DOI 10.1109/MNET.2018.1700146. – ISSN 0890–8044

[132] MCU GmbH & Co. KG: *Toolinspect Process Monitoring*. https://sequoia-vibrationmonitoring.com/wp-content/uploads/2020/12/MCU-Broschu%CC%88re-DeuEng-2021.pdf. Version: 2020

[133] Fraunhofer-Institut für Produktionstechnologie IPT: *vBox – Industrie 4.0 als Retrofit*. https://www.ipt.fraunhofer.de/de/kompetenzen/Produktionsmaschinen/praezisionstechnik-und-kunststoffreplikation/vbox.html. Version: 2023

[134] Montronix GmbH: *SpectraNG*. https://www.montronix.com/de/produkte/produktserien/spectrang/spectrang.html. Version: 2022

[135] Ceratazit S.A.: *Werkzeug- und Prozessüberwachung: ToolScope*. https://cuttingtools.ceratizit.com/de/de/services/toolscope.html.

Version: 2023

[136] Machine Metrics Inc.: *Industrial IoT Platform*. https://www.machinemetrics.com/predictive-maintenance. Version: 2023

[137] Siemens: *Industrial Edge*. https://new.siemens.com/de/de/produkte/automatisierung/themenfelder/industrial-edge.html. Version: 2022

[138] MARPOSS Monitoring Solutions GmbH: *Werkzeug- und Prozessüberwachung*. https://www.artis.de/ger/application/monitoring-solutions-for-machining-center. Version: 2023

[139] Nasir, Vahid ; Sassani, Farrokh: A review on deep learning in machining and tool monitoring: methods, opportunities, and challenges. In: *The International Journal of Advanced Manufacturing Technology* 115 (2021), Nr. 9-10, S. 2683–2709. http://dx.doi.org/10.1007/s00170-021-07325-7. – DOI 10.1007/s00170–021–07325–7. – ISSN 0268–3768

[140] Resende, Carlos ; Folgado, Duarte ; Oliveira, João ; Franco, Bernardo ; Moreira, Waldir ; Oliveira-Jr, Antonio ; Cavaleiro, Armando ; Carvalho, Ricardo: TIP4.0: Industrial Internet of Things Platform for Predictive Maintenance. In: *Sensors (Basel, Switzerland)* 21 (2021), Nr. 14. http://dx.doi.org/10.3390/s21144676. – DOI 10.3390/s21144676

[141] Fournaris, Apostolos P. ; Alexakos, Christos ; Anagnostopoulos, Christos ; Koulamas, Christos ; Kalogeras, Athanasios: Introducing Hardware-Based Intelligence and Reconfigurability on Industrial IoT Edge Nodes. In: *IEEE Design & Test* 36 (2019), Nr. 4, S. 15–23. http://dx.doi.org/10.1109/MDAT.2019.2908547. – DOI 10.1109/MDAT.2019.2908547. – ISSN 2168–2356

[142] Hao, Cong ; Dotzel, Jordan ; Xiong, Jinjun ; Benini, Luca ; Zhang, Zhiru ; Chen, Deming: Enabling Design Methodologies and Future Trends for Edge AI: Specialization and Codesign. In: *IEEE Design & Test* 38 (2021), Nr. 4, S. 7–26. http://dx.doi.org/10.1109/MDAT.2021.3069952. – DOI 10.1109/MDAT.2021.3069952. – ISSN 2168–2356

[143] Chongyu Zhou ; Chen-Khong Tham: GraphEL: A Graph-based Ensemble Learning Method for Distributed Diagnostics and Prognostics in the Industrial Internet of Things. (2018). https://ieeexplore.ieee.

org/servlet/opac?punumber=8635632

[144] Hiessl, Thomas ; Schall, Daniel ; Kemnitz, Jana ; Schulte, Stefan: Industrial Federated Learning – Requirements and System Design. (2020). http://arxiv.org/pdf/2005.06850v1

[145] Proakis, John G. ; Manolakis, Dimitris G.: *Digital signal processing: Principles, algorithms, and applications*. 3. ed. Upper Saddle River : Prentice Hall, 1996. – ISBN 0133737624

[146] Stoica, Petre ; Moses, Randolph L.: *Spectral analysis of signals*. Upper Saddle River N.J. : Pearson/Prentice Hall, 2005. – ISBN 0131139568

[147] Christ, Maximilian ; Braun, Nils ; Neuffer, Julius ; Kempa-Liehr, Andreas W.: Time Series FeatuRe Extraction on basis of Scalable Hypothesis tests (tsfresh – A Python package). In: *Neurocomputing* 307 (2018), 72–77. http://dx.doi.org/10.1016/j.neucom.2018.03.067. – DOI 10.1016/j. neucom.2018.03.067. – ISSN 0925–2312

[148] Barandas, Marília ; Folgado, Duarte ; Fernandes, Letícia ; Santos, Sara ; Abreu, Mariana ; Bota, Patrícia ; Liu, Hui ; Schultz, Tanja ; Gamboa, Hugo: TSFEL: Time Series Feature Extraction Library. In: *SoftwareX* 11 (2020), 100456. http://dx.doi.org/10.1016/j.softx.2020.100456. – DOI 10.1016/j. softx.2020.100456. – ISSN 2352–7110

[149] Takeyama, H. ; Murata, R.: Basic Investigation of Tool Wear. In: *Journal of Engineering for Industry* 85 (1963), Nr. 1, S. 33–37. http://dx.doi.org/10.1115/1.3667575. – DOI 10.1115/1.3667575. – ISSN 0022–0817

[150] Usui, E. ; Shirakashi, T. ; Kitagawa, T.: Analytical prediction of cutting tool wear. In: *Wear* 100 (1984), Nr. 1-3, 129–151. http://dx.doi.org/10.1016/0043-1648(84)90010-3. – DOI 10.1016/0043–1648(84)90010–3. – ISSN 0043–1648

[151] Hosseinkhani, Keyvan ; Ng, Eu-Gene: A Unique Methodology for Tool Life Prediction in Machining. In: *Journal of Manufacturing and Materials Processing* 4 (2020), Nr. 1, S. 16. http://dx.doi.org/10.3390/jmmp4010016. – DOI 10.3390/jmmp4010016

[152] Liu, Zhibo ; Yue, Caixu ; Li, Xiaochen ; Liu, Xianli ; Liang, Steven Y. ; Wang, Lihui: Research on Tool Wear Based on 3D FEM Simulation for

Milling Process. In: *Journal of Manufacturing and Materials Processing* 4 (2020), Nr. 4, S. 121. http://dx.doi.org/10.3390/jmmp4040121. – DOI 10.3390/jmmp4040121

[153] Binder, M. ; Klocke, F. ; Doebbeler, B.: An advanced numerical approach on tool wear simulation for tool and process design in metal cutting. In: *Simulation Modelling Practice and Theory* 70 (2017), S. 65–82. http://dx.doi.org/10.1016/j.simpat.2016.09.001. – DOI 10.1016/j.simpat.2016.09.001. – ISSN 1569190X

[154] Salvatore, F. ; Saad, S. ; Hamdi, H.: Modeling and Simulation of Tool Wear During the Cutting Process. In: *Procedia CIRP* 8 (2013), S. 305–310. http://dx.doi.org/10.1016/j.procir.2013.06.107. – DOI 10.1016/j.procir.2013.06.107. – ISSN 22128271

[155] Li, Bin: A review of tool wear estimation using theoretical analysis and numerical simulation technologies. In: *International Journal of Refractory Metals and Hard Materials* 35 (2012), S. 143–151. http://dx.doi.org/10.1016/j.ijrmhm.2012.05.006. – DOI 10.1016/j.ijrmhm.2012.05.006. – ISSN 02634368

[156] Su, Yinrui: Remaining Useful Life Prediction of Cutting Tool Based on Monotonic Feature Selection and Floating Weighted Regression. In: *2022 8th International Conference on Control, Automation and Robotics (ICCAR)*, IEEE, 08.04.2022 - 10.04.2022. – ISBN 978–1–6654–8116–8, S. 66–70

[157] Yen-Chun Liu ; Yuan-Jen Chang ; Sheng-Liang Liu ; Szu-Ping Chen: *Data-driven prognostics of remaining useful life for milling machine cutting tools*. Piscataway, NJ : IEEE, 2019 https://ieeexplore.ieee.org/servlet/opac?punumber=8809669. – ISBN 9781538683576

[158] Wang, Xuefei ; Liu, Zepeng ; Lu, Enze: Remaining Useful Life Estimation of Cutting Tools Using Bayesian Augmented Lagrangian Algorithm. In: *2022 IEEE 31st International Symposium on Industrial Electronics (ISIE)*, IEEE, 01.06.2022 - 03.06.2022. – ISBN 978–1–6654–8240–0, S. 1165–1169

[159] Salehi, M. ; Wald, G. ; Schmitz, T. L. ; Haas, R. ; Ovtcharova, J.: Probabilistische Modellierung und Vorhersage der Standzeit und Zuverlässigkeit eines Fräswerkzeugs mittels der Bayesianischen Statistik.

In: *Forschung im Ingenieurwesen* 84 (2020), Nr. 2, S. 129–139. http://dx.doi.org/10.1007/s10010-019-00391-0. – DOI 10.1007/s10010–019–00391–0. – ISSN 0015–7899

[160] Hu, Ya-Wei ; Zhang, Hong-Chao ; Liu, Shu-Jie ; Lu, Hui-Tian: Sequential Monte Carlo Method Toward Online RUL Assessment with Applications. In: *Chinese Journal of Mechanical Engineering* 31 (2018), Nr. 1. http://dx.doi.org/10.1186/s10033-018-0205-x. – DOI 10.1186/s10033–018–0205–x. – ISSN 1000–9345

[161] Karandikar, Jaydeep M. ; Abbas, Ali E. ; Schmitz, Tony L.: Tool life prediction using Bayesian updating. Part 1: Milling tool life model using a discrete grid method. In: *Precision Engineering* 38 (2014), Nr. 1, S. 9–17. http://dx.doi.org/10.1016/j.precisioneng.2013.06.006. – DOI 10.1016/j.precisioneng.2013.06.006. – ISSN 01416359

[162] Lin, Muquan ; Wanqing, Song ; Chen, Dongdong ; Zio, Enrico: Evolving Connectionist System and Hidden Semi-Markov Model for Learning-Based Tool Wear Monitoring and Remaining Useful Life Prediction. In: *IEEE Access* 10 (2022), S. 82469–82482. http://dx.doi.org/10.1109/ACCESS.2022.3196016. – DOI 10.1109/ACCESS.2022.3196016

[163] Zhu, Kunpeng ; Liu, Tongshun: Online Tool Wear Monitoring Via Hidden Semi-Markov Model With Dependent Durations. In: *IEEE Transactions on Industrial Informatics* 14 (2018), Nr. 1, S. 69–78. http://dx.doi.org/10.1109/TII.2017.2723943. – DOI 10.1109/TII.2017.2723943. – ISSN 1551–3203

[164] Liu, Weichao ; Yang, Wen-An ; You, Youpeng: Three-Stage Wiener-Process-Based Model for Remaining Useful Life Prediction of a Cutting Tool in High-Speed Milling. In: *Sensors (Basel, Switzerland)* 22 (2022), Nr. 13. http://dx.doi.org/10.3390/s22134763. – DOI 10.3390/s22134763

[165] Jinjiang Wang ; Peng Wang ; R. Gao: Tool life prediction for sustainable manufacturing. (2013). https://www.semanticscholar.org/paper/Tool-life-prediction-for-sustainable-manufacturing-Wang-Wang/9e069dbeb943d2c7478fecfbacb964e13e791f63

[166] Wang, Jinjiang ; Wang, Peng ; Gao, Robert X.: Enhanced particle filter for tool wear prediction. In: *Journal of Manufacturing Systems* 36

(2015), S. 35–45. http://dx.doi.org/10.1016/j.jmsy.2015.03.005. – DOI 10.1016/j. jmsy.2015.03.005. – ISSN 02786125

[167] Li, Yifan ; Xiang, Yongyong ; Pan, Baisong ; Shi, Luojie: *A Hybrid Remaining Useful Life Prediction Method for Cutting Tool Considering the Wear State*. 2022. http://dx.doi.org/10.21203/rs.3.rs-1237427/v1. http://dx.doi.org/10.21203/rs.3.rs-1237427/v1

[168] Krupp, Lukas ; Hennig, Andreas ; Wiede, Christian ; Grabmaier, Anton: A Hybrid Framework for Bearing Fault Diagnosis using Physics-guided Neural Networks. In: *2020 27th IEEE International Conference on Electronics, Circuits and Systems (ICECS)*, IEEE, 23.11.2020 - 25.11.2020. – ISBN 978–1–7281–6044–3, S. 1–2

[169] Sammut, Claude ; Webb, Geoffrey I.: *Encyclopedia of machine learning*. New York, NY : Springer, 2011 (Springer reference). http://dx.doi.org/10.1007/978-0-387-30164-8. http://dx.doi.org/10.1007/978-0-387-30164-8. – ISBN 978–0–387–30768–8

[170] Botchkarev, Alexei: Performance Metrics (Error Measures) in Machine Learning Regression, Forecasting and Prognostics: Properties and Typology. In: *Interdisciplinary Journal of Information, Knowledge, and Management* 14 (2019), 045–076. http://dx.doi.org/10.28945/4184. – DOI 10.28945/4184. – ISSN 1555–1229

[171] Helwig, Nikolai: *Zustandsbewertung industrieller Maschinen mittels multivariater Sensordatenanalyse*. Saarbrücken, Universität des Saarlandes, Dissertation, 2018

[172] Deng, Difan ; Karl, Florian ; Hutter, Frank ; Bischl, Bernd ; Lindauer, Marius: *Efficient Automated Deep Learning for Time Series Forecasting*. http://arxiv.org/pdf/2205.05511v3

[173] Herzen, Julien ; Lässig, Francesco ; Piazzetta, Samuele G. ; Neuer, Thomas ; Tafti, Léo ; Raille, Guillaume ; van Pottelbergh, Tomas ; Pasieka, Marek ; Skrodzki, Andrzej ; Huguenin, Nicolas ; Dumonal, Maxime ; Kościsz, Jan ; Bader, Dennis ; Gusset, Frédérick ; Benheddi, Mounir ; Williamson, Camila ; Kosinski, Michal ; Petrik, Matej ; Grosch, Gaël: Darts: User-Friendly Modern Machine Learning for Time Series. In: *Journal of Machine Learning Research 23 (* (2022). https:

//arxiv.org/pdf/2110.03224

[174] Sherstinsky, Alex: Fundamentals of Recurrent Neural Network (RNN) and Long Short-Term Memory (LSTM) network. In: *Physica D: Nonlinear Phenomena* 404 (2020), 132306. http://dx.doi.org/10.1016/j.physd.2019.132306. – DOI 10.1016/j. physd.2019.132306. – ISSN 0167–2789

[175] Hutter, Frank ; Kotthoff, Lars ; Vanschoren, Joaquin: *Automated Machine Learning*. Cham : Springer International Publishing, 2019. http://dx.doi.org/10.1007/978-3-030-05318-5. http://dx.doi.org/10.1007/978-3-030-05318-5. – ISBN 978–3–030–05317–8

[176] Feurer, Matthias ; Klein, Aaron ; Eggensperger, Katharina ; Springenberg, Jost ; Blum, Manuel ; Hutter, Frank: Efficient and Robust Automated Machine Learning. In: *Advances in Neural Information Processing Systems* 28 (2015)

[177] Feurer, Matthias ; Eggensperger, Katharina ; Falkner, Stefan ; Lindauer, Marius ; Hutter, Frank: Auto-Sklearn 2.0: Hands-free AutoML via Meta-Learning. In: *Journal of Machine Learning Research 23(261)* (2022). http://arxiv.org/pdf/2007.04074v3

[178] Li, Liam ; Jamieson, Kevin ; Rostamizadeh, Afshin ; Gonina, Ekaterina ; Hardt, Moritz ; Recht, Benjamin ; Talwalkar, Ameet: A System for Massively Parallel Hyperparameter Tuning. In: *Conference on Machine Learning and Systems* (2018). https://arxiv.org/pdf/1810.05934

[179] Möhring, H.-C. ; Eschelbacher, S. ; Georgi, P.: Machine learning approaches for real-time monitoring and evaluation of surface roughness using a sensory milling tool. In: *Procedia CIRP* 102 (2021), S. 264–269. http://dx.doi.org/10.1016/j.procir.2021.09.045. – DOI 10.1016/j. procir.2021.09.045. – ISSN 22128271

[180] Lin, Wan-Ju ; Lo, Shih-Hsuan ; Young, Hong-Tsu ; Hung, Che-Lun: Evaluation of Deep Learning Neural Networks for Surface Roughness Prediction Using Vibration Signal Analysis. In: *Applied Sciences* 9 (2019), Nr. 7, 1462. http://dx.doi.org/10.3390/app9071462. – DOI 10.3390/app9071462

[181] Denkena, B. ; Dittrich, M.-A. ; Lindauer, M. ; Mainka, J. ; Stürenburg, L.: Using AutoML to optimize shape error prediction in milling

processes. (2020)

[182] Y. Li ; Y. Zhang ; Y. Chang ; Z. Liu: Remaining useful life prediction of tool with BiGRU-Attention and improved Particle Filter. In: *2021 CAA Symposium on Fault Detection, Supervision, and Safety for Technical Processes (SAFEPROCESS)*, 2021, S. 1–6

[183] X. Li ; B. S. Lim ; J. H. Zhou ; S. Huang ; S. J. Phua ; K. C. Shaw ; M. J. Er: Fuzzy Neural Network Modelling for Tool Wear Estimation in Dry Milling Operation. In: *Annual Conference of the PHM Society* 1 (2009), Nr. 1. https://papers.phmsociety.org/index.php/phmconf/article/view/1403. – ISSN 2325–0178

[184] Goebel: Management of Uncertainty in Sensor Validation, Sensor Fusion, and Diagnosis of Mechanical Systems Using Soft Computing Techniques. (1996)

[185] Sun, Sharon: *CNC Mill Tool Wear: Variational CNC machining data*. https://www.kaggle.com/datasets/shasun/tool-wear-detection-in-cnc-mill/versions/1. Version: 2018. – [Online; accessed 27.03.2023]

[186] J. Niu ; C. Liu ; L. Zhang ; Y. Liao: Remaining Useful Life Prediction of Machining Tools by 1D-CNN LSTM Network. In: *2019 IEEE Symposium Series on Computational Intelligence (SSCI)*, 2019, S. 1056–1063

[187] Huang, Qingqing ; Qian, Chunyan ; Li, Chao ; Han, Yan ; Zhang, Yan ; Xie, Haofei: Tool Remaining Useful Life Prediction Method Based on Multi-Sensor Fusion under Variable Working Conditions. In: *Machines* 10 (2022), Nr. 10, S. 884. http://dx.doi.org/10.3390/machines10100884. – DOI 10.3390/machines10100884

[188] Nie, Lei ; Zhang, Lvfan ; Xu, Shiyi ; Cai, Wentao ; Yang, Haoming: Remaining Useful Life Prediction of Milling Cutters Based on CNN-BiLSTM and Attention Mechanism. In: *Symmetry* 14 (2022), Nr. 11, 2243. http://dx.doi.org/10.3390/sym14112243. – DOI 10.3390/sym14112243

[189] Wan, Lanjun ; Chen, Keyu ; Li, Yuanyuan ; Wu, Yuezhong ; Wang, Zhibing ; Li, Changyun: A Novel Remaining Useful Life Prediction Method Based on CEEMDAN-IFTC-PSR and Ensemble CNN/-BiLSTM Model for Cutting Tool. In: *IEEE Access* 10 (2022), S.

2182–2195. http://dx.doi.org/10.1109/ACCESS.2021.3140165. – DOI 10.1109/ACCESS.2021.3140165. – ISSN 2169–3536

[190] Zegarra, Fabio C. ; Vargas-Machuca, Juan ; Coronado, Alberto M.: Tool wear and remaining useful life (RUL) prediction based on reduced feature set and Bayesian hyperparameter optimization. In: *Production Engineering* 16 (2022), Nr. 4, 465–480. http://dx.doi.org/10.1007/s11740-021-01086-8. – DOI 10.1007/s11740–021–01086–8. – ISSN 0944–6524

[191] H. Jia ; Z. Zhang ; Y. Gao ; F. Shi: A Dual-Stage Attention-Based LSTM Neural Network for Tool Remaining Useful Life Prediction. In: *2021 3rd International Symposium on Robotics & Intelligent Manufacturing Technology (ISRIMT)*, 2021, S. 273–277

[192] Wang, Yahui ; Zheng, Lianyu ; Wang, Yiwei: Event-driven tool condition monitoring methodology considering tool life prediction based on industrial internet. In: *Journal of Manufacturing Systems* 58 (2021), S. 205–222. http://dx.doi.org/10.1016/j.jmsy.2020.11.019. – DOI 10.1016/j.jmsy.2020.11.019. – ISSN 02786125

[193] Zhang, Xiaoyang ; Lu, Xin ; Li, Weidong ; Wang, Sheng: Prediction of the remaining useful life of cutting tool using the Hurst exponent and CNN-LSTM. In: *The International Journal of Advanced Manufacturing Technology* 112 (2021), Nr. 7-8, 2277–2299. http://dx.doi.org/10.1007/s00170-020-06447-8. – DOI 10.1007/s00170–020–06447–8. – ISSN 0268–3768

[194] Huang, Cheng-Geng ; Yin, Xianhui ; Huang, Hong-Zhong ; Li, Yan-Feng: An Enhanced Deep Learning-Based Fusion Prognostic Method for RUL Prediction. In: *IEEE Transactions on Reliability* 69 (2020), Nr. 3, S. 1097–1109. http://dx.doi.org/10.1109/TR.2019.2948705. – DOI 10.1109/TR.2019.2948705. – ISSN 0018–9529

[195] J. Mun ; J. Jeong: Design and Analysis of RUL Prediction Algorithm Based on CABLSTM for CNC Machine Tools. In: *2020 7th International Conference on Soft Computing & Machine Intelligence (ISCMI)*, 2020. – ISBN 2640–0146, S. 83–87

[196] Sun, Huibin ; Zhang, Jiduo ; Mo, Rong ; Zhang, Xianzhi: In-process tool

condition forecasting based on a deep learning method. In: *Robotics and Computer-Integrated Manufacturing* 64 (2020), 101924. http://dx.doi.org/10.1016/j.rcim.2019.101924. – DOI 10.1016/j.rcim.2019.101924. – ISSN 0736–5845

[197] A. K. Jain ; B. K. Lad: Predicting Remaining Useful Life of high speed milling cutters based on Artificial Neural Network. In: *2015 International Conference on Robotics, Automation, Control and Embedded Systems (RACE)*, 2015, S. 1–5

[198] Benkedjouh, T. ; Medjaher, K. ; Zerhouni, N. ; Rechak, S.: Health assessment and life prediction of cutting tools based on support vector regression. In: *Journal of Intelligent Manufacturing* 26 (2015), Nr. 2, 213–223. http://dx.doi.org/10.1007/s10845-013-0774-6. – DOI 10.1007/s10845–013–0774–6. – ISSN 0956–5515

[199] Drouillet, Cyril ; Karandikar, Jaydeep ; Nath, Chandra ; Journeaux, Anne-Claire ; El Mansori, Mohamed ; Kurfess, Thomas: Tool life predictions in milling using spindle power with the neural network technique. In: *Journal of Manufacturing Processes* 22 (2016), 161–168. http://dx.doi.org/10.1016/j.jmapro.2016.03.010. – DOI 10.1016/j.jmapro.2016.03.010. – ISSN 1526–6125

[200] Liu, Yingchao ; Hu, Xiaofeng ; Jin, Jian: Remaining Useful Life Prediction of Cutting Tools based on Deep Adversarial Transfer Learning. (2019), S. 434–439. http://dx.doi.org/10.1145/3373509.3373543. – DOI 10.1145/3373509.3373543

[201] Bagri, Sumant ; Manwar, Ashish ; Varghese, Alwin ; Mujumdar, Soham ; Joshi, Suhas S.: Tool wear and remaining useful life prediction in micro-milling along complex tool paths using neural networks. In: *Journal of Manufacturing Processes* 71 (2021), 679–698. http://dx.doi.org/10.1016/j.jmapro.2021.09.055. – DOI 10.1016/j. jmapro.2021.09.055. – ISSN 1526–6125

[202] An, Qinglong ; Tao, Zhengrui ; Xu, Xingwei ; El Mansori, Mohamed ; Chen, Ming: A data-driven model for milling tool remaining useful life prediction with convolutional and stacked LSTM network. In: *Measurement* 154 (2020), 107461. http://dx.doi.org/10.1016/j.measurement.2019.

107461. – DOI 10.1016/j.measurement.2019.107461. – ISSN 0263–2241

[203] Guo, Liang ; Yu, Yaoxiang ; Gao, Hongli ; Feng, Tingting ; Liu, Yuekai: Online Remaining Useful Life Prediction of Milling Cutters Based on Multisource Data and Feature Learning. In: *IEEE Transactions on Industrial Informatics* 18 (2022), Nr. 8, 5199–5208. http://dx.doi.org/10.1109/TII.2021.3118994. – DOI 10.1109/TII.2021.3118994. – ISSN 1551–3203

[204] Hu, Ning ; Liu, Zhenguo ; Jiang, Shixin ; Li, Quanzhou ; Zhong, Shuqi ; Chen, Bingquan: Remaining Useful Life Prediction of Milling Tool Based on Pyramid CNN. In: *Shock and Vibration* 2023 (2023), 1–14. http://dx.doi.org/10.1155/2023/1830694. – DOI 10.1155/2023/1830694. – ISSN 1070–9622

[205] Liu, Y. C. ; Hu, X. F. ; Sun, S. X.: Remaining Useful Life Prediction of Cutting Tools Based on Support Vector Regression. In: *IOP Conference Series: Materials Science and Engineering* 576 (2019), Nr. 1, 012021. http://dx.doi.org/10.1088/1757-899X/576/1/012021. – DOI 10.1088/1757–899X/576/1/012021. – ISSN 1757–899X

[206] Li, Weidong ; Zhang, Xiaoyang ; Wang, Sheng ; Lu, Xin ; Huang, Zhiwen: Distributed deep learning enabled prediction on cutting tool wear and remaining useful life. In: *Proceedings of the Institution of Mechanical Engineers, Part B: Journal of Engineering Manufacture* (2023), Nr. 7, 095440542211487. http://dx.doi.org/10.1177/09544054221148776. – DOI 10.1177/09544054221148776. – ISSN 0954–4054

[207] Wang, Biao ; Lei, Yaguo ; Li, Naipeng ; Wang, Wenting: Multiscale Convolutional Attention Network for Predicting Remaining Useful Life of Machinery. In: *IEEE Transactions on Industrial Electronics* 68 (2021), Nr. 8, S. 7496–7504. http://dx.doi.org/10.1109/TIE.2020.3003649. – DOI 10.1109/TIE.2020.3003649. – ISSN 0278–0046

[208] W. Wang ; B. Wang ; N. Li ; Y. Lei ; T. Yan: Remaining Useful Life Prediction Based on Multi-channel Attention Bidirectional Long Short-term Memory Network. In: *2021 IEEE International Conference on Sensing, Diagnostics, Prognostics, and Control (SDPC)*, 2021, S. 7–12

[209] Marei, Mohamed ; Li, Weidong: Cutting tool prognostics enabled by hybrid CNN-LSTM with transfer learning. In: *The International Journal of*

Advanced Manufacturing Technology 118 (2022), Nr. 3-4, 817–836. http://dx.doi.org/10.1007/s00170-021-07784-y. – DOI 10.1007/s00170–021–07784–y. – ISSN 0268–3768

[210] Mebrahitom Asmelash Gebremariam ; Seow Xiang Yuan ; Azmir Azhari ; Tamiru Alemu Lemma: Remaining Tool Life Prediction Based on Force Sensors Signal During End Milling of Stavax ESR Steel, 2017, V002T02A094

[211] Zhang, Jianlei ; Zeng, Yukun ; Starly, Binil: Recurrent neural networks with long term temporal dependencies in machine tool wear diagnosis and prognosis. In: *SN Applied Sciences* 3 (2021), Nr. 4, 1–13. http://dx.doi.org/10.1007/s42452-021-04427-5. – DOI 10.1007/s42452–021–04427–5. – ISSN 2523–3963

[212] Zhou, Jing-Tao ; Zhao, Xu ; Gao, Jing: Tool remaining useful life prediction method based on LSTM under variable working conditions. In: *The International Journal of Advanced Manufacturing Technology* 104 (2019), Nr. 9-12, 4715–4726. http://dx.doi.org/10.1007/s00170-019-04349-y. – DOI 10.1007/s00170–019–04349–y. – ISSN 0268–3768

[213] Lutz, B. ; Reisch, R. ; Kisskalt, D. ; Avci, B. ; Regulin, D. ; Knoll, A. ; Franke, J.: Benchmark of Automated Machine Learning with State-of-the-Art Image Segmentation Algorithms for Tool Condition Monitoring. In: *Procedia Manufacturing* 51 (2020), 215–221. http://dx.doi.org/10.1016/j.promfg.2020.10.031. – DOI 10.1016/j.promfg.2020.10.031. – ISSN 23519789

[214] Kisskalt, Dominik ; Mayr, Andreas ; Lutz, Benjamin ; Rögele, Annelie ; Franke, Jörg: Streamlining the development of data-driven industrial applications by automated machine learning. In: *Procedia CIRP* 93 (2020), S. 401–406. http://dx.doi.org/10.1016/j.procir.2020.04.009. – DOI 10.1016/j.procir.2020.04.009. – ISSN 22128271

[215] Saleh Valizadeh Sotubadi ; Rui Liu ; Vinh Nguyen: MSEC2023-104127 DRAFT: EXPLAINABLE AI FOR TOOL WEAR PREDICTION IN TURNING, 2023

[216] Li, Yilin ; Wang, Jinjiang ; Huang, Zuguang ; Gao, Robert X.: Physics-informed meta learning for machining tool wear prediction. In: *Journal of*

Manufacturing Systems 62 (2022), 17–27. http://dx.doi.org/10.1016/j.jmsy.2021.10.013. – DOI 10.1016/j.jmsy.2021.10.013. – ISSN 02786125

[217] A. Schmetz ; C. Vahl ; Z. Zhen ; D. Reibert ; S. Mayer ; D. Zontar ; J. Garcke ; C. Brecher: Decision Support by Interpretable Machine Learning in Acoustic Emission Based Cutting Tool Wear Prediction. In: *2021 IEEE International Conference on Industrial Engineering and Engineering Management (IEEM)*, 2021, S. 629–633

[218] Wang, Jinjiang ; Li, Yilin ; Zhao, Rui ; Gao, Robert X.: Physics guided neural network for machining tool wear prediction. In: *Journal of Manufacturing Systems* 57 (2020), Nr. 1, 298–310. http://dx.doi.org/10.1016/j.jmsy.2020.09.005. – DOI 10.1016/j. jmsy.2020.09.005. – ISSN 02786125

[219] Jia, Wenjie ; Wang, Wei ; Li, Ziwei ; Li, Hai: Prediction of tool wear in sculpture surface by a new fusion method of temporal convolutional network and self-attention. In: *The International Journal of Advanced Manufacturing Technology* 121 (2022), Nr. 3-4, S. 2565–2583. http://dx.doi.org/10.1007/s00170-022-09396-6. – DOI 10.1007/s00170–022–09396–6. – ISSN 0268–3768

[220] MATSUMURA, Rei ; NISHIDA, Isamu ; SHIRASE, Keiichi: Tool life prediction in end milling using a combination of machining simulation and tool wear progress data. In: *Journal of Advanced Mechanical Design, Systems, and Manufacturing* 17 (2023), Nr. 2, JAMDSM0025-JAMDSM0025. http://dx.doi.org/10.1299/jamdsm.2023jamdsm0025. – DOI 10.1299/jamdsm.2023jamdsm0025. – ISSN 1881–3054

[221] ISO International Organization for Standardization: *DIN ISO 10816-7:2009-08 - Mechanical vibration - Evaluation of machine vibration by measurements on non-rotating parts.* 2009

[222] Kistler Group: *Test & Measurement acceleration, acoustic emission and dynamic force: Measuring equipment for demanding T&M applications.* https://www.kistler.com/INT/en/c/accelerometers/CG21-accelerometers. Version: 2021

[223] Marposs S.p.A.: *VA-3D MEMS: 3-Axis Acceleration Sensor.* https://www.marposs.com/eng/product/vibration-sensors. Version: 2022

[224] Montronix GmbH: *PulseNG Sensor*. https://www.montronix.com/en/products/functionality/sensors/accelerometer/pulseng-en.html. Version: 2022

[225] TE Connectivity: *830M1 Triaxial Condition Monitoring Accelerometer*. https://www.te.com/deu-de/product-20018122-00.html. Version: 2022

[226] Analog Devices: *ADXL1001/ADXL1002: Low Noise, High Frequency MEMS Accelerometers*. https://www.analog.com/en/products/adxl1002.html. Version: 2017

[227] Analog Devices: *ADXL1005: Low Noise, Wide Bandwidth, MEMS Accelerometer*. https://www.analog.com/en/products/adxl1005.html. Version: 2018

[228] Analog Devices: *CN-0549: IEPE-Compliant, CbM Machine Learning Enablement Platform*. https://www.analog.com/en/design-center/reference-designs/circuits-from-the-lab/cn0549.html#rd-overview. Version: 2020

[229] Analog Devices: *CN-0532: IEPE-Compatible Interface for Wideband MEMS Accelerometer Sensors*. https://www.analog.com/en/design-center/reference-designs/circuits-from-the-lab/cn0532.html. Version: 2020

[230] Analog Devices: *CN-0540: 24-Bit Data Acquisition System for IEPE Sensors*. https://www.analog.com/en/design-center/reference-designs/circuits-from-the-lab/cn0540.html. Version: 2020

[231] Digilent: *Cora Z7*. https://digilent.com/reference/programmable-logic/cora-z7/start. Version: 2023

[232] Intel Corporation: *Intel® NUC Kit NUC8i5BEK*. https://www.intel.com/content/www/us/en/products/sku/126147/intel-nuc-kit-nuc8i5bek/specifications.html. Version: 2023

[233] DR. JOHANNES HEIDENHAIN GmbH: *iTNC 530: Benutzerhandbuch*. https://content.heidenhain.de/doku/tnc_guide/pdf_files/iTNC530/340422-xx/bhb/375_738-15.pdf. Version: 2004

[234] Hermle AG: *Betriebsanleitung C 30 U (iTNC 530)*

[235] Abele, Eberhard ; Hohenstein, Julien ; Kolaric, Sascha: Fliehkraftadäquate Auslegung von Fräswerkzeugen. In: *Zeitschrift für wirtschaftlichen Fabrikbetrieb* 105 (2010), Nr. 7-8, 681–686. http://dx.doi.org/10.3139/104.110367. – DOI 10.3139/104.110367. – ISSN 2511–0896

[236] Karpuschewski, Bernhard ; Kalhöfer, Eckehard ; Joswig, Dirk ; Rief, Markus: Energiebedarf bei der Herstellung von Hartmetall-Wendeschneidplatten. In: *Zeitschrift für wirtschaftlichen Fabrikbetrieb* 106 (2011), Nr. 9, 602–605. http://dx.doi.org/10.3139/104.110629. – DOI 10.3139/104.110629. – ISSN 2511–0896

[237] Analog Devices: *EVAL-XLMOUNT1: Mechanically optimized mounting block for accelerometer breakout (Z) boards.* https://www.analog.com/en/design-center/evaluation-hardware-and-software/evaluation-boards-kits/eval-xlmount1.html#eb-overview. Version: 2021

[238] Analog Devices: *What is libiio?* https://wiki.analog.com/resources/tools-software/linux-software/libiio. Version: 2023

[239] Analog Devices: *pyadi-iio: Device Specific Python Interfaces For IIO Drivers.* https://wiki.analog.com/resources/tools-software/linux-software/pyadi-iio. Version: 2022

[240] Diaz, Michel: *Petri Nets: Fundamental Models, Verification and Applications.* 1st ed. Hoboken : John Wiley & Sons Incorporated, 2008 https://ebookcentral.proquest.com/lib/kxp/detail.action?docID=477662. – ISBN 9780470394304

[241] Krupp, Lukas ; Wiede, Christian ; Grabmaier, Anton: Approximate Fast Fourier Transform-based Preprocessing for Edge AI. In: *2022 IEEE 27th International Conference on Emerging Technologies and Factory Automation (ETFA)*, IEEE, 06.09.2022 - 09.09.2022. – ISBN 978–1–6654–9996–5, S. 1–8

[242] Sause, Markus G.: Investigation of Pencil Lead Breaks as Acoustic Emission Sources. In: *e-Journal of Nondestructive Testing* 18 (2013), Nr. 07. https://www.ndt.net/search/docs.php3?id=14487

[243] Marius Kintel: *OpenSCAD: The Programmers Solid 3D CAD Modeller.*

https://openscad.org/documentation.html. Version: 2023

[244] SolidCAM GmbH: *SolidCAM*. https://www.solidcam.com/21/de/. Version: 2023

[245] ISO International Organization for Standardization: *ISO 10303-242:2022-12 - Industrial automation systems and integration - Product data representation and exchange - Part 242: Application protocol: Managed model-based 3D engineering*. 2022

[246] Hoffmann SE: *The GARANT measuring microscope family*. https://www.hoffmann-group.com/GB/en/houk/areas-of-application/measurement-technology/garant-video-measuring-microscopes/e/68118/. Version: 2023

[247] Mahr GmbH: *MarSurf PS 10*. https://metrology.mahr.com/de/produkte/artikel/6910230-mobiles-rauheitsmessgeraet-marsurf-ps-10. Version: 2023

[248] Helton, J. C. ; Davis, F. J.: Latin hypercube sampling and the propagation of uncertainty in analyses of complex systems. In: *Reliability Engineering & System Safety* 81 (2003), Nr. 1, 23–69. http://dx.doi.org/10.1016/S0951-8320(03)00058-9. – DOI 10.1016/S0951–8320(03)00058–9. – ISSN 0951–8320

[249] Liaw, Richard ; Liang, Eric ; Nishihara, Robert ; Moritz, Philipp ; Gonzalez, Joseph E. ; Stoica, Ion: *Tune: A Research Platform for Distributed Model Selection and Training*. https://arxiv.org/pdf/1807.05118

[250] Akiba, Takuya ; Sano, Shotaro ; Yanase, Toshihiko ; Ohta, Takeru ; Koyama, Masanori: *Optuna: A Next-generation Hyperparameter Optimization Framework*. https://arxiv.org/pdf/1907.10902

Appendix

A CN-0549 Hardware Specification

Figure A.1a depicts the schematic of the CN-0532 IEPE-comaptible acceleration sensor circuit. The main components of the circuit besides the ADXL1002 include a low-pass filter (LPF), a zero-gain buffer amplifier and two shunt regulators. The shunt regulator IC3 adds a voltage offset to the output voltage of the ADXL1002 such that the final circuit output conforms the IEPE standard. The shunt regulator IC4 provides the other components with a supply current. Figure A.1b shows the schematic of the CN-0540 signal acquisition circuit to which the CN-0532 IEPE-compatible acceleration sensor is connected. As the IEPE standard is based on the supply of acceleration sensors with a constant current, one of the main components of the CN-0540 is a constant current source. Furthermore, the CN-0540 includes a programmable voltage level shifting unit capable of compensating arbitrary IEPE-typical voltage offsets. The offset-compensated voltage is then further processed by an anti-aliasing filter (AAF) with a cut-off frequency of 54 kHz that determines the maximum input bandwidth of the circuit. The final stage of the signal acquisition circuit includes a fully-differential amplifier (FDA), preparing the signal for the following digitization with the 24-bit Σ-Δ-ADC by transforming it from single-ended to differential and by increasing its signal-to-noise ratio (SNR). Given the 24-bit resolution M of the ADC and an ADC reference voltage of $U_{REF} = 4.096$ V, the least significant bit (LSB) voltage U_{LSB} can be derived according to Equation 1a. The sensitivity of the final output of the ADC S_{ADC} in LSBs per acceleration can be derived according to Equation 1b, based on U_{LSB}, the peak-to-peak acceleration range $a_{P-P} = 100$ g of the ADXL1002 and the knowledge that the FDA amplifies the input voltage such that its output voltages match the range $\pm U_{REF}$.

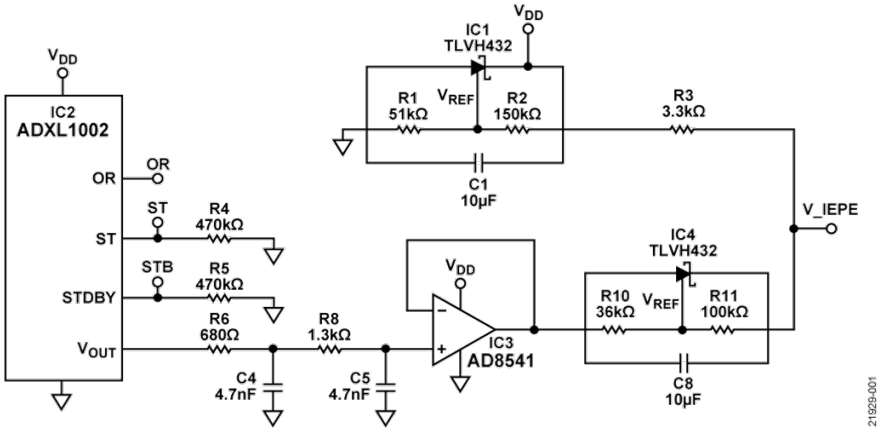

(a) CN-0532 [229]

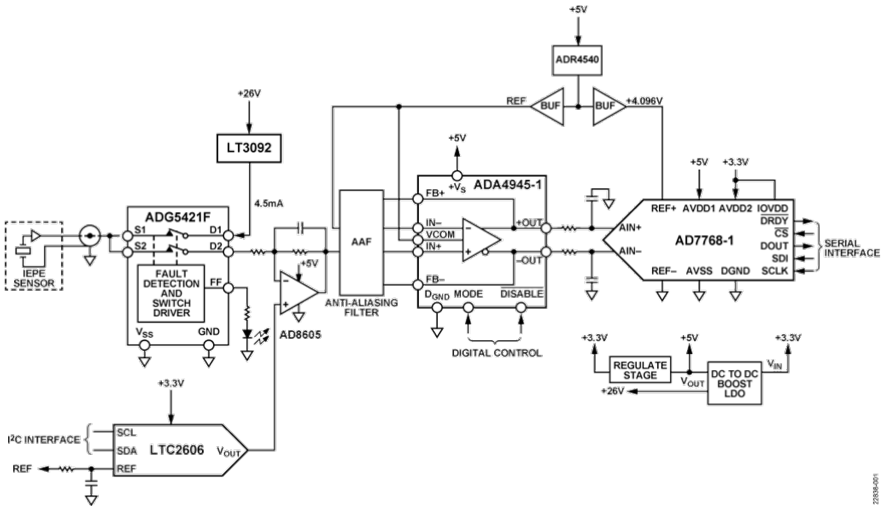

(b) CN-0540 [230]

Figure A.1: Schematics of CN-0532 sensor unit boards [229] and the CN-0540 signal acquisition units [230]. The two subsystems are the core components of the CN-0549 platform.

$$U_{LSB} = \frac{2 \cdot U_{REF}}{2^M} = 488 \ \frac{nV}{LSB} \tag{1a}$$

$$S_{ADC} = \frac{2 \cdot U_{REF}}{a_{P-P} \cdot U_{LSB}} = 167868 \ \frac{LSB}{g} \tag{1b}$$

Although the ADXL1002 acceleration sensor has a ± 3 dB bandwidth of 11 kHz and a resonance frequency of 21 kHz, it still provides an output signal pass band beyond the resonance frequency range. The output amplifier of the ADXL1002 has a small signal bandwidth of 70 kHz. Therefore, it is recommended by Analog Devices to apply measures avoiding aliasing of high frequency noise beyond 70 kHz, when there are frequency bands of interest beyond 10 kHz. In this

work, a filtering is achieved by choosing the sampling rate such that it exceeds twice the equivalent noise bandwidth (ENBW) of a single-pole LPF according to Equation 2 [229].

$$ENBW = \frac{\pi}{2} \cdot 70\ kHz \approx 110\ kHz \tag{2}$$

Therefore, the sampling rate has to exceed $2 \cdot ENBW = 220$ kHz which can be achieved with the CN-0540 signal acquisition system by setting its maximum sampling frequency of 256 kHz.

B CN-0549 Software Specification

Table B.1 gives an overview of the computing systems used throughout this work.

Table B.1: Specification of the computing systems used in this work.

Computing System	Part of Sensor System	Purpose	Operating System
Cora Z7-07S	✓	Single-axis signal aggregation	Kuiper Linux (2019-R2)
Raspberry Pi 4B+	✓	Control data aggregation	Raspberry Pi OS (11)
Intel NUC8i5BEK	✓	Centralized data aggregation and processing	Ubuntu (20.04.02 LTS)
Workstation PC	✗	Offline data analysis and machine learning development	Ubuntu (20.04.02 LTS)

The LibIIO library is the foundation for the data acquisition in the sensor system developed in this work. Therefore, its working principle on the computing systems, especially the Cora Z7-07S and the Intel NUC8i5BEK, according to Table B.1 is explained in the following. Figure B.2 visualizes the relationships of the hardware-software system.

The core of the LibIIO library [238] are the local and the network backend. The local backend implements the direct interfacing between the corresponding Linux-running computing system and the connected IIO device. The local backend is based on the IIO subsystem and device drivers that are part of the Linux kernel. As shown in Figure B.2, the local backend on the Cora Z7-07S communicates with the CN-0540 signal acquisition circuit via the SPI engine running on the FPGA fabric. The required IIO subsystem and device drivers are part of the Kuiper Linux by default. The network backend of LibIIO is required to stream data from an IIO device over a locally connected computing system to a remote client

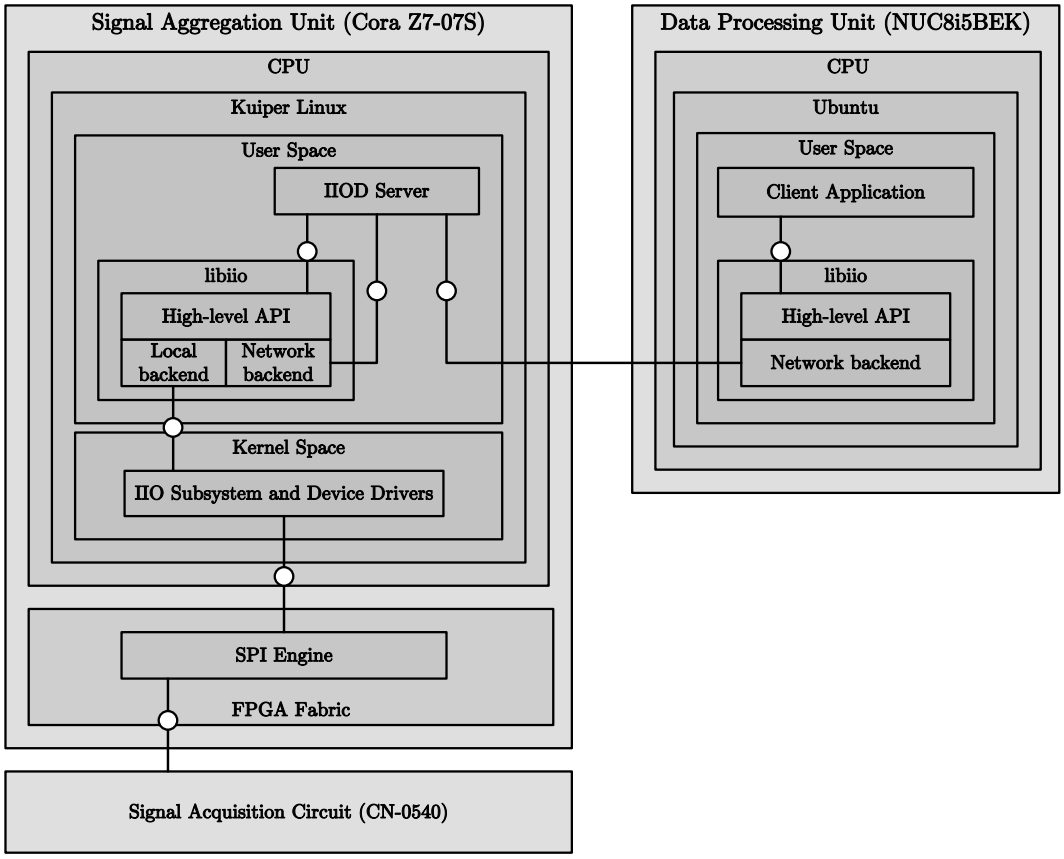

Figure B.2: Interaction between hard- and software components of the acceleration sensor system for the data acquisition based on the LibIIO library.

connected via network. In this work, the remote client is the data processing unit that also runs an instance of LibIIO. However, on the data processing unit the local backend is not required, as the CN-0549 sensor systems are connected via Ethernet. The network link between the NUC8i5BEK and the particular Cora Z7-07S is managed by an IIO daemon server running on the Cora Z7-07S. The IIO daemon server allows to remotely execute client applications developed based on the LibIIO high-level API. In this work, the client applications on the NUC8i5BEK are developed using the PyADI-IIO library [239], mapping the high-level API of the C-based LibIIO library to Python.

C Experimental Setup Details

The following Figures C.5a, C.5b and C.5c show the installation of the CN-0532 sensor boards on the spindle housing of the Hermle C 30 U CNC milling center. The mounting cube by Analog Devices [237] is fixed on an adapter plate. The installed adapter plate with the sensor housing is shown Figure C.5c.

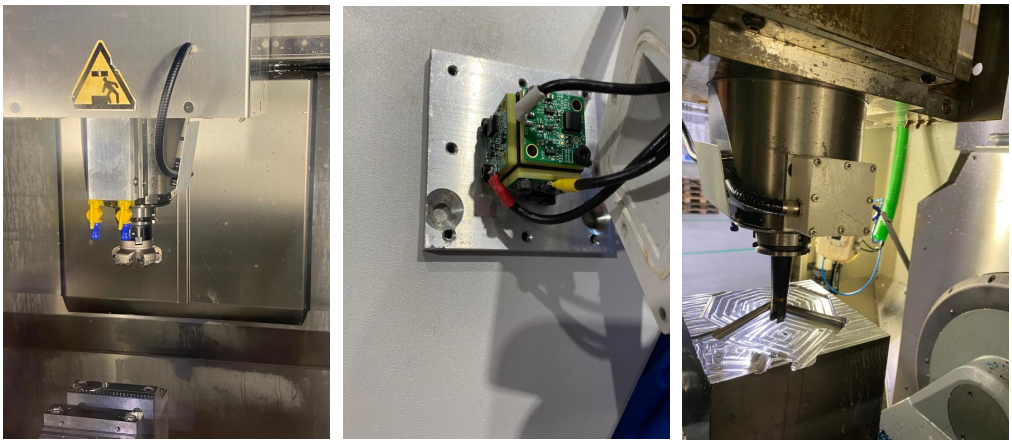

(a) Front View **(b)** Sensor Mounting **(c)** Installed Sensor Box

Figure C.3: Installation of the CN-0532 sensor unit boards on the spindle housing of the Hermle C 30 U CNC machining center.

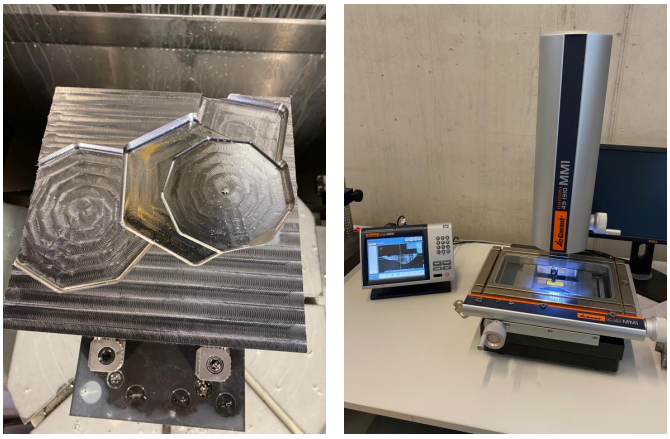

(a) Pocket Geometries **(b)** Garant MM1 [246]

Figure C.4: Pocket geometries milled during dataset generation and Garant MM1 video measuring microscope for determination of the tool wear.

During the dataset generation based on the sensor systems, the pocket geometries shown in Figure C.4a are manufactured. Intermediately, the tool wear

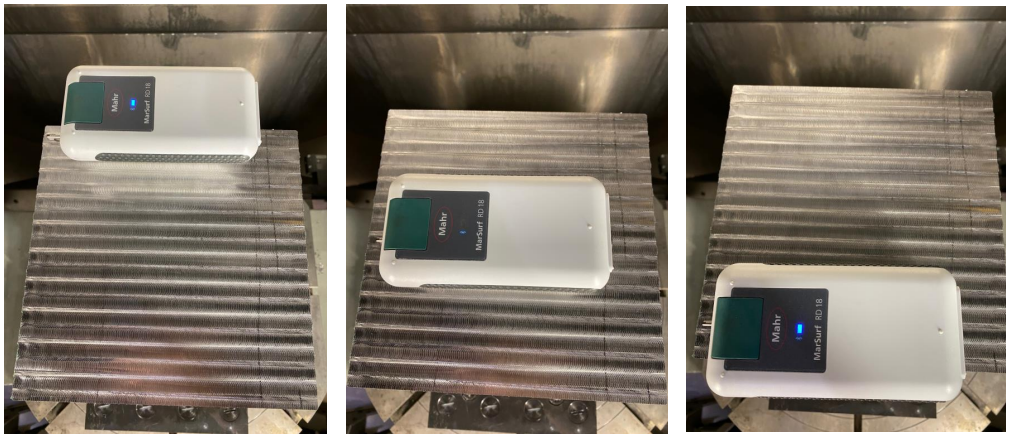

(a) Position 1 **(b)** Position 2 **(c)** Position 3

Figure C.5: Measurement procedure of the workpiece surface roughness using the MarSurf PS 10 roughness measuring device [247].

is measured using the Garant MM1 video measuring microscope shown in Figure C.4b. The flank wear mark width VB is determined for all tool cutting edges.

After each face milling process, the surface roughness is also determined at three positions on the workpiece, according to Figure C.5. Since face milling is performed using the zig-zag strategy, one up-milling and one down-milling path are measured at each position.

D Ternary-Quantized Fast Fourier Transform

Looking at the value distribution of the FFT twiddle factors based on the sine and cosine functions for arbitrary signal lengths N, it becomes clear that the decisive proportion of the values lies around ± 1. Therefore, it is essential to take ± 1 into account in the quantization to minimize the approximation error. Furthermore, the twiddle factors with value 0 simplify the calculations of the butterfly units since multiplications with the inputs are omitted. Based on these considerations, a ternary quantization scheme is used in the following. The ternary quantization is characterized by a mid-tread quantization function $q_T(w, \Delta_t)$ that assigns to every value $w \in \{w^m_{N,r}, w^m_{N,i}\}$ in the interval $[-1, 1]$ a representative level according to the decision thresholds $\Delta_t \in \{-\Delta^T_t, \Delta^T_t\}$ such that $q_T(w, \Delta_t) \in \{-1, 0, 1\}$. The quantization function $q_T(w, \Delta_t)$ is given by:

$$q_T(w, \Delta_t) = (w)_T = \begin{cases} -1, & w < -\Delta_t^T \\ 0, & |w| \leqslant \Delta_t^T \\ 1, & w > \Delta_t^T \end{cases} \tag{3}$$

For simplification, the ternary quantization of the complex twiddle factors $\underline{w}_N^m$ is further written as:

$$(\underline{w}_N^m)_T = \left(w_{r,N}^m\right)_T - j\left(w_{i,N}^m\right)_T \tag{4}$$

Applying the quantization function to the twiddle factors omits the multiplications with the inputs $a_2 \in \{a_{2,r}, a_{2,i}\}$ of the butterfly units contained in Equation 4.8, as a conditional decision with $(w)_T \in \left\{\left(w_{r,N}^m\right)_T, \left(w_{i,N}^m\right)_T\right\}$ can replace them:

$$a_2 \cdot (w)_T = \begin{cases} -a_2, & (w)_T = -1 \\ 0, & (w)_T = 0 \\ a_2, & (w)_T = 1 \end{cases} \tag{5}$$

Since the ternary quantization of the twiddle factors is accompanied by calculation errors, it is necessary to minimize them. The minimization can be achieved by optimal selection of the decision threshold Δ_t of the quantization function and by introducing a general correction factor α according to Equation 6:

$$\begin{aligned} w_N^m &\approx \alpha (w_N^m)_T \\ w_{N,r}^m - j w_{N,i}^m &\approx \alpha\Big(\left(w_{N,r}^m\right)_T - j\left(w_{N,i}^m\right)\Big) \end{aligned} \tag{6}$$

The correction factor α reduces the error to the twiddle factors in full precision. The optimal correction factor can be derived by solving the optimization problem according to Equation 7:

$$\begin{aligned} J(\alpha) &= |w_N^m - \alpha (w_N^m)_T| \\ &\underset{\alpha}{\operatorname{argmin}}\, J(\alpha) \end{aligned} \tag{7}$$

By taking the derivative of $J(\alpha)$ with respect to α and setting it to 0, α can be optimized:

$$\alpha_{opt} = \frac{w_{N,r}^m \cdot \left(w_{N,r}^m\right)_T + w_{N,i}^m \cdot \left(w_{N,i}^m\right)_T}{\left(\left(w_{N,r}^m\right)_T\right)^2 + \left(\left(w_{N,i}^m\right)_T\right)^2} \tag{8}$$

Equation 3 is a special case with $\alpha = 1$. For the TQ- and α-TQ-FFT it is required to derive an optimal decision threshold Δ_t by solving the optimization problem:

$$\begin{gathered} E_\alpha(\Delta_t) = \frac{2}{N} \sum_{k=0}^{\frac{N}{2}-1} |w_N^m - \alpha(w_N^m)_T| \\ \underset{\Delta_t}{\operatorname{argmin}}\, E_\alpha(t) \end{gathered} \tag{9}$$

Since the optimal correction factors depend on the decision threshold, Equation 9 can only be solved iteratively.

List of Publications

The following articles and papers were published as part of the work:

- Krupp, L.; Wiede, C.; Friedhoff, J.; Grabmaier, A.: Explainable Remaining Tool Life Prediction for Individualized Production Using Automated Machine Learning. In: MDPI Sensors (Basel, Switzerland) 23 (2023)

- Krupp, L.; Wiede, C.; Friedhoff, J.; Grabmaier, A.: A Cognitive Sensor System Architecture for the Monitoring of Flexible Machining Systems. In: 2023 IEEE SENSORS, Vienna, Austria, 2023

- Hoyer, I.; Berg, O.; Krupp, L.; Utz, A.; Wiede, C.; Seidl, K.: Hardware Accelerators for a Convolutional Neural Network in Condition Monitoring of CNC Machines. In: 2023 IEEE SENSORS, Vienna, Austria, 2023

- Krupp, L.; Wiede, C.; Grabmaier, A.: Approximate Fast Fourier Transform-based Preprocessing for Edge AI. In: 2022 IEEE 27th International Conference on Emerging Technologies and Factory Automation (ETFA), Stuttgart, Germany, 2022

- Krupp, L.; Hennig, A.; Wiede, C.; Grabmaier, A.: A Hybrid Framework for Bearing Fault Diagnosis using Physics-guided Neural Networks. In: 2020 27th IEEE International Conference on Electronics, Circuits and Systems (ICECS), Glasgow, UK, 2020

DOI: 10.17185/duepublico/81423
URN: urn:nbn:de:hbz:465-20240119-143622-9